PB85-221729

Fundamental Studies of Sorbent Calcination and Sulfation for SO2 Control from Coal-Fired Boilers

Energy and Environmental Research Corp.
Irvine, CA

Prepared for

Environmental Protection Agency
Research Triangle Park, NC

Jun 85

U.S. Department of Commerce
National Technical Information Service
NTIS

EPA/600/7-85/027
June 1985

FUNDAMENTAL STUDIES OF SORBENT CALCINATION AND SULFATION FOR SO_2 CONTROL FROM COAL-FIRED BOILERS

PB85-221729

by
J. A. Cole
W. D. Clark
M. P. Heap
J. C. Kramlich
G. S. Samuelsen
W. R. Seeker

Energy and Environmental Research Corporation
18 Mason
Irvine, CA 92718

EPA Contract No. 68-02-3633

EPA Project Officer: G. Blair Martin

Engineering Applications Division
Air and Energy Engineering Research Laboratory
Research Triangle Park, NC 27711

AIR AND ENERGY ENGINEERING RESEARCH LABORATORY
OFFICE OF RESEARCH AND DEVELOPMENT
U.S. ENVIRONMENTAL PROTECTION AGENCY
RESEARCH TRIANGLE PARK, NC 27711

REPRODUCED BY
NATIONAL TECHNICAL
INFORMATION SERVICE
U.S. DEPARTMENT OF COMMERCE
SPRINGFIELD, VA. 22161

TECHNICAL REPORT DATA

(Please read Instructions on the reverse before completing)

1. REPORT NO. EPA/600/7-85/027	2.	3. RECIPIENT'S ACCESSION NO. PB85 221729 /AS
4. TITLE AND SUBTITLE Fundamental Studies of Sorbent Calcination and Sulfation for SO2 Control from Coal-fired Boilers		5. REPORT DATE June 1985
		6. PERFORMING ORGANIZATION CODE
7. AUTHOR(S) J. A. Cole, W. D. Clark, M. P. Heap, J. C. Kramlich, G. S. Samuelsen, and W. R. Seeker		8. PERFORMING ORGANIZATION REPORT NO.
9. PERFORMING ORGANIZATION NAME AND ADDRESS Energy and Environmental Research Corporation 18 Mason Irvine, California 92718		10. PROGRAM ELEMENT NO.
		11. CONTRACT/GRANT NO. 68-02-3633
12. SPONSORING AGENCY NAME AND ADDRESS EPA, Office of Research and Development Air and Energy Engineering Research Laboratory Research Triangle Park, NC 27711		13. TYPE OF REPORT AND PERIOD COVERED Final; 7/82 - 9/83
		14. SPONSORING AGENCY CODE EPA/600/13

15. SUPPLEMENTARY NOTES AEERL project officer is G. Blair Martin, Mail Drop 4, 919/541-7504.

16. ABSTRACT The report gives results of a laboratory-scale investigation of the reactivity of calcium-based sorbents for SO2 capture after calcination at furnace operating temperatures (1200-1950 C). This work was undertaken to provide fundamental information for developing SO2 emission control technology in pulverized-coal-fired utility boilers. Pulverized sorbents (< 100 micrometer diameter) were calcined by injection into a laboratory gas flame reactor. Experimental variables were time, temperature, gas composition, limestone type, and particle size. Samples were collected for analysis of surface area, extent of calcination, particle size distribution, and reactivity toward SO2. Particle heating, calcination, and surface area development occurred typically in 25-35 ms. Measured surface areas increased with decreasing calcination temperature; the range for a calcite (Vicron 45-3) was 3-15 sq m/g at 1200-1830 C. Surface areas for dolomite reached 25 sq m/g. The general order of SO2 reactivity was dolomite > calcium hydroxide > calcite. Flyash materials reduced both the surface area and the SO2 reactivity of the sorbents tested: calcite was affected the most, and dolomite the least. An approximately linear correlation was found between SO2 reactivity and specific surface area which covered both limestones and limestone/mineral mixtures.

17. KEY WORDS AND DOCUMENT ANALYSIS

a. DESCRIPTORS		b. IDENTIFIERS/OPEN ENDED TERMS	c. COSATI Field/Group	
Pollution	Sorbents	Pollution Control	13B	11G
Sulfur Oxides	Calcium	Stationary Sources	07B	
Coal	Roasting	Calcium-based Sorbents	21D	13H
Pulverized Fuels	Sulfation			07C
Boilers			13A	
Utilities				

18. DISTRIBUTION STATEMENT Release to Public	19. SECURITY CLASS *(This Report)* Unclassified	21. NO. OF PAGES 186
	20. SECURITY CLASS *(This page)* Unclassified	22. PRICE

EPA Form 2220-1 (9-73)

The information is this document has been funded wholly or in part by the U.S. Environmental Protection Agency under contract 68-02-3633 to Energy and Environmental Research Corporation. It has been subject to the Agency's peer and administrative review, and it has been approved for publication as an EPA document. Mention of trade names or commercial products does not constitute endorsement or recommendation for use.

Abstract

Results are presented from a laboratory-scale investigation of limestone reactivity for SO_2 capture after calcination at furnace operating temperatures (1200-1950°C). This work was undertaken to provide fundamental information in support of the U.S. EPA program on Limestone Injection for Multistaged Burners (LIMB) for SO_2 emissions control in pulverized-coal-fired utility boilers.

Pulverized limestones (<100 μm diameter) were calcined by injection into a laboratory gas flame reactor. Experimental variables were time, temperature, gas composition, limestone type and particle size. Samples were collected at short residence times (10-250 ms) using either of two sampling systems. A water-cooled, rapid-quench probe was used to collect samples for analysis of surface area, extent of calcination and particle size distribution. A "dispersed-phase SO_2 reactivity probe" was used to obtain a relative measure of limestone reactivities. The reactivity probe provided a controllable thermal environment for sulfation of calcines independent of the calcination conditions in the reactor. Typical operating conditions were 0.6s at 1100°C with six percent SO_2.

Other areas of investigation were: 1. comparison of fuel-rich versus fuel-lean in-flame sulfur capture, 2. regeneration of solid sulfur species into the gas phase and, 3. the effects of fly ash and minerals on specific surface area and SO_2 capture.

Particle heating, calcination and surface area development occurred typically in 25-35 ms. Measured surface areas increased with decreasing calcination temperature; the range for a calcite, Vicron 45-3, was from 3- to 15 m^2/g. Surface areas for dolomite reached 25 m^2/g. The general order of SO_2 reactivity was dolomite > calcium hydroxide > calcite. Mineral and ash addition to the limestones were detrimental both to surface area and to SO_2 reactivity, with calcite affected the most and dolomite the least. An approximately linear correlation was found between SO_2 reactivity and

specific surface area which covered both limestones and limestone-mineral mixtures.

This work was submitted in partial fulfillment of EPA contract number 68-02-3633 by Energy and Environmental Research Corporation under the sponsorship of the U.S. Environmental Protection Agency. This report covers a period from 1 October 1980 to 30 September 1983 and work was completed as of 31 October 1983.

CONTENTS

Section | Page

Abstract iii
Figures. vii
Tables xii
Nomenclature xiii
Acknowledgments. xv

1.0 INTRODUCTION 1

2.0 BACKGROUND 3
2.1 Sulfur Capture Chemistry. 3
2.2 Previous Studies. 5

3.0 EXPERIMENTAL 13
3.1 Reactor System. 13
3.1.1 Reactor Design 14
3.1.2 Particle Feed Technique. 17
3.2 Diagnostics 20
3.2.1 Sampling Techniques. 20
3.2.2 Physical Diagnostics 25
3.2.3 Chemical Diagnostics 26
3.2.4 Thermal Analyses 27
3.3 Flame Conditions. 30
3.3.1 Flame Temperature Profiles 30

4.0 RESULTS AND DISCUSSION 33
4.1 Limestone Activation and Sulfation. 34
4.1.1 Particle Heat-Up and Calcination 34
4.1.2 Limestone Activation 40
4.1.3 Limestone Reactivity to Sulfation. 54
4.1.4 Limestone Regeneration 59
4.2 Alternate Sorbents. 59

CONTENTS (Continued)

Section Page

4.2.1 Calcination and Activation of Alternate Sorbents 62
4.2.2 Alternate Sorbents Reactivity to Sulfation . . . 71
4.2.3 Summary 73
4.3 Sorbent Deactivation 74
4.3.1 Effect of Coal-Ash on Limestone Activation . . . 75
4.3.2 Effect of Pure Compounds on Limestone Activation 84
4.3.3 Effect of Mineral Matter on Sorbent Reactivity 91
4.3.4 Summary of Mixed Matter Interactions 96

5.0 CONCLUSIONS AND IMPLICATIONS 97

REFERENCES 101

APPENDICES

A--FLAME GAS TEMPERATURE MEASUREMENTS 104

B--SORBENT MATERIAL AND MINERAL DATA 121

C--TWO-COLOR PYROMETRIC PARTICLE TEMPERATURE MEASUREMENTS 123

D--CALCINATION AND SULFATION MODELS 125

E--LIMESTONE SAMPLES DATA 137

F--QUALITY ASSURANCE 152

LIST OF FIGURES

Figure Page

2-1 Effect of sorbent type and size on sulfur capture in (A) propane fired and (B) coal-fired boiler simulator furnace (Indiana coal, DMB with divergent injector) 7

2-2 Effect of fly ash on the sulfur-capture efficiency of Vicron 45-3; chemical analysis of sorbent/ash mixtures . . . 9

2-3 Effects of ash and mineral additives on sulfur-capture efficiency in a natural gas flame 10

3-1 Flat flame burner and particle injection system for the flame thermal decomposition reactor 15

3-2 Schematic of the flame thermal decomposition reactor system 16

3-3 Fluidized bed sorbent delivery system for injection of coal and dry limestone sorbents at low flow rates (0.1-1.0 g/min) 18

3-4 Water-cooled stainless steel sorbent sampling probe and mounting flange 22

3-5 Schematic of the dispersed-phase SO_2 reactivity probe as installed in the TDR 24

3-6 Schematic of the two-color pyrometry system 29

3-7 Radial temperature profiles for four CH_4-air flames at 2 cm from the burner face 31

4-1 Thermocouple gas temperatures compared with two-color particle temperature measurements for Vicron 45-3 injected into a CH_4-air flame. Peak particle temperature V1830°C . . 35

4-2 Calcination dependence on residence time for Vicron 45-3 injected into four methane-air flames 37

4-3 Effect of gas composition on the extent of calcination of Vicron 45-3. T_{max} = 1630°C 38

4-4 Comparison of the degree of calcination of Vicron 45-3 samples injected into H_2 and CH_4 flames 39

4-5 Comparison of present study with other data for calcination of Vicron 45-3 and similar limestone 41

LIST OF FIGURES (Continued)

Figure | | Page
4-6 Residence time dependence of specific surface area of Vicron 45-3 injected into CH_4-air flames 42

4-7 Ultimate specific surface area dependence on peak particle temperature during calcination. Data are taken from differential reactor studies and dispersed-phase reactor studies 44

4-8 Effect of gas-phase composition on the specific surface area development of Vicron 45-3. $T_{max} = 1630^o$ 45

4-9 Vicron 45-3 surface area correlation with extent of calcination 47

4-10 Effect of peak calcination temperature on the ultimate particle size distribution of Vicron 45-3 injected into methane-air flames 48

4-11 SEM examination of Vicron 45-3 51

4-12 The effect of temperature on both rich and lean flame sulfur capture (residence time 150 msec) 56

4-13 Results of scoping tests in the dispersed-phase SO_2 reactivity probe 57

4-14 Calcium utilization efficiency of Vicron 45-3. Residence time 600 msec; nominal reaction zone temperature, 1100^oC; 6 percent SO_2 by volume 58

4-15 Percent regeneration of CaS vs. residence time in the TDR for fuel-lean methane flames 60

4-16 Specific surface area and extent of calcination of alternate sorbents. Peak calcination temperature 1360^oC 63

4-17 Specific surface area and percent calcination of alternate sorbents. Peak calcination temperature 1515^oC 65

4-18 Specific surface area and extent of calcination of alternate sorbents. Peak calcination temperature 1630^oC 66

4-19 SEM analysis of dolomite Michigan Marl and calcium hydroxide 67

4-20 Comparison of surface area development and calcium utilization efficiency for three sorbents 72

LIST OF FIGURES (Continued)

Figure		Page
4-21	Comparison of surface area development for Vicron 45-3 and a Vicron/fly ash mixture. T_{max} = 1515°C	76
4-22	Ultimate specific surface area of Vicron 45-3/Bentonite mixtures for different peak calcination temperatures	77
4-23	Effect of temperature on the ultimate specific surface area of calcined Vicron 45-3/kaolin mixtures	79
4-24	SEM analysis of a Vicron 45-3/5 percent Kaolin mixture calcined in an H_2-air flame, T_{max} = 1200°C	80
4-25	SEM analysis of a Vicron 45-3/5 percent Kaolin mixture calcined in an H_2-air flame, T_{max} = 1200°C	81
4-26	Effect of 5 percent kaolin addition on the particle size distribution of limestone injected into a flame with a peak calcination temperature of 1200°C	82
4-27	Effect of 5 percent kaolin addition on the particle size distribution of limestone injected into a flame with a peak calcination temperature of 1630°C	83
4-28	Sorbent/mineral co-injection techniques	85
4-29	Surface area of Vicron 45-3 after injection into flames at peak temperatures of 1200°C and 1630°C	86
4-30	Effect of Na_2CO_3 and Fe_2O_3 addition on the ultimate surface area of Vicron 45-3 after calcination	88
4-31	Effect of Al_2O_3 and SiO_2 addition on the ultimate surface area of Vicron 45-3 after calcination	89
4-32	Effect of bentonite and kaolin on the ultimate surface area of Vicron 45-3 after calcination	90
4-33	Comparison of calcium utilization efficiency with specific surface area of Vicron 45-3/kaolin mixtures after calcination. T_{max} = 1200°C	93
4-34	Comparison of surface area development and calcium utilization efficiency of limestone in the presence mineral matter	94
4-35	Effect of kaolin on the calcium utilization efficiency of three sorbents	95

LIST OF FIGURES (Continued)

Figure | Page

5-1 Calcium utilization efficiency of sorbents and sorbent-mineral mixtures as a function of specific surface area of sample calcined under identical conditions 99

A-1 Gas temperature profile in a CH_4-air flame. SR = 0.92, V_o = 38.0 $cm \cdot s^{-1}$ 107

A-2 Gas temperature profile in a CH_4-air flame. SR = 1.03, V_o = 38.0 $cm \cdot s^{-1}$ 108

A-3 Gas temperature profile in a CH_4-air flame. SR = 1.16, V_o = 37.0 $cm \cdot s^{-1}$ 109

A-4 Gas temperature profile in a CH_4-air flame. SR = 1.0, V_o = 77.8 $cm \cdot s^{-1}$ 110

A-5 Gas temperature profile in a CH_4-air flame. SR = 0.96, V_o = 50.2 $cm \cdot s^{-1}$ 111

A-6 Gas temperature profile in a CH_4-air flame. SR = 1.58, V_o = 45.2 $cm \cdot s^{-1}$ 112

A-7 Gas temperature profile in a CH_4-air flame. SR = 1.01, V_o = 48.0 $cm \cdot s^{-1}$ 113

A-8 Gas temperature profile in a CH_4-air flame. SR = 1.18, V_o = 47.3 $cm \cdot s^{-1}$ 114

A-9 Gas temperature profile in a CH_4-air flame. SR = 1.30, V_o = 47.0 $cm \cdot s^{-1}$ 115

A-10 Gas temperature profile in a CH_4-air flame. SR = 1.52, V_o = 23.2 $cm \cdot s^{-1}$ 116

A-11 Gas temperature profile in a CH_4-air flame. SR = 2.09, V_o = 49.8 $cm \cdot s^{-1}$ 117

A-12 Gas temperature profile in a CH_4-air flame. SR = 0.98, V_o = 47.6 $cm \cdot s^{-1}$ 118

A-13 Gas temperature profile in a CH_4-air flame. SR = 0.98, V_o = 45.8 $cm \cdot s^{-1}$ 119

A-14 Gas temperature profile in a CH_4-air flame. SR = 1.67, V_o = 49.0 $cm \cdot s^{-1}$ 120

D-1 Comparison of different kinetic models for calcination of 30 m limestone particles at 1730°C 129

LIST OF FIGURES (Concluded)

Figure		Page
D-2	The effect of particle size assumptions on the heating and calcination rates of limestone	130
D-3	The effect of gas temperature on model assumptions for 30 m limestone particle heating and calcination	131
D-4	Times for 50 percent calcination of Vicron 45-3 (this work) and similar limestones over the temperature range of 500°C-1750°C	132
D-5	Comparison of measured ata for Vicron 45-3 with the calcination model using the measured gas temperature profile . . .	134
D-6	Measured gas and Vicron 45-3 particle temperatures compared with model predictions for 11 m and 30 m limestone particles at 1830°C	136
F-1	Calibration of the SO_2 flowmeter at room temperature with negligible outlet pressure	154
F-2	H_2-rotometer calibration curve. Data were obtained using a dry-test volume displacement meter corrected for pressure and ambient temperature	155
F-3	Configuration for stagnation pressure measurement at rotometer outlet. Pressure measurements are used to correct measured gas flow rates	156

LIST OF TABLES

Table   Page

3-1 Diagnostics 21

4-1 SEM Examination of Vicron 45-3 subjected to different temperatures 50

4-2 SEM Examination of fragmentation 61

4-3 Appearance of sorbents, minerals, and mixtures after heating at 950°C for 12 hours 70

4-4 Appearance of sorbent, minerals and mixtures after heating at 950°C for 12 hours 92

A-1 Flame conditions 106

B-1 Physical and chemical properties of sorbents and minerals 122

C-1 Two-color pyrometric particle temperature measurements for Vicron 45-3 co-injected with CH_4-air into a stoichiometric hydrogen-air flame at T_0 = 1917°C and $V_0 = 77.8$ cm·s^{-1} 124

E-1 BET surface area samples data 139

E-2 Vicron 45-3/Kaolin separate injection results 148

E-3 Sulfur capture data (reactivity probe) 149

E-4 In-flame sulfur capture data 151

F-1 Reproducibility of sorbent flow rates before and after sample collection 159

F-2 Reproducibility of BET specific surface area measurements . . 162

F-3 BET specific surface area standards testing 162

F-4 Accuracy and precision tests for the Perkin-Elmer 240B elemental analyser 164

F-5 Accuracy and relative standard deviation determinations for the Leco SC-32 sulfur analyser 166

NOMENCLATURE

a,b = stoichiometric coefficients

C = local concentration of fluid

C_p = heat capacity of $CaCO_3$

C_p = heat capacity of CaO

D = particle density

D_e = effective diffusivity of fluid in particle

D_p = effective diffusivity of fluid in product layer

ΔHr = heat of reaction

K_s = thermal conductivity

k_x = rate constant for surface reaction

K_{rxn} = reaction rate constant

L_o = total length of pore system per unit volume, at $t = 0$

m = mass of sample

M = molecular weight of solid

M_1 = molecular weight of $CaCO_3$

M_2 = molecular weight of CaO

Nu = Nusselt number

r = pore radius

R_o = particle radius

S_o = initial pore surface area per unit volume

t = time

T = temperature

T_g = gas temperature

T_p = particle temperature

T_w = wall temperature

X = local conversion of $CaCO_3$ to CaO

Z = ratio of volume of solid phase after reaction to that before reaction

GREEK LETTERS

α = fraction of original $CaCO_3$ remaining at any time

β = $\dfrac{2k_x\alpha\rho(1 - \varepsilon_o)}{MbD_pS_o}$

ε = porosity

ε_o = ε at $t = 0$

ε_r = emissivity at particle surface

σ = Stefan-Boltzmann constant

ω_0 = mass fraction of reactant in initial solid particles

ψ = $\dfrac{4\pi L_o\ (1 - \varepsilon_o)}{{S_o}^2}$ stuctural parameter

ρ = mass of solid per unit volume of solid phase

ρ_b = initial bulk density of solid

ρ_p = particle density

ACKNOWLEDGMENTS

The authors gratefully acknowledge R. L. Garcia and R. K. Nihart for performing much of the experimental and analytical work. Thanks also for EPA support under contract EPA 68-02-3633 and for many technical discussions with D. W. Pershing, P. L. Case, R. Payne, and the EPA project staff, W. S. Lanier and G. B. Martin. We could not have completed this work without their input.

1.0 INTRODUCTION

The injection of pulverized sorbents into the radiant section of a pulverized-coal-fired boiler as a method of SO_2 control is being investigated by the Engineering Applications Division of the EPA. This activity is largely a development effort designed to elucidate the principal controlling parameters of SO_2 capture and, as a result, allow for process optimization and generalization. Results from bench-scale studies indicate that the overall process involves a complex interaction of physical, thermal, and chemical subprocesses. In order to interpret the bench-scale results, the major parameters must be uncoupled. This suggests the need for fundamental experiments in which major processes, particle heat-up, calcination, and sulfation, are uncoupled, and in which sufficient experimental flexibility is available to match the conditions found in the heat-release zone of a pulverized-coal-fired boiler. Specifically, this implies high temperatures, fast heating rates, both fuel-rich and fuel-lean combustion, and the capability to achieve a broad range of these conditions.

A task within the Fundamental Combustion Research (FCR) program is to study the use of sorbent injection to reduce sulfur oxide emissions from pulverized coal flames. The goal of this task is to obtain information on the high-temperature, short residence time reactions involving sorbents under conditions typical of those existing in coal flames. This information supports data interpretation, model development and verification, and future work in the Engineering Applications Division.

The objectives of the FCR task noted above and addressed here are:

1. To determine the physical and thermal phenomena occurring during high-temperature calcination of calcium-based sorbents.

2. To determine the interrelationship between physical changes and the ability of the sorbent to absorb sulfur compounds.

3. To determine the impact of controllable parameters on physical structure changes, e.g., sorbent type, sorbent size, temperature, stoichiometry, and gas-phase composition.

The approach employed in this effort was to inject a variety of pulverized sorbents into the high-temperature region of a laboratory gas flame. By providing a high temperature (>1200°C) vitiated atmosphere with moderate concentrations of H_2O and CO_2 the gas flame simulated the environment in the radiant zone of a boiler furnace. Several diagnostic techniques were used to define the changes that affect the sorbent particles during calcination and that are likely to affect the ability of the sorbent to absorb SO_2. Both *in-situ* and laboratory analyses were performed in determining the physical and chemical changes of the particles during the short residence times at high temperatures. The conditions sorbents were subjected to were controlled by the laboratory flame environment in order to assess the impact of such parameters as gas-phase temperature and stoichiometry on sorbent properties. The sorbents were also co-injected with different minerals to determine the impact of specific ash constituents on the physical structure of the sorbents. The measured physical changes were then compared with direct measurements of the ability of the sorbent to absorb sulfur dioxide under optimum conditions. In this manner the link between physical changes and sulfur reactivity of the sorbent was made.

2.0 BACKGROUND

Dry calcium-based sorbent injection for sulfur dioxide control has been of interest now for nearly a generation. The attractiveness of the process stems from the low cost and ready availability of the raw materials and the ease with which the dry waste products may be disposed. Early tests in pilot and commercial scale furnaces, however, found that desired levels of SO_2 removal (>70%) could not be attained even with a large excess of limestone (1). Alternative sorbents, such as sodium carbonate and sodium bicarbonate, have yielded much greater success (2). Nonetheless, their greater cost and tendency to increase furnace slagging and corrosion--as well as waste management difficulties--present economic barriers to their implementation.

2.1 Sulfur Capture Chemistry

Sulfur capture by sorbent injection involves four main processes, namely:

- Sorbent activation--the sorbent particles are heated, calcined and rendered reactive toward SO_2.

- Deactivation--the sorbent may experience physical or chemical changes which vitiate its sulfur sorption ability.

- Capture--sulfur species (H_2S, COS SO_2) react with the sorbent producing mainly either sulfate or sulfide.

- Regeneration--the spent sorbent may decompose regenerating gas-phase sulfur species (e.g., $CaS + 3/2\ O_2 \longrightarrow CaO + SO_2$).

Sorbent reactivity depends on many factors, including particle size, composition, surface area, calcination conditions, particle heating rate, and peak particle temperature. Overheating the sorbent can result in the sintering of the solid and, hence, a loss of surface area and reactivity (deadburning).

Substantial experimental effort has been devoted to fundamental studies of limestone calcination and reaction with SO_2 (3). This work, however, generally has been carried out for long exposure times at relatively low temperatures. The general reaction describing sulfur capture under oxidizing conditions:

$$CaO + SO_2 + 1/2\ O_2 \longrightarrow CaSO_4 \qquad (2\text{-}1)$$

has been studied extensively in thin-bed and dispersed-flow reactors by several workers (4,5). However, none of these studies have duplicated the time/temperature conditions that prevail in pulverized coal flames (i. e. 1000°C-1900°C, 100-500 ms). In recent EPA studies, Borgwardt (4) has suggested that reactions such as:

$$CaCO_3 + H_2S \longrightarrow CaS + H_2O + CO_2 \qquad (2\text{-}2)$$

$$CaO + H_2S \longrightarrow CaS + H_2O \qquad (2\text{-}3)$$

could be significant under fuel-rich conditions. Extrapolation of rate data for such reactions (4) indicates that Reaction (2-2) is slow compared to calcination and therefore unimportant for sulfur capture in coal flames. However, low-temperature rate data indicate that Reaction (2-3) would be an important reaction for sulfur capture if the sorbent has high surface area and if H_2S is present in significant concentration. Equilibrium calculations further support this possibility (6).

Low NO_x coal burners produce extensive fuel-rich regions in addition to the usual fuel-lean burnout regions of the flame. Consequently, there may be two possible modes by which calcium-based sorbents can capture sulfur species in a pulverized-coal-fired combustor operating under low NO_x conditions. In fuel-lean regions, Reaction (2-1) may proceed because the lower peak temperature will minimize deadburning. In the fuel-rich region the formation of calcium sulfide may be significant. Furthermore, reaction (2-3) will take place at a much higher temperature (1400°C vs. 1250°C) than Reaction (2-1); the higher temperature enhances the reaction rate. Unfortunately, very little information is available on the fate of the CaS when it enters the fuel-lean burnout region. It can be inferred from thermodynamics, however, that at least some of the CaS will be oxidized to CaO and SO_2 (7).

2.2 Previous Studies

The work carried out to date under Contract 68-02-2667 and 68-02-3921 has involved two parallel investigations at different scales. These are:

- Bench-scale investigations using a boiler-simulator furnace (BSF) firing at a nominal rate of 300 kW (10^6 Btu/hr). The main purpose of these studies has been to define the phenomena controlling sulfur capture in pulverized coal flames.

- Pilot-scale investigations involving full-scale low-NO_x coal burners tested in an environment designed to simulate the burner heat release zones of small utility boilers.

Data were obtained with the EPA prototype distributed mixing burner (DMB) at 21 MW (70 x 10^6 Btu/hr) burning two coals, a low sulfur Utah coal (0.6 percent) and a medium sulfur coal from Indiana (2.5 percent). Sulfur capture is dependent upon coal sulfur content and for the Indiana coal, captures of 50 percent were possible at full load with a calcium-to-sulfur molar ratio of 2:1.

A range of sulfur captures was obtained in the BSF for the Indiana coal and the same sorbent (a commercial calcium carbonate) used in the pilot-scale studies. In a series of screening studies designed to investigate the influence of combustion parameters and thermal environment, the range of captures was achieved by varying heat extraction in the radiant zone, load and tertiary (staged) air velocity.

There have been a number of anomalous findings in the bench-scale results for which our present knowledge does not permit a clear explanation. Notable among these is that sorbent utilization values in excess of 40 percent can be achieved in lean propane flames doped with H_2S. For coal fired under similar conditions, sorbent utilizations below 10 percent are measured, despite similarity in all the known parameters which affect calcination and sulfur capture. At the pilot scale, other differences have been observed which also cannot be explained adequately. These are associated primarily with the inability to predict the effects of different furnace designs on sulfur capture. The furnace effect does not relate to a simple thermal environment change even when using similar DMB-type burners and similar sorbent injection techniques (tertiary air ports).

The effect of sorbent type on sulfur capture is another factor (see bench-scale studies under EPA Contract 68-02-2667 and 68-02-3921) which requires explanation if the process is to be understood. Figure 2-1 shows sulfur capture for various calcium/sulfur ratios and for a variety of sorbent types injected into the BSF firing propane or an Indiana coal at a nominal rate of 300 kW (10^6 Btu/hr). The different results for these sorbents may be attributable to a number of different features, such as:

- Inherent chemical reactivity for sulfur absorption
- Sintering (deadburning) rate and temperature
- Calcination rate
- Physical changes during calcination (e.g., fragmentation)
- Initial particle size distribution
- Tendency to agglomerate
- Surface area or porosity
- Pore size distribution
- Regeneration of sulfur

These combine to make different sorbents behave strikingly different in sulfur capture efficiency; however, which of these parameters controls the process was previously unclear. Figure 2-1B is the capture data for the same sorbents in the same furnace as for Figure 2-1A, but now the sorbents are co-fired with pulverized coal instead of propane. The efficiency of capture dropped dramatically for all sorbents except dolomite.

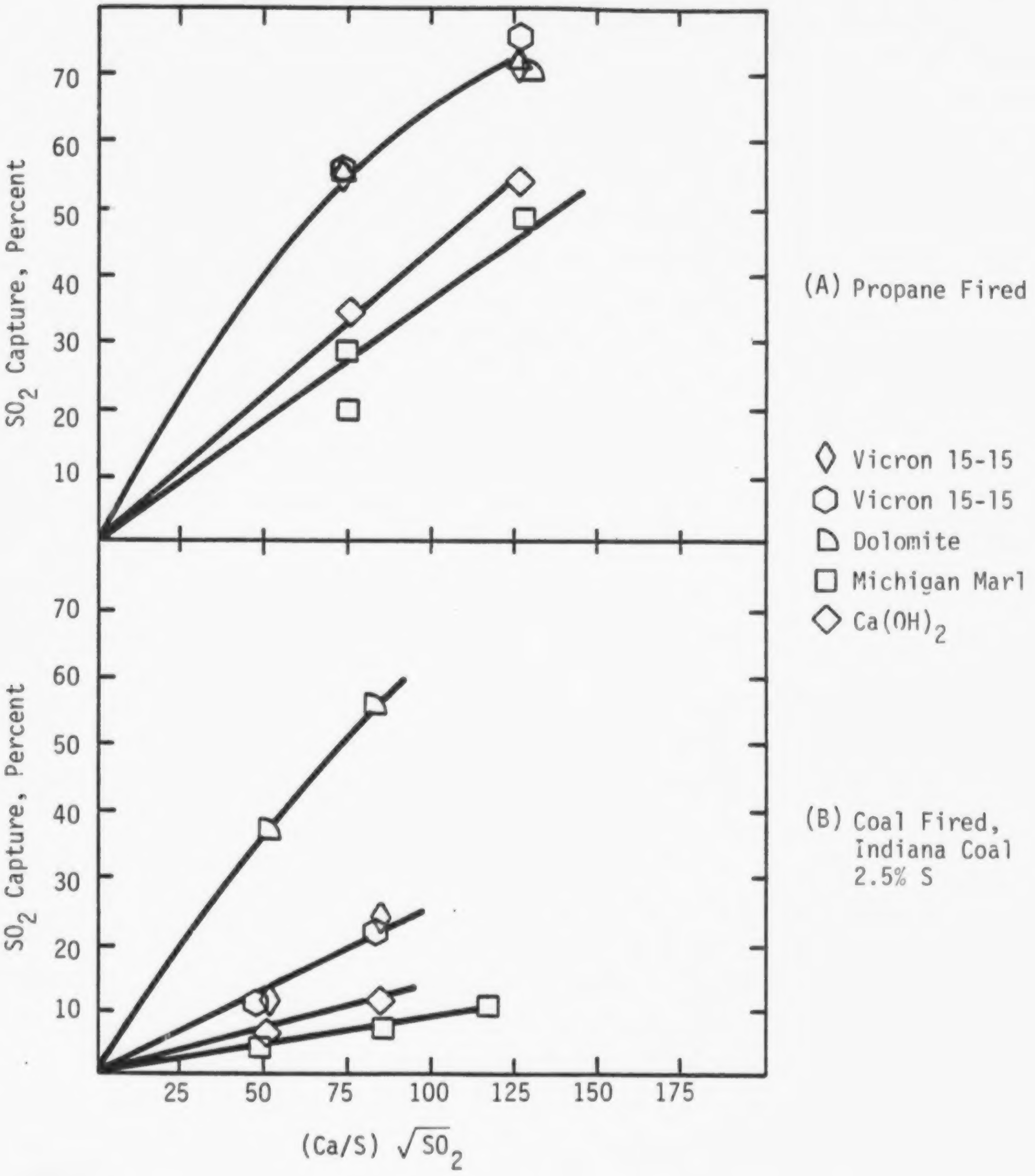

Figure 2-1. Effect of sorbent type and size on sulfur capture in (A) propane fired and (B) coal fired boiler simulator furnace (Indiana coal, DMB with divergent injector). (Case, et al. (8)).

An example of the effects of coal ash on SO_2 capture is shown in Figure 2-2. In the previously mentioned BSF a commercial limestone, Vicron 45-3, was injected neat and in mixtures with fly ash into a natural gas flame doped with H_2S (which quickly oxidizes to SO_2 under fuel lean to slightly rich conditions). The presence of fly ash significantly reduced sulfur capture; the capture for the 25:75 sorbent/ash mixture was less than one-quarter of that for the neat sorbent.

Data shown in Figure 2-3 attempt to relate the loss of sulfur capture efficiency to specific minerals contained in fly ash. Vicron 45-3 was again introduced neat and with fly ash and also with two alumina/silica compounds. Kaolinite is a relatively pure material with a 2:1 (molar) silica:alumina ratio. Bentonite contains proportionately more silica than kaolinite in addition to significant iron, sodium, and potassium fractions. The data indicate that bentonite is roughly half as detrimental, by weight, as fly ash, while kaolinite effects a three-fold greater decrease in sulfur capture efficiency. It is impossible, however, to assess the cause for this loss of efficiency without further information generated under similar, but more controlled laboratory-scale conditions.

A final example of fundamental information required by development programs is fuel-rich-zone chemistry. Pulverized coal flames, particularly when operated under low-NO_x conditions, have large volume fuel-rich zones. Combustion modification techniques for combined control of SO_x and NO_x would have interactions of sorbent particles with fuel-rich flame reactants. It has been suggested from lower temperature data (4, 9, 10) that reduced sulfur species (i.e., H_2S) may react directly with calcium oxide or calcium carbonate to form calcium sulfide in these fuel-rich zones. To what extent these rich-zone reactions take place is not known. The assessment of their importance is critical information for the direction of development efforts.

Although considerable data have been collected from the bench-scale investigations, no clear picture has emerged concerning the precise sequence of events and controlling parameters which dictate overall sulfur capture. It has been established, however, that under fuel-lean conditions thermal

	Mineral Matter Constituents, wt. pct.										
Sample	Ash*	CaO	SiO_2	Al_2O_3	TiO_2	Fe_2O_3	MgO	Na_2O	K_2O	P_2O_5	SO_3
SWS Ash/Sorbent (Vicron 45-3) 50-50	76.3	31.7	26.6	9.5	.3	3.6	1.0	.2	.6	.1	1.3
SWS Ash/Sorbent (Vicron 45-3) 75-25	85.6	17.9	42.2	15.0	.5	5.6	.9	.4	.9	.2	1.0

*Based on ignition weight loss, will include CaO from sorbent as ash.

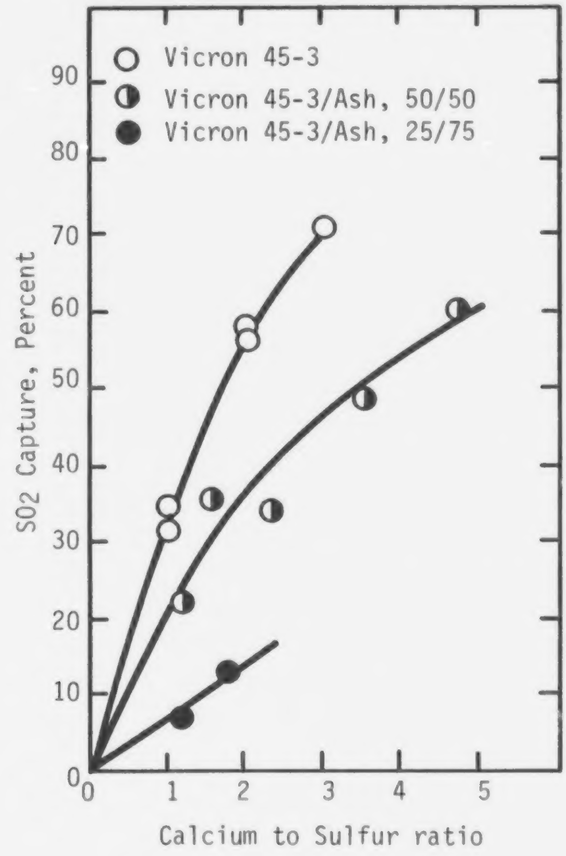

Figure 2-2. Effect of Fly-Ash on the Sulfur-Capture efficiency of Vicron 45-3 at various calcine to sulfur ratios; chemical analysis of Sorbent/Ash mixtures (8).

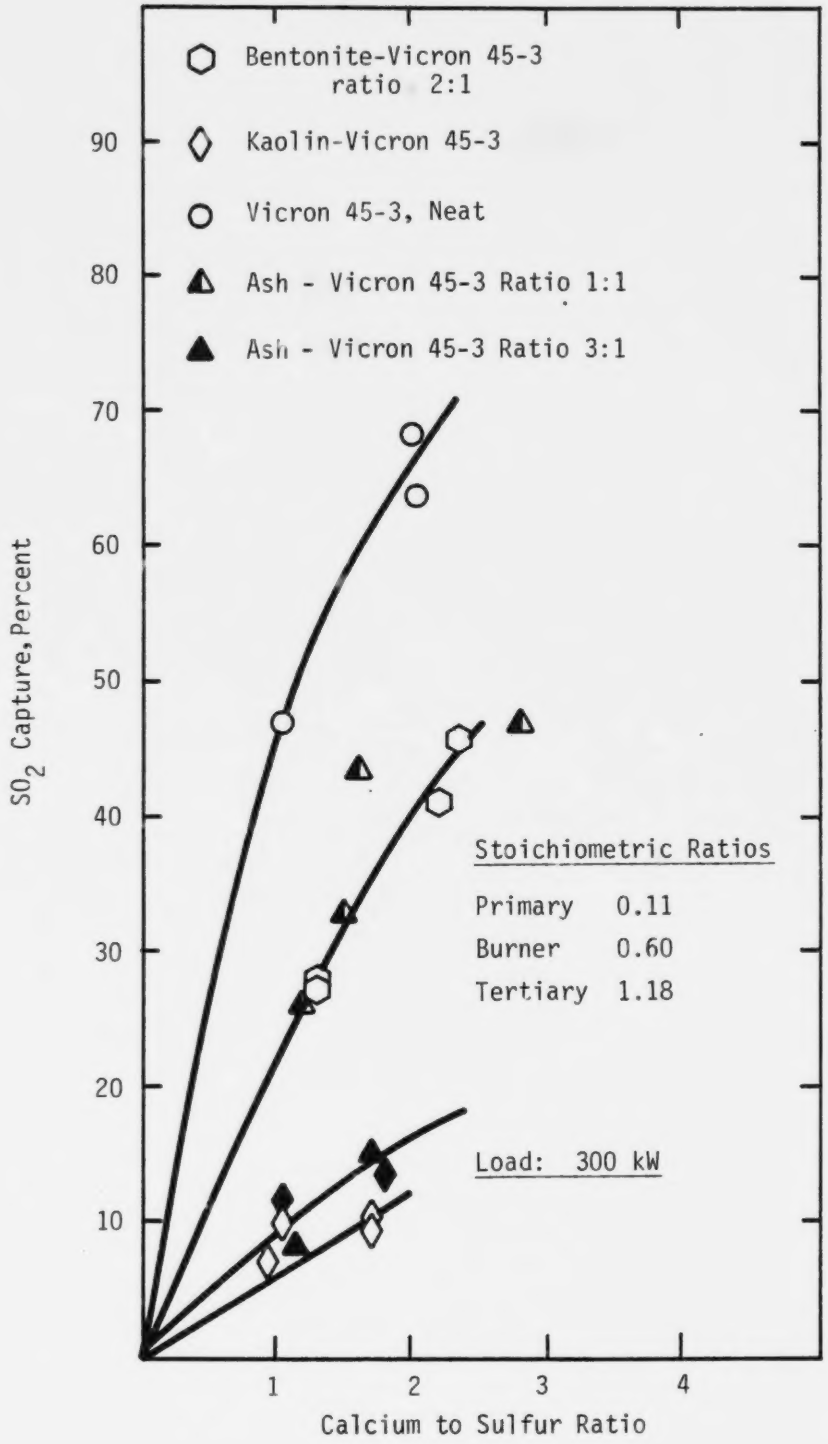

Figure 2-3. Effects of Ash and Mineral Additives on Sulfur-Capture Efficiency in a Natural Gas Flame (8).

environment dominates sorbent utilization and that certain events which occur in short times during the early particle history may be key to determining final reactivity. Results obtained under fuel-rich conditions are less clear and have not shown any significant advantage over the fuel-lean route to sulfur capture (11). Also, it is yet to be demonstrated that significant concentrations of reduced sulfur species are present in large-scale flames, even when these are operated under staged combustion conditions.

Bench-scale and pilot-scale research to date have indicated the need for more detailed information if the development goals of process optimization and generalization are to be accomplished. The following areas were identified for investigation in the laboratory-scale flame thermal decomposition reactor (TDR):

- Temperature necessary to complete calcination in times available in pulverized-coal-fired utility boilers.
- Time/temperature relationships which result in sorbent deactivation or deadburning.
- Time-temperature for maximum sorbent reactivity.
- Characterization of sorbent reactivity.
- Local stoichiometry effects on sorbent calcination.
- Physical and chemical properties of solid reaction products and influence of time/temperature.
- Particle heating rate and maximum temperature achieved upon injection into high-temperature reacting combustion gases.
- Effect of particle size and sorbent type on rates of heating, calcination, and sulfation.

- Effects of mineral matter on physical and chemical changes occurring to sorbents upon injection into high-temperature environment.

The critical information gap exists in the area of the physical and thermal behavior of sorbents under high-temperature dispersed-phase conditions with gas-phase products resembling the gases of pulverized-coal flames. This area has been found to be especially amenable to investigation with the Thermal Decomposition Reactor (TDR) and other existing FCR equipment.

3.0 EXPERIMENTAL APPARATUS AND TECHNIQUES

The experimental phase of this program involved the injection of calcium-based sorbents into high-temperature flames. Physical and chemical processes occurring as a result of flame injection were studied on-line and by subsequent laboratory analysis. Temperature and time in the flame were the most important factors in determining the eventual characteristics of the sorbent.

3.1 Reactor System

Any reactor system has to meet several criteria if it is to yield useful data concerning particle reactions representative of those occurring in gas and pulverized coal flames. These criteria were first delineated by Badzioch (12) as follows:

1. The particle heating rate must be fast, in the range of 10^4 to 10^5 K/s.

2. The reaction time should be controllable and the products rapidly quenched.

3. The temperature (both particle and gas) of reaction should be well defined and be in the appropriate range of pulverized coal flames (1000-2000°C).

4. The particles should be in suspension to match the contacting between the volatiles and char in a flame.

5. The time/temperature history should be precisely known.

In addition to these general criteria, there are a few specific design criteria that arise from the process under investigation and the diagnostic techniques utilized. A partial list of these includes:

1. Since the experimental objective is to simulate a pulverized coal flame environment, the gas-phase environment should be vitiated air composed of volatile products, partially oxidized products, and coal particles along with free oxygen. Stoichiometry and sulfur levels, as well as the mineral content of the solids should be controllable.

2. The system should have optical and mechanical probing access suitable for the selected diagnostic techniques.

3. Coal and sorbent concentrations should be controllable from single particle to concentrations up to those found in flames (200 mg/L).

3.1.1 Reactor Design

The technique which is employed to meet the criteria above is injection of sorbent particles into a one-dimensional laminar flame reactor previously designed for optical and mechanical probing (13). This flame thermal decomposition reactor consists of a sintered metal, flat-flame burner manufactured to specification by McKenna Products Co. The burner (Figure 3-1) has a 27.6-cm (3-in.) diameter active area of 1.6-cm (0.6-in.) thick sintered bronze (-100, +150 mesh) and is mounted in a stainless steel housing. The burner size was chosen in an attempt to thoroughly insulate the centerline gas and particles from the cool ambient. The burner is water-cooled by a tubular copper coil embedded in the sintered disk. Along the centerline a 6.35-mm (0.250-in.) i.d.. copper tube is incorporated into the burner, perpendicular to the face, through which coal or sorbent particles can be injected.

The flat flame is downfired into a 10-cm (4-in.) square stainless steel chimney in order to reduce heat loss and prevent cross-flow interaction (Figure 3-2). High quality fused silica windows (7.6-cm (3.0-in.) diameter x 3.2-mm (.13-in.) thick, Optosil 1) are mounted on two opposing sides of the 91-cm (36-in.) long chimney for visualization measurements. A 7.6 x 30.5-cm (3.0 x 12.0-in.) flat plate of Vycor is mounted on a third side for measuring

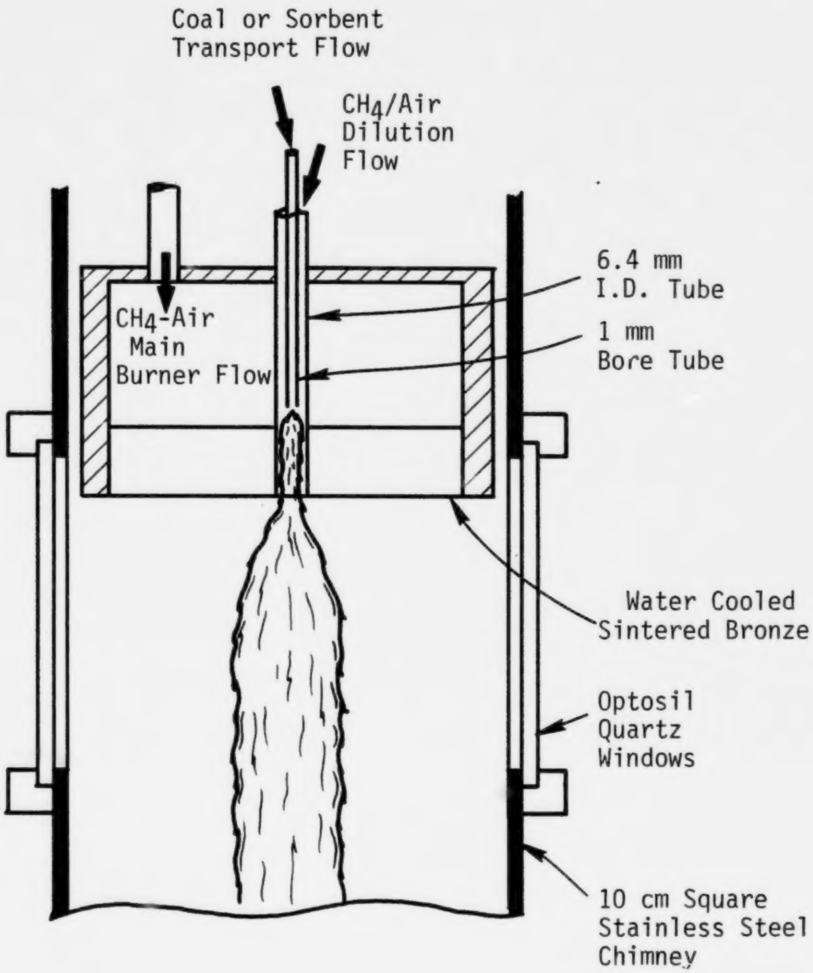

Figure 3-1. Flat-flame burner and particle injection system for the flame thermal decomposition reactor.

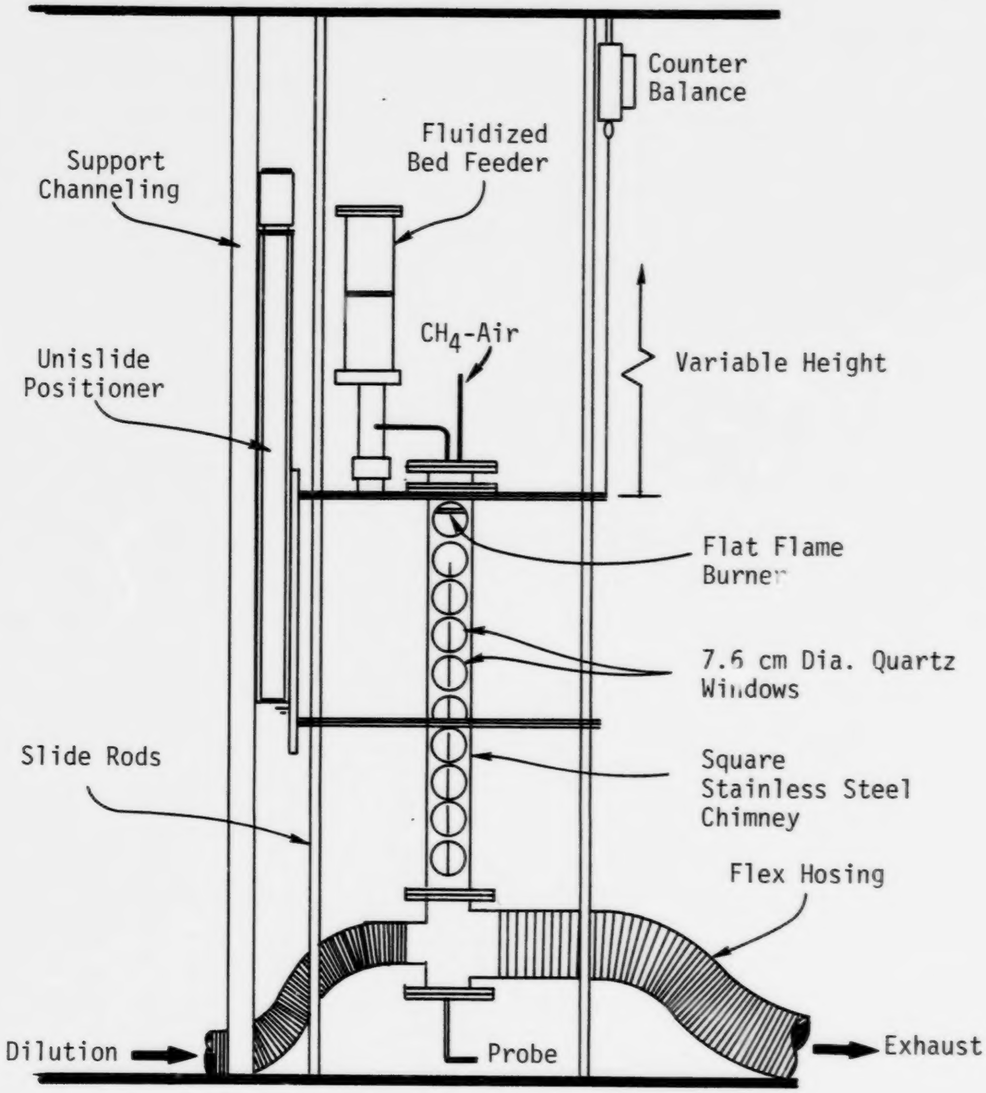

Figure 3-2. Schematic of the flame thermal decomposition reactor system.

particle/droplet temperatures using the two-color pyrometry system and for general visual access. The vertical positioning of the burner and chimney relative to a stationary optical probing height is accomplished through the use of a Unislide assembly.

3.1.2 Particle Feed Technique

One of the most difficult technical problems associated with any dispersed-phase study of sorbents is feeding the fine hydrophilic particles. This problem is exacerbated when ultra-fine particles are used which tend to agglomerate. A Smith-type fluidized bed feeder (14, 15) has been used in the past for feeding pulverized coal in the range of 0.5 to 5 g/min (0.07-0.66 lb/h). However, feed rate instability was encountered when feeding particles smaller than 20 μm. Several alternative approaches were considered for feeding fine and ultra-fine sorbents at the appropriate flow rate of 0.5 g/min. However, it was found that the conventional fluidized bed feeder was adaptable to the fine sorbent particles.

In this technique, sorbent particles are fed directly from a fluidized bed (FB). The particles are suspended in the FB and forced from the suspension by a slight positive pressure in the FB chamber. The resulting particle/gas stream is then diluted with air to an empirically determined air-to-sorbent mass ratio of approximately 1:1. This allows the sorbent to flow freely through a 2-mm (0.08 in.) i.d. delivery tube to the burner. The dilution air also dampens pulsations in the particle flow and regulates the feed pressure in the delivery tube. The FB is vibrated to prevent particle agglomeration, which results in clogging of the sorbent off-take tube. Figure 3-3 shows a schematic of the sorbent delivery system.

In order to check against the possibility of size segregation and discrimination in the feed, raw sorbent samples were collected from the sorbent delivery system and analyzed for sized and surface area. Sedigraph size analyses and BET surface area analyses of batch samples taken from the bulk supply of sorbent and samples fed from the FB were found to be very similar for the Vicron sorbent. Despite these indications of no physical

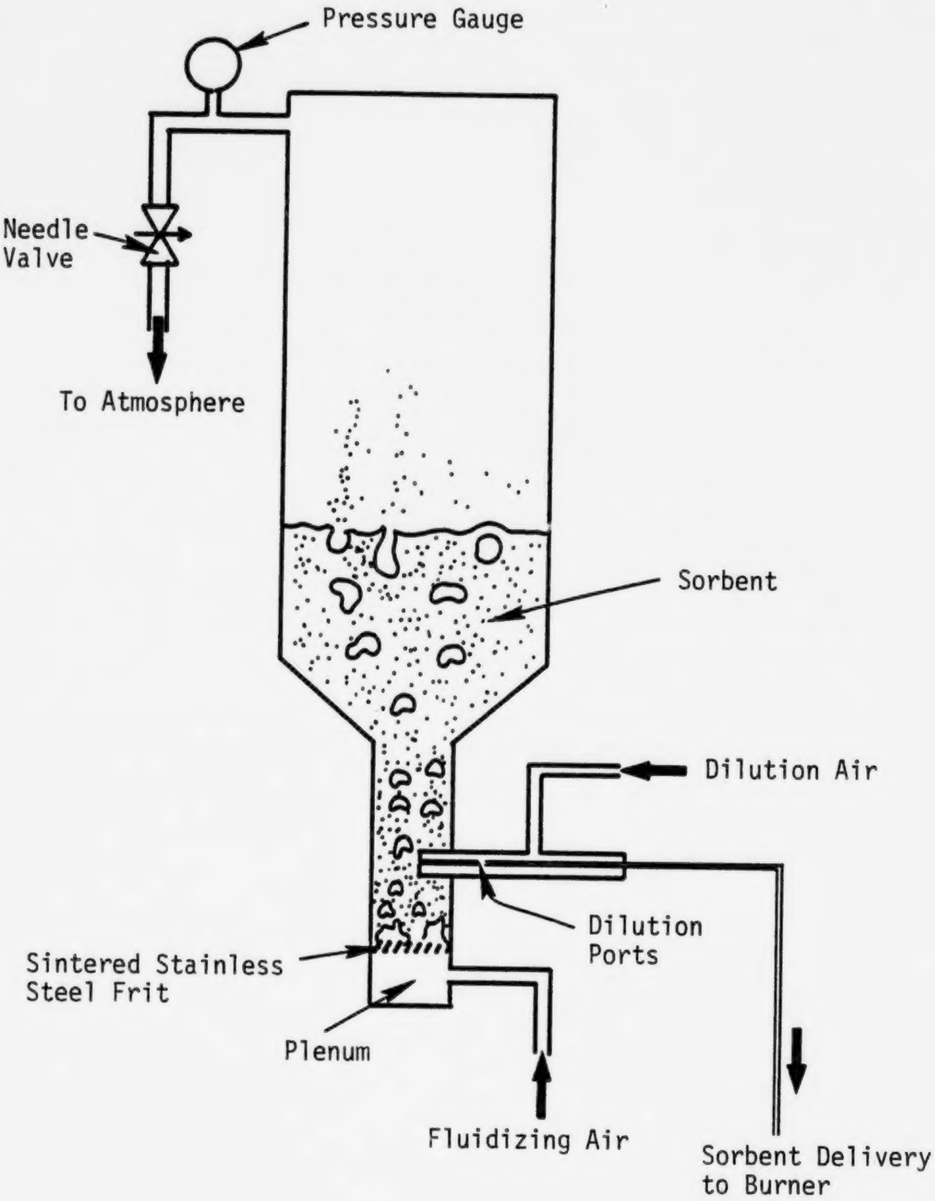

Figure 3-3. Fluidized bed sorbent delivery system for injection of coal and dry limestone sorbents at low flow rates (0.1-1.0 g/min).

segregation within the delivery system, raw samples are always taken via the particle feed and sampling system in the same manner as the flame injected samples.

The feed rate of the sorbent to the flame was maintained at less than 1.0 g/min (0.13 lb/h). This value was established initially for limestone by thermodynamic considerations. A flow rate of 1 g/min results in a temperature drop of 50°C for a typical burner output value of 4.3 kW. For flowrates below 1 g/min, at constant burner load, the extents of calcination and specific surface areas of resulting samples were found to be unaffected by the sorbent flow rate. For flow rates in excess of 5 g/min (0.66 lb/h), particle/particle interactions reduced the aerodynamic dispersion of the sorbent. This produced a stream of particles that traversed the reactor essentially unheated and uncalcined. For burner operation at lower heat outputs, the feed rate was scaled down accordingly.

The flow rates of sorbents, independent of feed system parameters, were affected by the size distribution, shape, and composition of the sorbent particles. Feed rate equations for monodisperse particle diameters (15) were inadequate for predicting particle delivery in the present system. In general, sorbents with narrower size distributions fed easier. Also, sorbents with higher levels of impurities such as silica and alumina (see Appendix B) flowed more steadily and at higher feed rates at the same fluidized bed conditions. Lastly, when pulverized coal (New Mexico -30/+50 mesh) or coal fly-ash (12.6 percent residual carbon, 100 percent < 50 mesh) were added to Vicron 45-3, a noticeable improvement in flow characteristics resulted.

Control of the sorbent feed rate was established by changing the fluidized bed pressure, fluidization velocity, dilution gas flow and the delivery tube diameter. Pressures and gas flow rates were determined experimentally. There was enough flexibility to allow the velocity of sorbent carrier gas to be matched to within ± 50 percent of that of the flame gases at the burner face. The sorbent delivery tube material was standard poly-flow or teflon tubing sold as nominal 1/8 in. o.d.

3.2 Diagnostics

A large number of analytical techniques lend themselves to the study of physical and chemical processes associated with sorbent injection into a furnace. However, the emphasis of this program was to relate the physical, chemical, and thermal responses of sorbents to the thermal and chemical environment to which they might be subjected in a furnace. Physical responses include changes in phase, surface morphology, particle size, and the development or loss of porosity and surface area. Chemical responses may be evolution of CO_2(calcination), solid- or liquid-phase chemical reaction, and sulfation or sulfidation. Thermal responses include changes in internal and surface temperature. Physical and chemical changes, as well as particle heating rate, are interdependent but, in general, were measured independently of each other.

The full analysis of the solids was a mix of standard characterization techniques which allowed comparison with existing data from the literature and more advanced techniques which extended the understanding of sorbent structure and the influence of high-temperature reactions. Table 3-1 provides a list of the diagnostics used in this study. These techniques required that both solids sampling and *in-situ* visualization be utilized.

3.2.1 Sampling Techniques

The method of solid sampling depended upon the subsequent analytical technique. Batch sampling of solids from the flame reactor for physical and chemical analyses was performed with an isokinetic water-cooled stainless-steel probe (Figure 3-4). The solids were collected in a large volume filter (47 mm Nuclepore filter holder using Nuclepore polycarbonate, or Gelman triacetate filter elements with 0.8 μm pore size). The probe was operated above the dew point of the sampled gas (~70°C) by restricting the cooling water flow rate. The filter was maintained at 100°C by keeping it in an electrically heated oven. The sample and flame gases were drawn through the probe by a vacuum pump downstream of the filter holder. If any condensation

TABLE 3-1. DIAGNOSTICS

Classification	Technique	Parameter
Physical	BET N_2 - adsorption isotherm	Specific surface area
	Scanning electron microscopy (SEM)	Particle size, surface morphology, grain structure
	Auto-pycnometry by liquid displacement	Apparent specific gravity
	Auto-pycnometry by helium displacement	Specific gravity
	X-ray sedimentation (Sedigraph)	Particle size distribution
Chemical	Instrumental C,H,N (Perkin-Elmer 240B) determination	Extent of calcination Calcium utilization efficiency
	Loss on ignition (LOI) 1 hr, 950°C	Extent of calcination
	ASTM D2795 Calcium determination	Calcium utilization efficiency
	Instrumental S determination (Leco SC-32)	Calcium utilization efficiency
	Instrumental O_2	Flame stoichiometry
Thermal	Thermocouple	Flame gas temperature, Sampling probe temperature
	Two-color pyrometry	Particle surface temperature

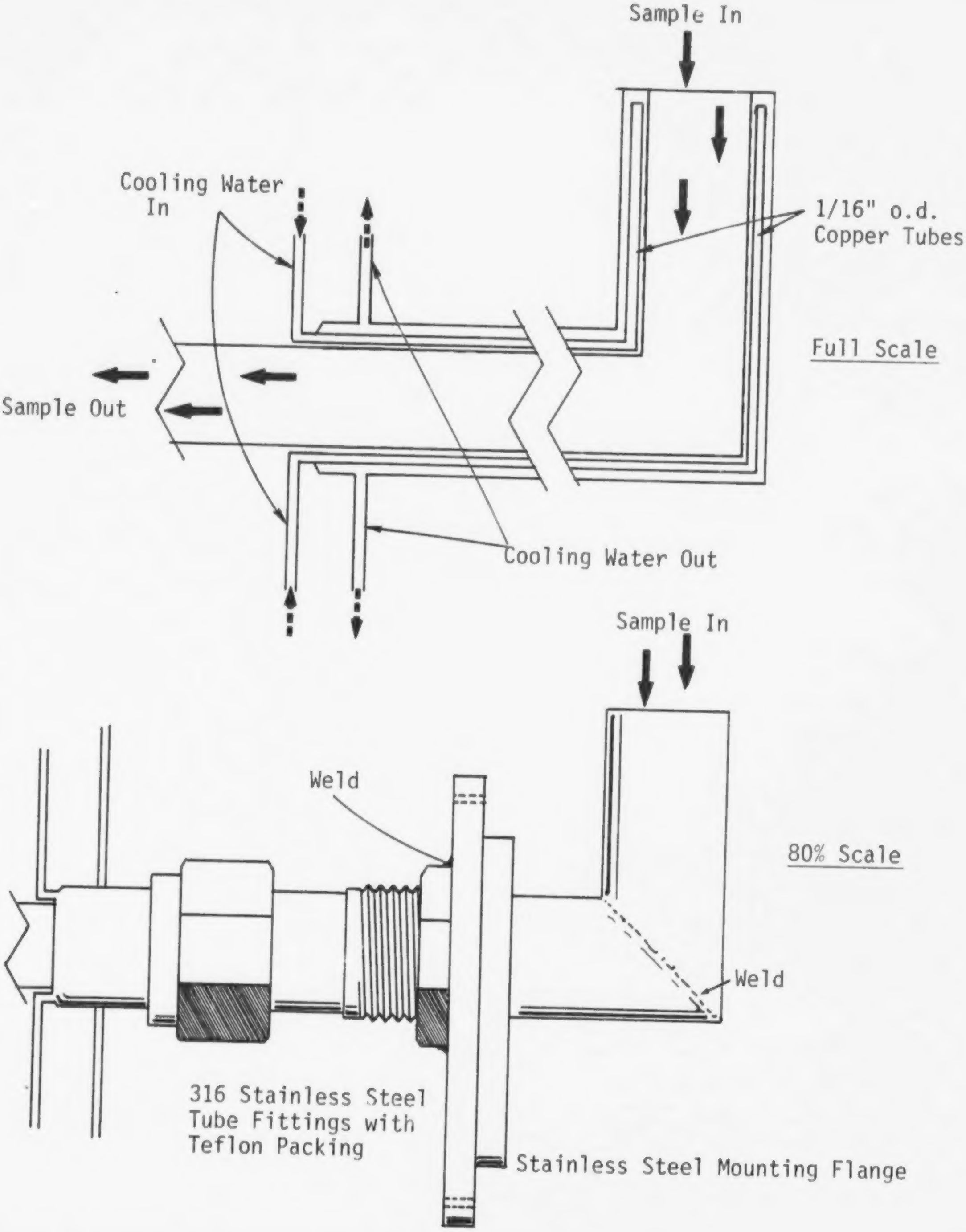

Figure 3-4. Water-cooled stainless steel sorbent sampling probe and mounting flange. (Probe is used for iso-kinetic in-flame sampling of sorbents and sorbent-mineral mixtures).

was observed in the sample train, the sample was discarded because of the potential for slaking of the CaO component of the sample.

The probe was intended for isokinetic sampling. That is, it should not have produced any particle size discrimination. The same test applied to ensure against discrimination in the feed system was used to confirm that the probe was operating isokinetically.

In order to determine the ability of a flame-injected sorbent to uptake sulfur, a "sulfur reactivity probe" was constructed. The basic approach of the probe was first to inject the sorbent into the flame and then subject it to SO_2 in a controlled environment without fully quenching the sample to ambient conditions. In this manner the ability of the sorbent to take up sulfur was directly measured without quenching the sample to ambient, which has uncertain impacts on the sorbent properties. Considerations which went into this design include:

- Quench of sorbent/gas stream to a uniform temperature
- Control over sorbent temperature after quench and before and during exposure to SO_2
- Isokinetic sampling
- Sample recovery

The dispersed-phase reactivity probe is shown in Figure 3-5. This probe permitted samples to be extracted from the flame and quenched to prevent further calcination or sintering. The sorbent, still in the dispersed phase, was then drawn into a heated zone where it was mixed with SO_2 and allowed to react. After a fixed residence time, the sorbent passed through a cooled zone and was collected on a microporous glass fiber filter. It was necessary to keep the sorbent temperature above 650°C in order to prevent recarbonation (absorption of CO_2) of the calcined limestone prior to exposure to SO_2. Quench of the sample stream was regulated to provide a gas temperature

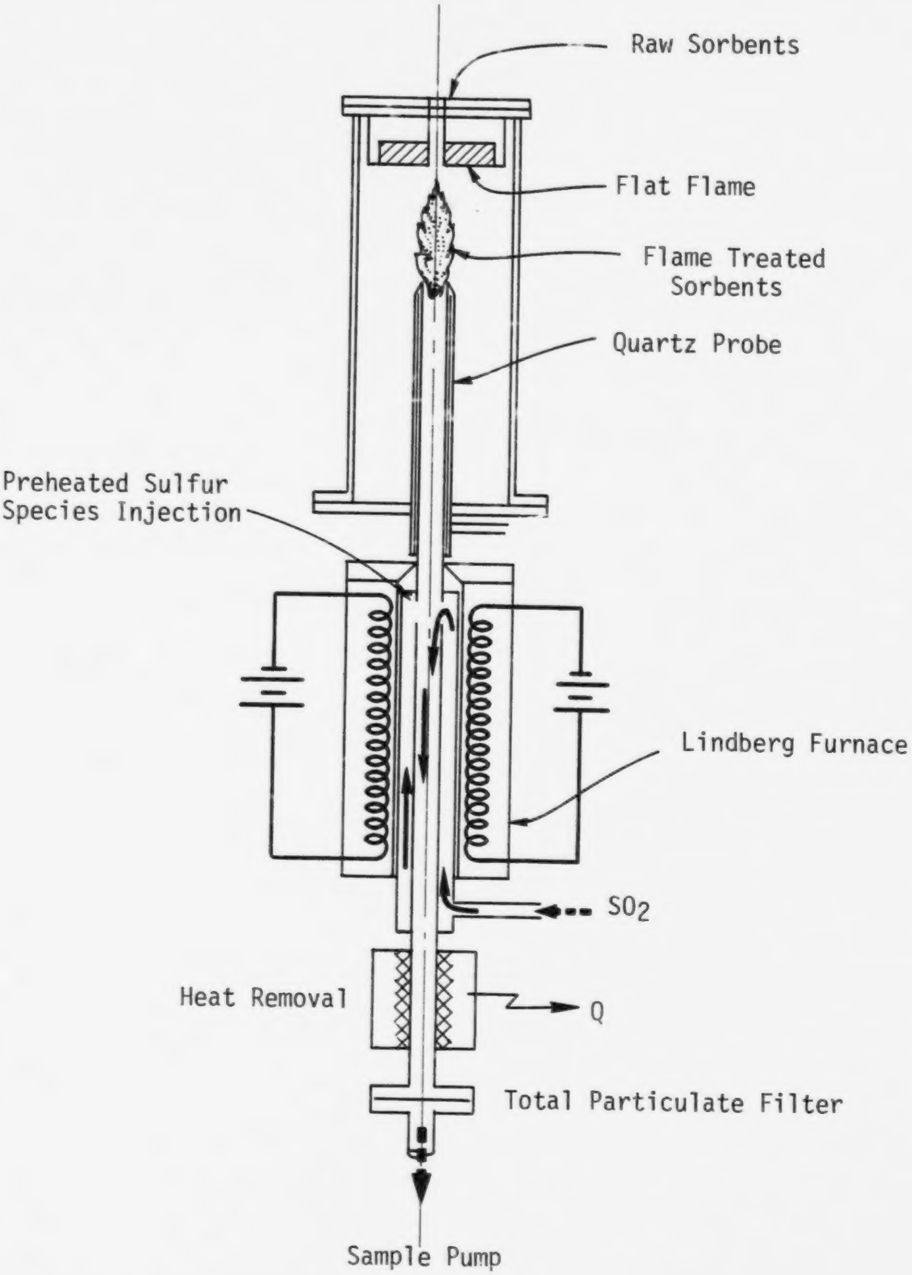

Figure 3-5. Schematic of the dispersed-phase SO_2 reactivity probe as installed in the TDR.

(measured by a type K thermocouple) of 650-670°C at the entrance to the reaction zone. The reaction zone was heated by a tube furnace (Lindburg 55035), which maintained a temperature of 1100 ± 30°C at its midpoint. These conditions were reproducible independent of the flame condition.

SO_2 was preheated before it was mixed with the sample stream by passing it through a quartz tube inside the furnace. A volume fraction of 6 percent SO_2 was added to ensure that the SO_2 concentration did not change appreciably along the length of the reaction zone. Transport calculations showed that the sample stream and SO_2 should be well mixed very early in the reaction zone.

Total residence time of the sample stream in the reaction zone was about 600 ms as estimated by jet-penetration theory (16) and the measured volume of gas leaving the reactor. At the exit of the furnace the sample stream was cooled by natural convection to approximately 150°C when it reached the sample filter holder. Tests were run which showed that additional sulfur uptake in the holder was small. Upon removal, the sulfated samples were analyzed for total sulfur, carbon, hydrogen, and calcium as well as LOI at 950°C.

3.2.2 Physical Diagnostics

The surface area of the solid sorbents and of ash/sorbent samples from the furnace were determined by gas absorption using an instrument manufactured by Quantachrome, Inc. Operation of the instrument is based on the Brunauer-Emmett-Teller (BET) method where surface area is related to the monolayer adsorption capacity of an adsorbent. The BET surface areas of porous and non-porous samples were determined from N_2 adsorption isotherms measured at 77 K (-196°C).

Scanning electron microscopy (SEM) was used for qualitative and semi-quantitative characterization of raw and flame-calcined sorbents and sorbent ash mixtures. SEM samples were collected with the same probe shown in Figure 3-4. In this case the sampling time was reduced to only a few seconds and the result was a light dusting of material on the filter. The filter itself was then used as the stage. Examination of samples collected in this way showed that the particles, in most cases, were well dispersed with a minimum of overlaying. The analyses were performed by an outside laboratory (Micrographics, Irvine, CA), which also conducted electron microprobe analyses on selected samples.

Auto-pycnometry and X-ray sedimentation, also performed by an outside laboratory (Micron Data Labs, Mission Viejo, CA), were used to determine particle size distributions of test materials before and after flame treatment. The analysis is fully automated and provides the mass distribution of particles from 0.1 μm to 100 μm equivalent spherical diameter.

3.2.3 Chemical Diagnostics

The measurement of the chemical characteristics of solid samples extracted from the reactor should allow the interrelationship between physical structure changes and sorbent reactivity to be determined. Of specific interest are the degree of calcination and the sulfur content of the reacted sorbent.

The extent of calcination of limestone sorbents was determined by measuring the residual CO_2 in the sample. The standard technique for CO_2 determination in limestone is ASTM C25-79, taken from Hildebrand, et al. (17). This involves digesting the sample in HCl to release the CO_2. The gaseous effluent is then dried and the CO_2 is collected on soda lime and weighed. This analysis has been performed on raw samples of calcite and dolomite and compared with the results both from weight loss on ignition (LOI) (also under ASTM C25-79) at 950°C and total carbon determination using a Perkin-Elmer 240B Elemental Analyzer. Agreement between the three techniques was within 1 percent overall. Because water of hydration is picked up by flame calcined limestones during sample quench, it is also necessary to take that into account in determining the extent of calcination. LOI is very accurate but nonspecific; it serves as a quality assurance verification for the elemental analysis instruments. For calcium hydroxide ($Ca(OH)_2$), residual H_2O content is the only way of determining the extent of calcination.

The instrument used for measuring sulfur content (Leco SC-32) is designed for combustible solids and had to be tested with sorbent and ash samples. This instrument burns the sample at high temperatures (>1300°C) in an oxygen-enriched atmosphere and measures the SO_2 evolved by infrared light absorption. The instrument is equipped with an analytical balance and a microprocessor system which are used to convert the measured SO_2 content of the gases to equivalent weight percent of sulfur in the sample. Noncombustible solids, including calcium salts, require the use of a combustion accelerator to ensure that all of the sulfur is evolved from the sample. Several combustion accelerators have been tested, including V_2O_5, Al_2O_3, and MgO. V_2O_5 was found best for our applications. This instrument has been successfully tested with several "known" samples, including reagent grades $CaSO_4$ and CaS (18).

Several models of on-line O_2 analyzers are available. These are employed regularly to check or confirm the stoichiometry of fuel-lean flames.

3.2.4 Thermal Analyses

Of paramount importance to the success of this program is the ability to characterize both the gas and solid temperatures. It is fortunate that techniques for both measurements already have been developed and thoroughly tested as part of the FCR study of the thermal decomposition of pulverized coal particles (13). The gas temperature profiles in the TDR were determined by the corrected thermocouple techniques discussed in Appendix A. Two-color pyrometry was used for the measurement of particle temperature.

While flame temperatures are important in estimating residence times and determining that the conditions are similar to those in a pulverized-coal-fired boiler furnace, a thorough analysis of the physical/chemical response of the sorbent requires knowledge of the sorbent temperature. The particle temperature is the temperature at which the gas-solid reactions occur and therefore requires definition. Two-color pyrometry is a simple technique based on the black-body radiation distribution curve. This described by Wien's Law which is adequately expressed by (19):

$$I_\lambda = 2\epsilon_\lambda A C_1 \lambda^{-5} \exp(-C_2/\lambda T) d\lambda \qquad (3\text{-}1)$$

Where: I_λ = intensity at λ
ϵ_λ = emissivity at λ
A = cross-sectional area
C_1 = first radiation constant
C_2 = second radiation constant
λ = wavelength
T = absolute temperature

If the emission of a radiator is measured at two different wavelengths, the ratio of the intensities can be used with considerable simplification to determine the temperature of the radiator. This is especially useful if A is changing or either A or ϵ are not well known. For a gray radiator $\epsilon_{\lambda_1}/\epsilon_{\lambda_2}$ can be considered to be unity. The intensity ratio, R, is then

$$R = \frac{I_{\lambda_1}}{I_{\lambda_2}} = \left(\frac{\lambda_2}{\lambda_1}\right)^5 \exp\left[C_2/T\left(\frac{1}{\lambda_2} - \frac{1}{\lambda_1}\right)\right] \qquad (3\text{-}2)$$

Temperature, T, is easily found since λ_1, λ_2, and C_2 all are constants. System biases were removed by calibrating the system against well-defined radiators including a tungsten-strip-filament lamp and a commercial black-body source.

The two-color system developed previously for high-temperature studies of pulverized coal combustion was not sensitive enough for these studies. It appeared that fragmentation and dispersion of the already ultra-fine particles severely reduced their emission within line-of-sight of the optical probe. For this reason, a fast-response, high-sensitivity, two-color system (Figure 3-6) was specially designed and assembled for in-situ sorbent

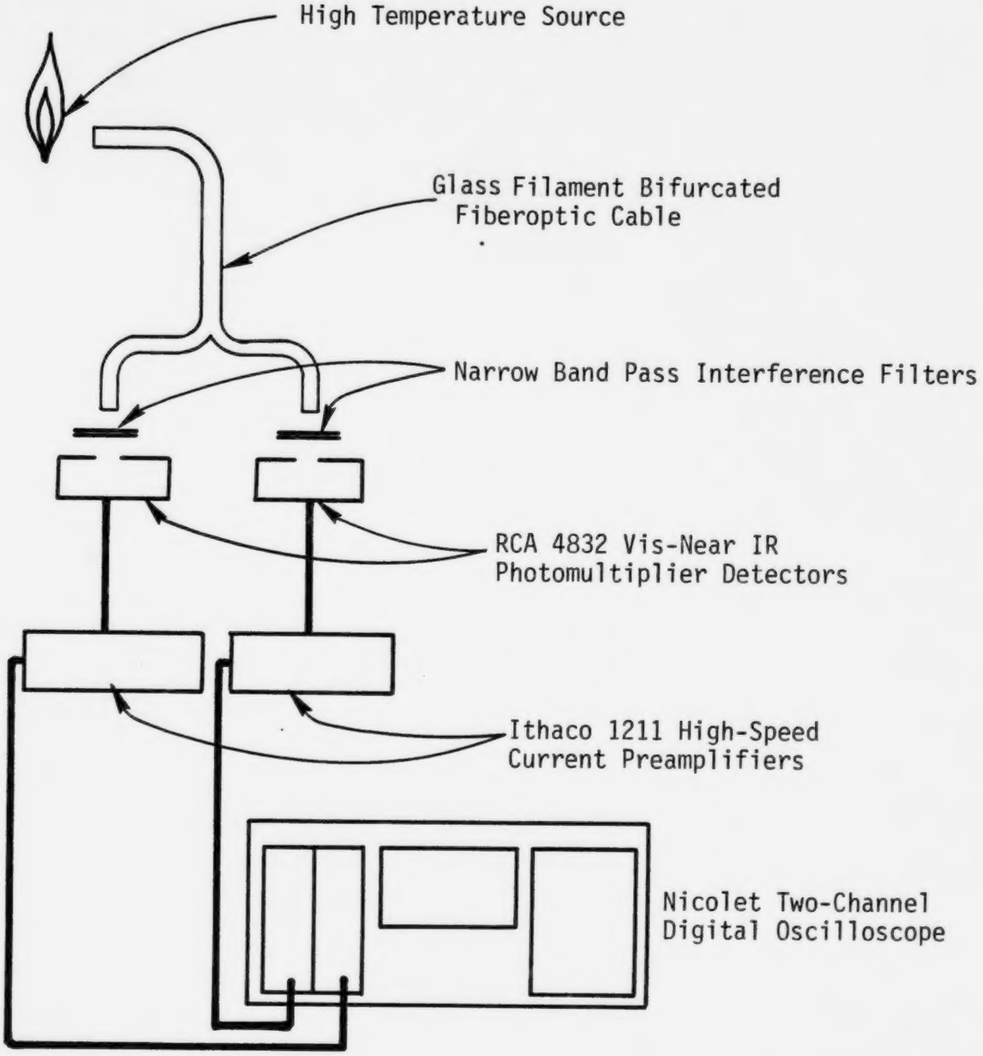
High Temperature Source
Glass Filament Bifurcated Fiberoptic Cable
Narrow Band Pass Interference Filters
RCA 4832 Vis-Near IR Photomultiplier Detectors
Ithaco 1211 High-Speed Current Preamplifiers
Nicolet Two-Channel Digital Oscilloscope

Figure 3-6. Schematic of the two-color pyrometry System.

particle temperature measurements. The key elements in this system are high-speed current amplifiers (Ithaco 1211) which permit measurement of weak signals over a high-level background. Photomultiplier tube detectors are indicated in Figure 3-6. These operate with narrow-band-pass filters at 750 nm and 850 nm. Alternatively, these could be replaced by photodiodes equipped with 750 nm and 950 nm filters. Both detection systems are current sources. The current was processed by the Ithaco 1211 amplifiers and read as voltage output on the digital oscilloscope.

3.3 Flame Conditions

The majority of the sorbent study was carried out with 13 different methane-air and hydrogen-air flames. Three of these flames used N_2, O_2, or CO_2 as diluent gases in an attempt to determine the effects of the combustion gas composition on the ultimate physical/chemical properties of the sorbents. Hydrogen flames were employed for two reasons: (1) first, to extend the temperature range of the study by utilizing the high flame speed and greater flammability range of H_2-air mixtures and (2) secondly, a hydrogen flame provides a CO_2-free environment so that complications involving calcination and possible recarbonation of the sorbent could be eliminated. Flame conditions used for this study are described in Appendix A.

3.3.1 Flame Temperature Profiles

Flame temperature profiles were measured with a type S (Pt/Pt-10%Rh) thermocouple monitored by an Omega model 199 Thermocouple Thermometer. Radiation corrections were applied in order to obtain true gas temperature within ±50K.

Injection of sorbents along the burner axis caused a disruption of the radial temperature profile because of the differences in gas velocity and composition. By adding small amounts of methane to the sorbent injection stream, the centerline temperature could be matched to the flame gas temperature at any convenient point away from the burner. Figure 3-7 shows radial temperature measurements for four methane-air flames where the

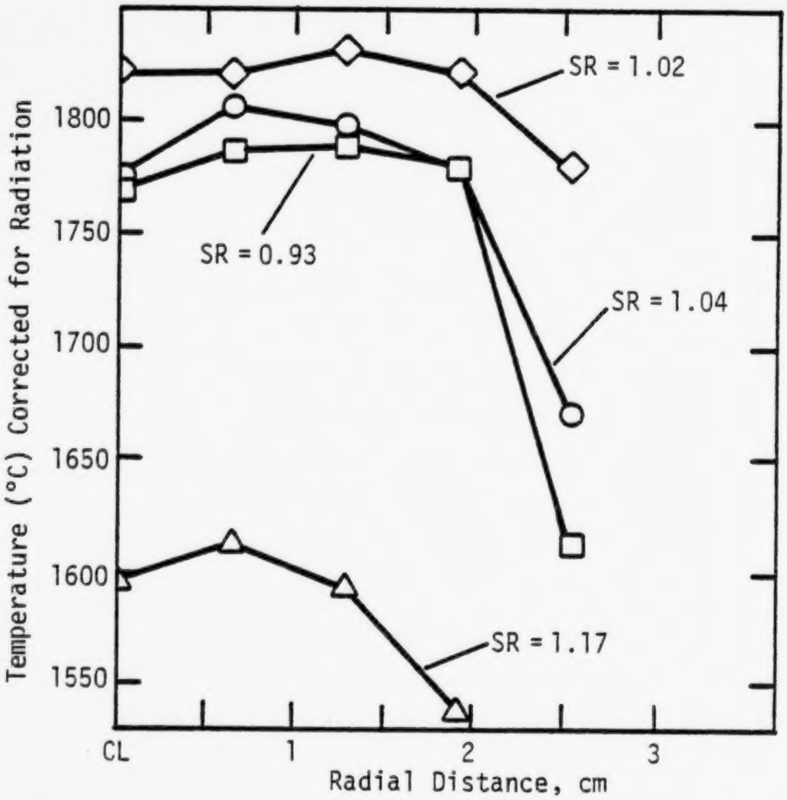

Figure 3-7. Radial temperature profiles for four methane-air flames at 2 cm from the burner face.

centerline temperature was matched to the flame gas temperature 2 cm (0.8 in.) from the burner face. The flatness of the temperature profiles was maintained well beyond the usual sampling distance.

All of the flame temperature profiles were linear with distance from the burner. This fact, coupled with the known cold-gas velocities, simplified the calculation of time temperature profiles. These also are shown in Appendix A.

4.0 RESULTS AND DISCUSSION

This work has centered on the collection and analysis of data on calcium-based sorbent samples which have been exposed to conditions simulating the radiant and convective regions of pulverized-coal-fired utility boilers. The samples were analyzed for changes in physical characteristics and chemical composition. Many were examined by SEM in order to observe both structural and size changes. Data were collected specifically to aid in the development of models for calcination, particle heating and sorbent reactivity to SO_2.

Two classes of sorbents were investigated--calcitic and dolomitic limestones. The calcitic limestones, including calcite, marl, and calcium hydroxide (calcined and slaked calcite), are characterized by a high concentration of calcium and small amounts of magnesium. Dolomitic limestones contain roughly equal amounts of calcium and magnesium as the mineral dolomite ($CaCO_3 \cdot MgCO_3$). Dolomitic limestones are generally disfavored as sorbents because the magnesium component is unreactive toward SO_2 (20) after high temperature calcination and therefore constitutes a voluminous inert which must be transported and handled at considerable extra cost (21). On the other hand, properties such as ease of calcination and resistance to sintering make it appealing as a sulfur capture sorbent.

The baseline sorbent for this work was a relatively pure calcitic limestone sold under the name of Vicron 45-3 (Pfizer Mineral and Pigments Co.). Descriptions and chemical analysis are provided for each of the sorbents in Appendix B.

In the following sections all of the data have been included unless indicated. Also, in general, curves were drawn as best fit by eye to follow the trends suggested by all of the data.

4.1 Limestone Activation and Sulfation

After sorbents are injected into a high temperature environment, a series of processes occur which ultimately dictate the level of sulfur capture which can be achieved. These are:

- Particle heatup
- Calcination
- Activation
- Sulfation
- Deactivation and/or regeneration

In the following section, each of these subprocesses is discussed separately along with the appropriate data for the baseline sorbent Vicron 45-3. Of primary importance is the time requirement for the sequential processes to occur at furnace temperatures. Of nearly equal importance is the impact of overall furnace conditions on the ability of the sorbent to uptake sulfur species. In the next section (4.2), the behavior other sorbents is compared with the pure calcitic limestone. The final section (4.3) contains data on the important deactivation process which results from sorbent interaction with coal mineral matter.

4.1.1 Particle Heatup and Calcination

The rate at which the sorbent particles heat up and the ultimate temperature attained determine the eventual reactivity of the sorbent. The time which the sorbent will spend in the furnace is only a few seconds so it is important that the process be optimized within this time frame. In addition, accurate data interpretation requires that the reaction temperature (i.e. the sorbent particle temperature) be known.

Using the two-color pyrometry system described in Section 3.2.4, particle temperatures were measured for Vicron 45-3 injected into a methane-air flame. These data are shown in Figure 4-1 along with the corrected gas temperatures both for the flame and for the sorbent carrier gas. The scatter

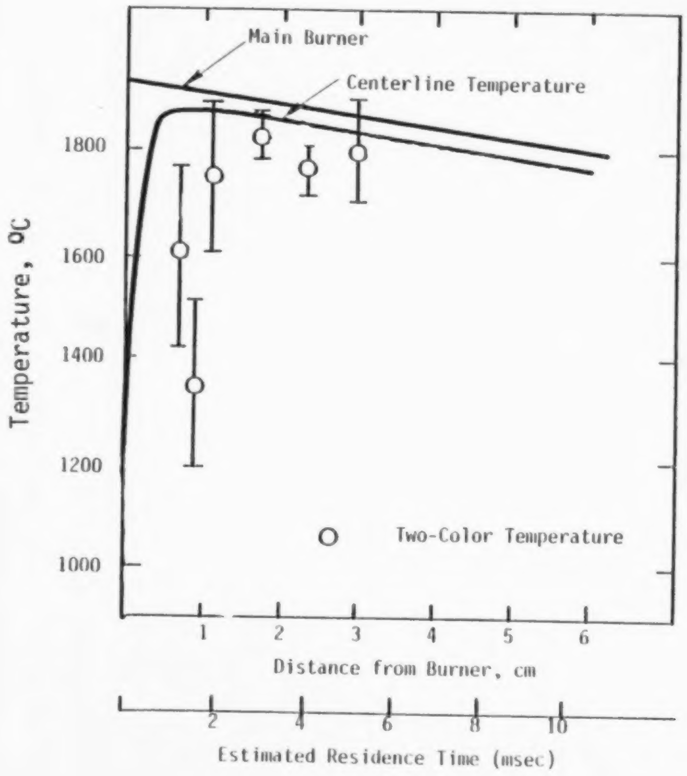

Figure 4-1. Thermocouple gas temperatures compared with two-color particle temperature measurements for Vicron 45-3 injected into a CH_4-air flame. Peak particle temperature=1830° C.

in the particle temperature measurements is expected because there are visible fluctuations in the particle flow rate near the injection point. These and other data taken at lower gas temperatures indicate that limestone sorbents heat up in a manner similar to inert particles. They heat rapidly (10^5 K/s) to the local gas temperature and effectively follow the local gas temperature. Thus, the reaction temperature can be taken to be the local gas temperature as measured by conventional means.

Prior to this study there was a distinct absence of time-to-calcine data for pulverized sorbents for temperatures and gas-phase compositions similar to those found in the radiant zone of pulverized-coal-fired furnaces. Much of the previous data was collected at lower temperatures and/or with larger particle sizes in inert (typically N_2 or air) atmospheres. In order to investigate the times to calcine under conditions representative of those in furnaces, Vicron 45-3 limestone was injected into a series of hydrocarbon and hydrogen flames. Solid samples were then collected at various distances (residence times) and analyzed for degree of calcination by techniques discussed in Section 3.2.3. Figure 4-2 shows the calcination of Vicron 45-3 at various residence times in four methane-air flames. The rate of calcination increases with increasing peak temperatures, and the curves approach asymptotic values somewhat below 100 percent calcination. Nonetheless, significant extent of calcination is attained in times less than 100 ms at all temperatures representative of commercial furnaces.

Because calcination involves the release of carbon dioxide from the sorbent, several tests were run for which the post-flame concentrations of CO_2 were varied. Figure 4-3 contains limestone calcination data for flames where N_2, O_2, and CO_2 were added in such a way as to change the burnt-gas composition while maintaining a constant time/temperature profile. The data indicate that doubling the CO_2 content had negligible effect on the ultimate level of calcination. However, the highest degree of calcination occurred in the flame with N_2 dilution which had the lowest concentration of CO_2. An additional set of experiments was run over a broad range of temperatures comparing calcination data from hydrogen-air flames--which contain no CO_2--with methane flame data. The data (Figure 4-4) indicate that the extent of

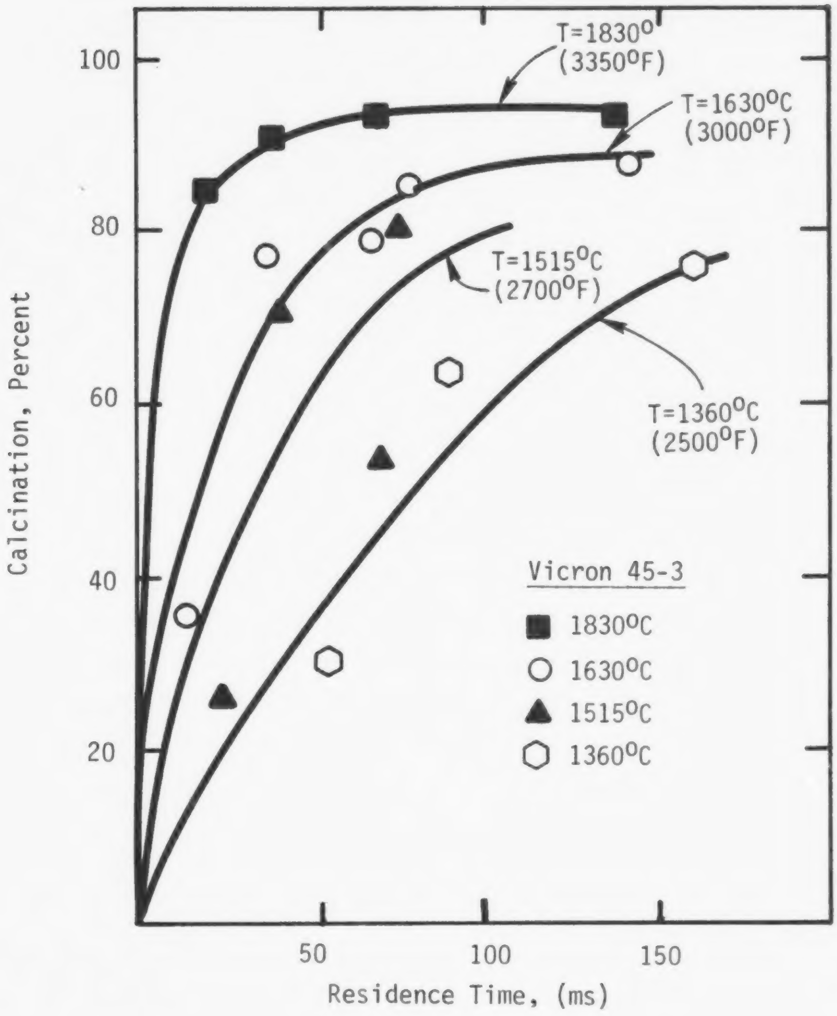

Figure 4-2. Calcination dependency on residence time for Vicron 45-3 injected into four methane-air flames.

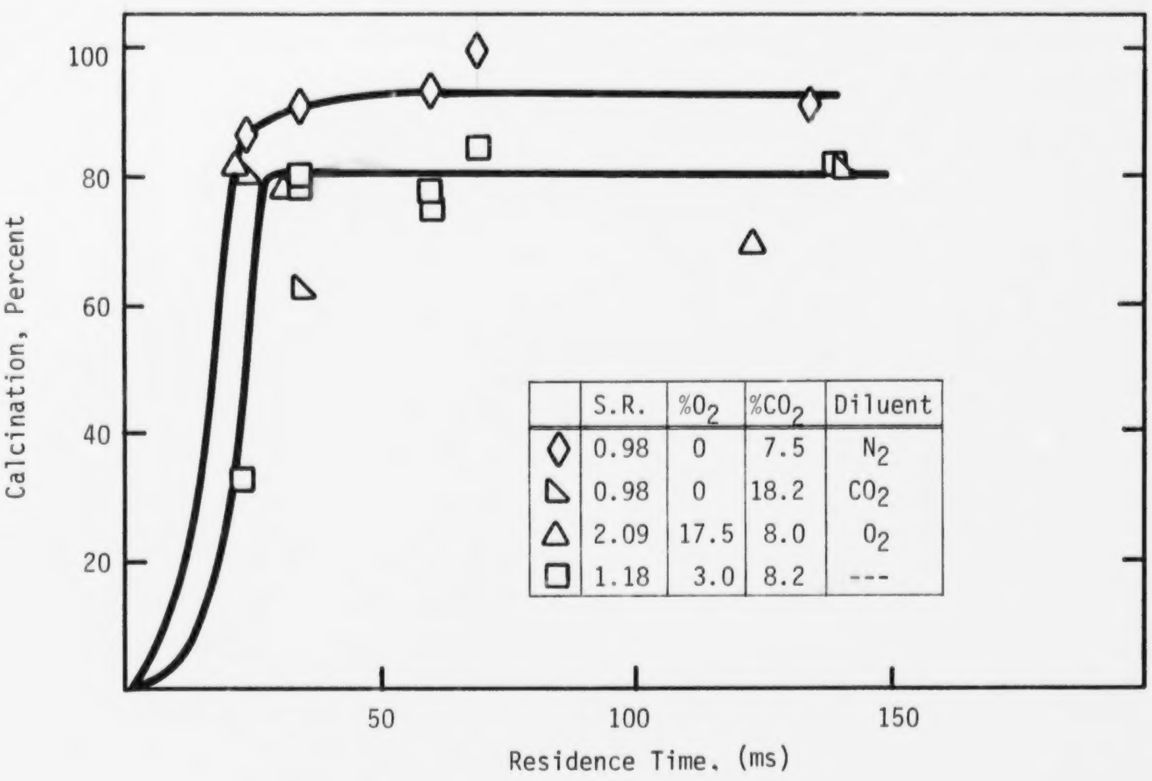

Figure 4-3. Effect of gas composition on the extent of calcination of Vicron 45-3. T_{max} = 1630°C.

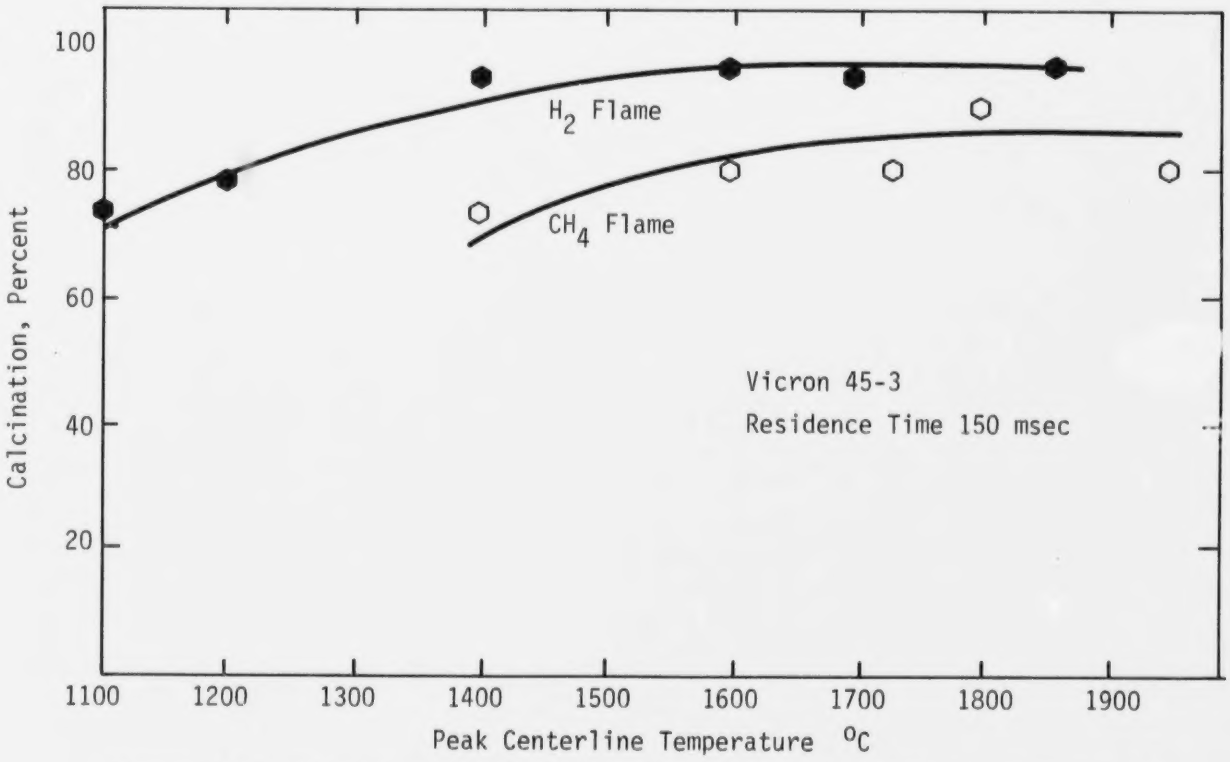

Figure 4-4. Comparison of the degree of calcination of Vicron 45-3 samples injected into H_2 and CH_4 flames.

calcination is higher when CO_2 is absent and that nearly 100 percent calcination can be achieved under this condition.

While studies have previously been performed on calcination, none of the earlier work has examined the temperature range of interest to utility boiler operation. The present data, however, are consistent with those of earlier studies. Figure 4-5 shows an Arrhenius plot of the present data as well as that of Borgwardt et al., (4) and of Greg and Sing (22). The zero order kinetic rate constant recommended by Borgwardt predicts a shorter time than was observed for calcination at furnace temperatures. The reason for this is that at these temperatures the particle heatup time has become a significant portion of the total time required for calcination. Nonetheless, the most significant conclusion from all of these data is that calcination is fast at the temperatures of interest and is not an impediment to the sulfur capture process. Only at temperatures below those typical of furnace exhaust (1150-1350°C) are the times to calcine significant in comparison to the available residence time.

4.1.2 Sorbent Activation

Several sorbent properties are believed to have a significant influence on reactivity toward sulfur capture (23). Properties which result from, and are affected by calcination include pore size, total porosity, total specific surface area, and degree of crystallinity. Also important is the initial sorbent particle size which is chosen at the outset. Pore size, porosity, and crystallinity after calcination appear to be functions of the particular rock under study (23). These properties, however, manifest themselves in the total specific surface area, which is a readily measurable parameter. It is important, therefore, to understand how the surface area of a calcined sorbent is affected by the calcination environment.

Surface area samples were collected at various residence times for Vicron 45-3 injected into four methane-air flames identical to those represented in Figure 4-2. The data are shown in Figure 4-6 as specific surface area versus residence time. The surface areas measured here (5-10

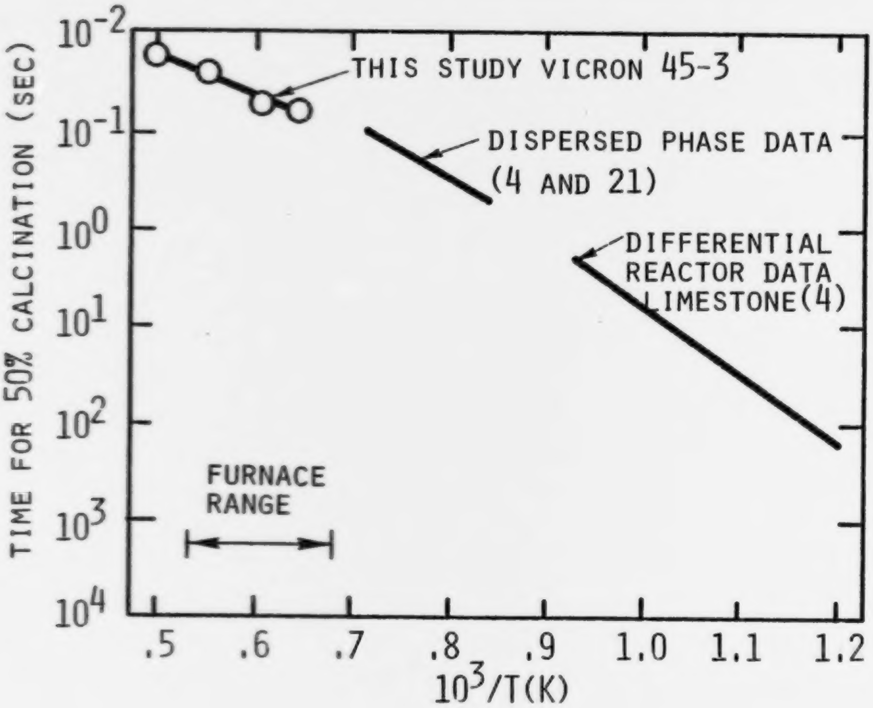

Figure 4-5. Comparison of present study with other data for calcination of Vicron 45-3 and similar limestone.

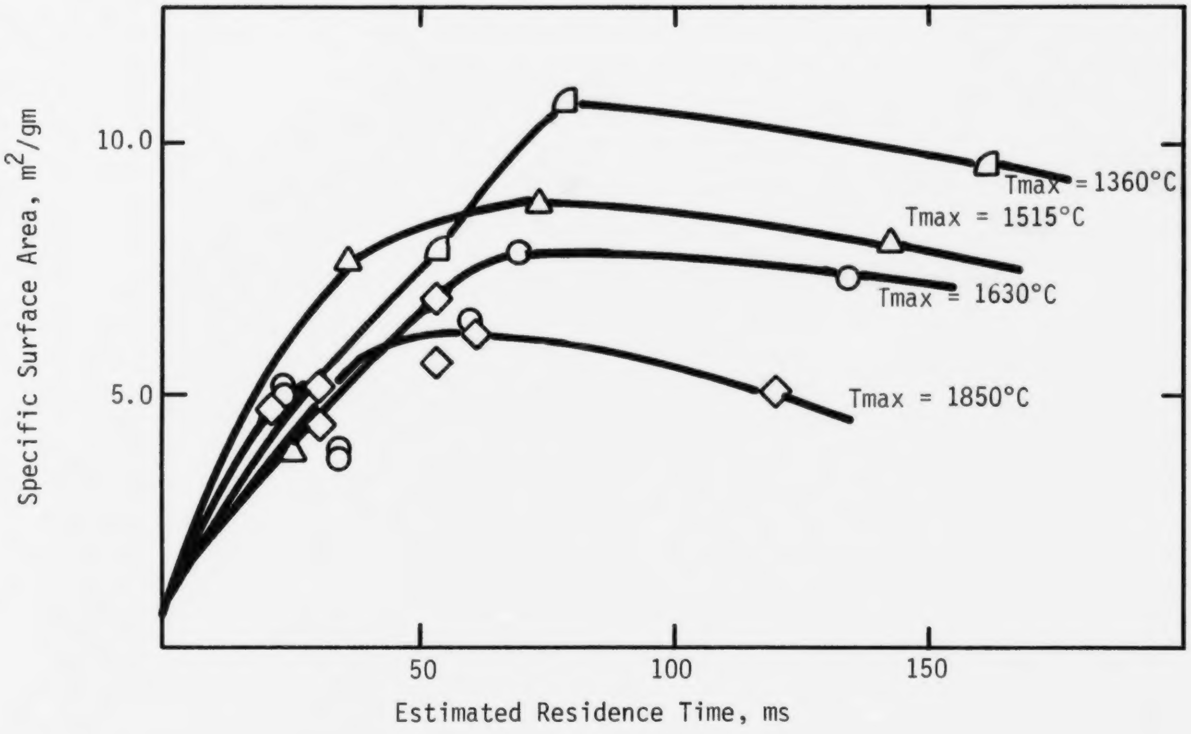

Figure 4-6. Specific surface area for Vicron 45-3 injected into CH_4-Air flames.

m^2/g) are low relative to those reported for similar stones in lower temperature work (5) and suggest that the calcine is not very reactive.

Two points are apparent from Figure 4-6. First, surface area develops rapidly and generally rises faster in higher temperature flames. Secondly, the ultimate surface area attained is higher in the lower temperature flames. These are very important observations since they suggest that there is a tradeoff between increasing surface area, requiring lower temperatures, and sintering which is enhanced by higher temperatures. Also, these data demonstrate that calcination and sintering are parallel processes since the surface areas do not rise to maxima and suddenly fall off. Rather, the competing processes are roughly in balance so that an ultimate surface area is reached which may or may not decline slowly, depending on the post-flame temperature.

Previous trends in surface areas for calcination at lower temperatures are consistent with those of this work. Data were taken from other studies which employed limestones similar in initial size, chemical composition, and crystal structure to Vicron 45-3. These are shown in Figure 4-7 along with the present results. As the temperature of calcination decreases in Figure 4-7, the time to attain the maximum surface area increases from tens of milliseconds at the right side of the plot to several minutes at the left side. This suggests a limitation to the process, namely, that the very high surface areas observed in some laboratory studies may not be attainable in the high-temperature environment found in conventional pulverized-coal-fired utility boilers.

The effect of flame gas composition on surface area development is indicated in Figure 4-8. The flames correspond to those indicated in Figure 4-3. Large variations in the CO_2 and O_2 concentrations have no significant effect on surface area development at these conditions. In addition, although the hydrogen-flame-calcined samples showed a higher level of calcination, it is not reflected in the surface areas attained.

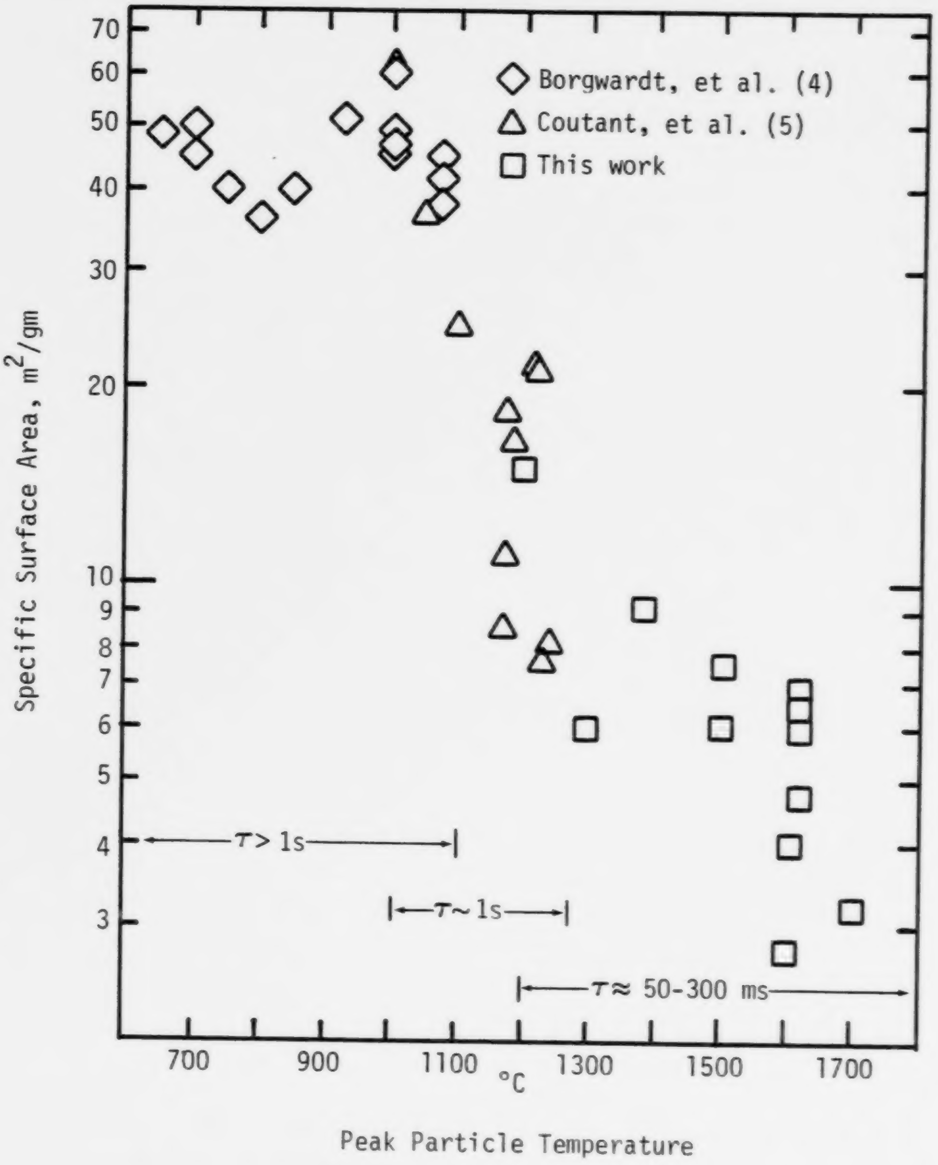

Figure 4-7. Ultimate specific surface area versus peak particle temperature during calcination. Data are taken from differential reactor studies (Borgwardt) and dispersed phase reactor studies (Borgwardt, Coutant, and this work). Present data for Vicron 45-3. Other data for similar calcitic limestones.

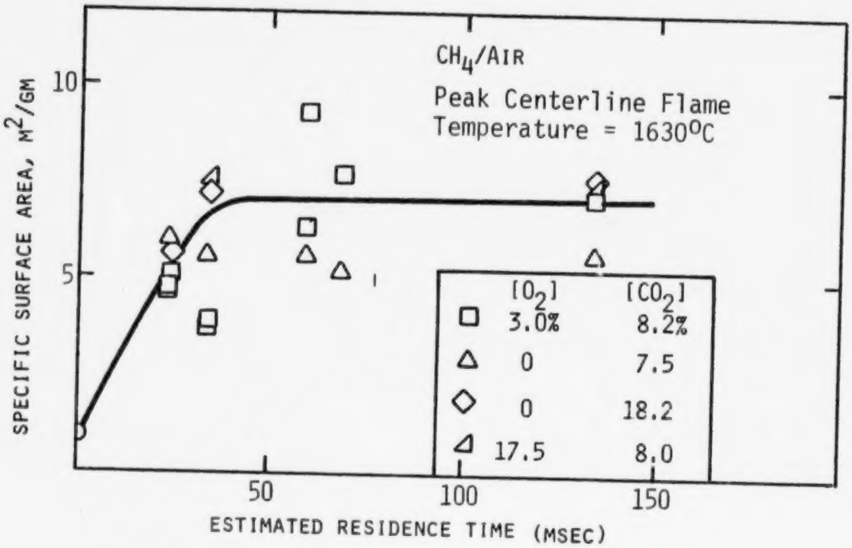

Figure 4-8. Effect of gas-phase composition on the specific surface area development of Vicron 45-3 in methane-air flames. $T_{max} = 1630^{\circ}C$.

In general, a correspondence was observed between extent of calcination and surface area development. Both, in turn, were found to be affected by the peak particle temperature. The relationship between surface area and extent of calcination as a function of peak temperature is shown in Figure 4-9. Although there is considerable scatter in the data, the curves show that if calcination is allowed to proceed far enough, the particles will begin to deadburn and lose surface area, even before calcination is complete. Figure 4-9 also indicates that maximum surface area is reached at about 70 percent calcination for these temperatures. However, the optimum level of calcination may increase at temperatures lower than studied here.

Surface area development at lower temperatures has been shown to occur mainly as a result of an increase in porosity during calcination (23). The furnace temperature data presented here suggest that some porosity is lost, however, as a result of sintering and that this loss increases with temperature. For uncalcined Vicron 45-3 it can be shown that the total specific surface area is due almost entirely to the external surface area of the ten percent of the sorbent mass at the small end of the size cut. These particles have diameters between 0.1 m and 2.0 m. The fraction of the sorbent in this range has a specific surface area of approximately 4-6 m^2/g. If high-temperature surface area development were to occur as a result of particle fragmentation down to this size range then high sorbent reactivities might be attained simply by grinding the limestone to a finer size.

In order to test this hypothesis three samples of Vicron 45-3 were collected in the TDR. The first sample was collected without a flame in order to check that no size discrimination was occurring in the sorbent delivery and sampling system. The other two samples were collected at long residence times (>150 ms) from methane flames providing peak particle temperatures of 1360°C and 1830°C. All three sorbent size distributions, as determined by X-ray sedimentation, are shown in Figure 4-10. It is clear from the figure that fragmentation does occur and that it increases with increasing temperature. Surface areas calculated from the fragmented sample size distributions are 0.65 m^2/g and 0.91 m^2/g respectively. These are insufficient to account for the measured surface areas of the samples. As a

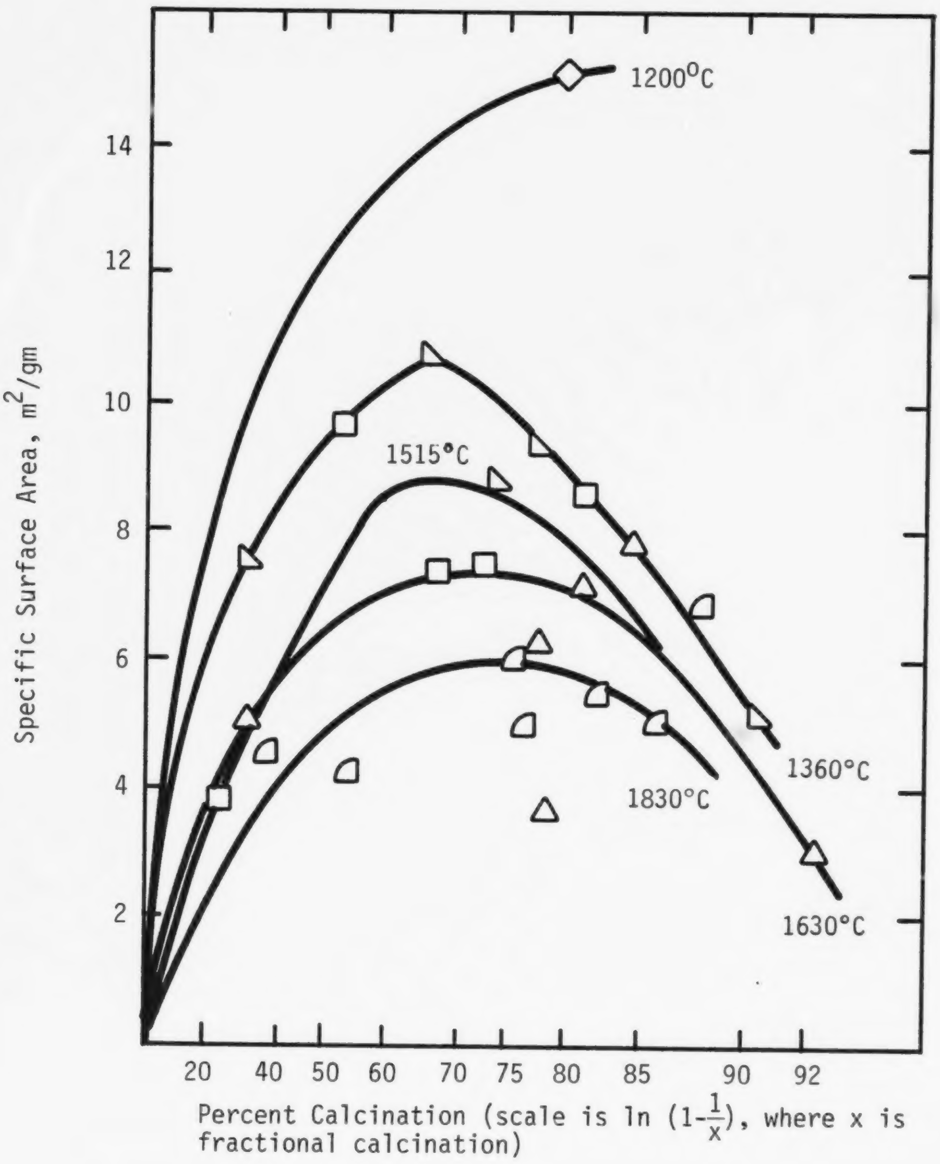

Figure 4-9. Vicron 45-3 surface area vs. extent of calcination.

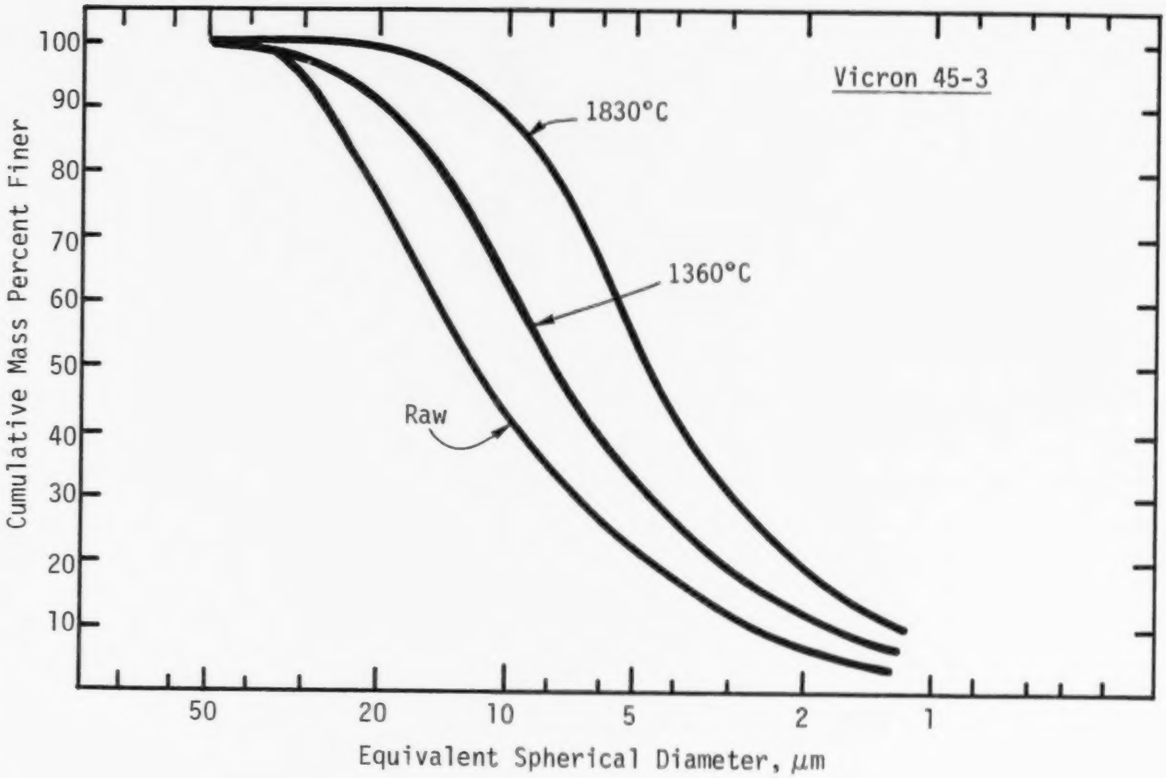

Figure 4-10. Effect of peak calcination temperature on the ultimate particle size distribution of Vicron 45-3 injected into methane-air flames.

result, it appears that particle fragmentation alone cannot account for sorbent activation at furnace temperatures.

The structural changes which occur as limestone is calcined at different temperatures are dramatic when viewed by scanning electron microscopy (SEM). Table 4-1 refers to the photographs shown in Figures 4-11A through 4-11F. Because of the small sample area taken in with the scanning electron microscope the micrographs shown do not necessarily represent the true particle size distribution.

Figures 4-11A and B are 2000x and 200x magnifications of a raw Vicron sample. Even the smallest resolvable particles in Figure 4-11A have straight edges, planar surfaces, and flat or pointed ends. In contrast with this is the sample shown in Figures 4-11C and D. This is a Vicron sample taken from a methane flame where the peak particle temperature was 1360°C. At both magnifications it is evident that all of the very large particles have fragmented. This is important because fragmentation has been shown to be a significant factor in reactivity toward SO_2 (5). Furthermore, there is a significant increase in the fraction of particles with $d < 1\,\mu m$. (The web-like material most visible in Figure 4-11C is a cellulose triacetate filter medium). Equally important is that, except for some of the largest particles, the sample shows no evidence of crystallinity. The smallest particles are nearly spherical and many appear to be "grape-like" clusters of these. Even the largest visible particles have slightly rounded edges.

Figures 4-11E and F are SEMs of Vicron 45-3 which have been calcined in 1630°C and 1850°C methane flames. The sample shown in Figure 4-11E shows roughly the same size distribution as Figure 4-11C although the smallest of particles now appear to be absent. In addition, many of what appeared to be clusters now seem to have fused or sintered together giving rise to a scalloped appearance. The particle at far left center seems to have several small spheres melting into it.

In Figure 4-11F particles larger than $10\,\mu m$ are again evident. These particles have flat surfaces and seem to have developed a crystal structure

TABLE 4-1. SEM EXAMINATION OF VICRON 45-3 SUBJECTED TO DIFFERENT TEMPERATURES

Peak Gas Temperature ^{o}C (^{o}F)	Figure	Fragmentation	Size Range (μm)	Visual Mean Size (μm)	Reference
Raw	4-11A,B	--	0.5-40	5	Crystalline particles with crevices and fissures
1360 (2500)	4-11C,D	Severe	0.1-10	2	Mixed crystalline and amorphous particles
1630 (3000)	4-11 E	Severe	1-8	2.5	Narrow size distribution some fused crystals
1850 (3350)	4-11 F	Severe	1-15	5	Larger particles than at lower temperature. Fused solid cores with crystal filaments

Vicron 45-3, Raw

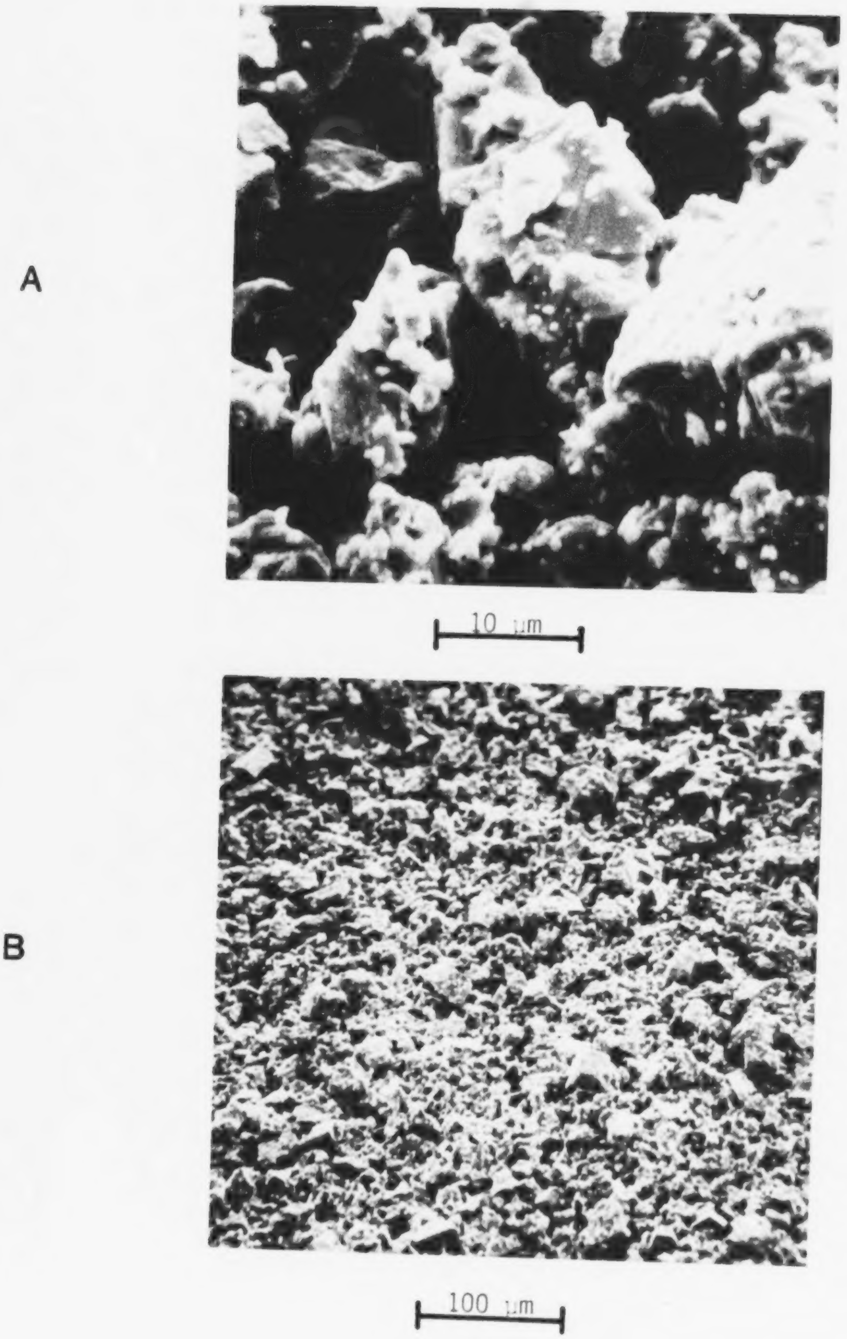

Figure 4-11. (A & B) SEM examination of raw Vicron 45-3.

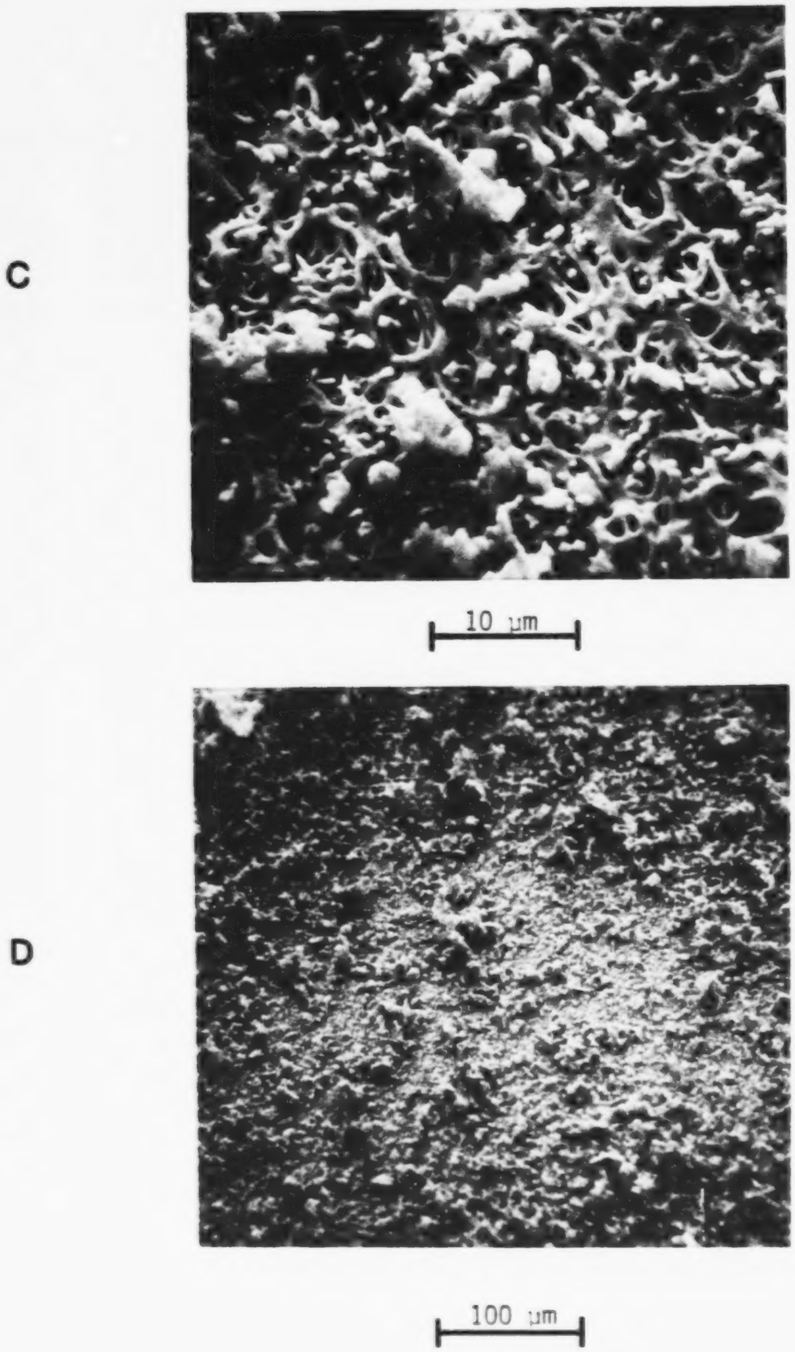

Vicron 45-3

Figure 4-11. (C & D) SEM examination of Vicron 45-3 calcined at T_{max} = 1360°C.

Vicron 45-3

E
Tmax = 1630°C

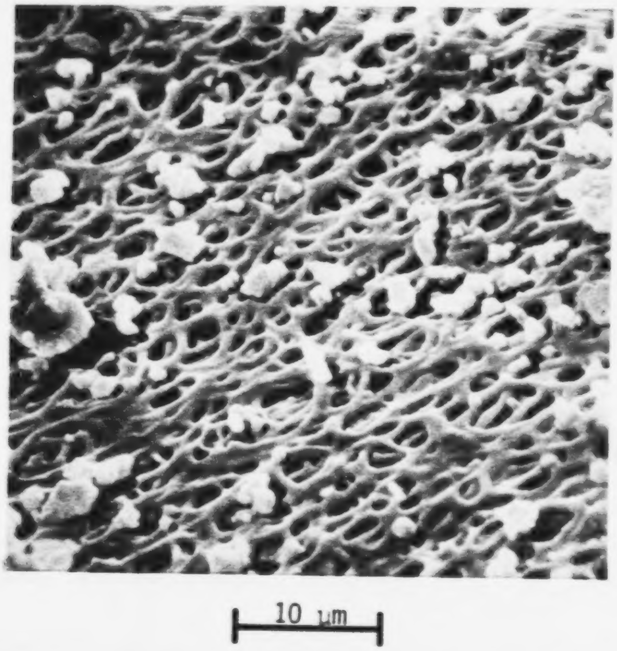

F
Tmax = 1830°C

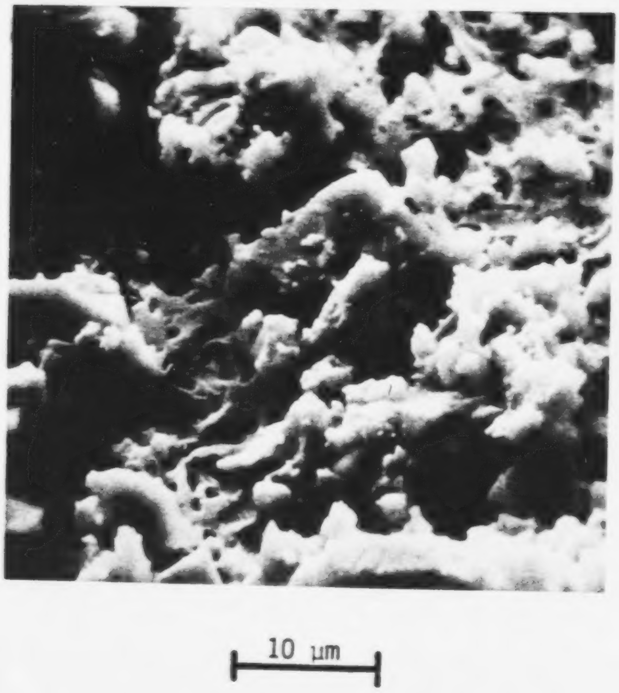

Figure 4-11. (E & F) SEM examination of Vicron 45-3 calcined at E - T_{max}=1630°C, F - T_{max} = 1830°C.

which is different than that of the raw sorbent. In addition, the larger particles are covered with small, short, whisker-like particles. This suggests that when subjected to extremely high temperatures, even for very short times, pulverized limestones calcine quickly enough and sinter efficiently to establish a stable calcium oxide crystal structure.

Among the conclusions drawn from the SEM study are:

1. Particle fragmentation is evident, even at the lowest temperature studied.

2. The surface morphology is altered by calcination and possibly by sintering.

3. At higher temperatures (e.g., T> 1630°C) the sorbent particles exhibit sintering and recrystallization, as well as some evidence of agglomeration.

If limestone activation is related to surface area it will benefit from lower calcination temperatures and longer calcination times. Since high surface areas were not observed in this study, it follows that the temperatures were too high for highly reactive sorbents to be produced.

4.1.3 Sorbent Reactivity to Sulfation

Experiments were done to determine the effect of peak particle temperature on both rich- and lean-flame sulfur capture. In these experiments a flame was established at SR = 1.0 with air and a mixture of 6.15 percent-H_2S in CH_4 (Matheson, specially prepared mixture). Flame stoichiometry and temperature were varied, keeping a constant 3750 ppm total sulfur, by replacing air with either N_2 or O_2. Using an adaptation of ASTM D2420-66, a lead acetate test for H_2S, the presence of H_2S in the rich flames and its absence in the lean and stoichiometric flames were confirmed. The actual levels of H_2S, however, were not determined. Vicron 45-3 was injected and collected at a residence time of 150 ms. The results of analysis for CaS and $CaSO_4$ are shown in Figure 4-12. An increase in temperature corresponds with the stoichiometric ratio approaching 1.0 under both rich and lean conditions. The calcium utilization increased precipitously as the peak flame temperature was lowered. In the lowest temperature flames, 15 percent of the calcium was sulfated in only 150 ms. The data indicate similar effectiveness of sulfur capture under rich and lean conditions.

Subsequent sulfur sorption tests were performed with the dispersed-phase, constant-temperature-reaction-zone probe discussed in Section 3. The results of scoping runs with this probe are shown in Figure 4-13. These initial measurements were undertaken to identify the important variables that should subsequently be investigated and to define the conditions under which the probe should be operated. These data demonstrate the trends that might be expected, especially the increase in reactivity with higher surface area. During the scoping runs, however, percent SO_2 and residence time in the probe were changed from 200-800 msec for the constant flame temperature of 1200°C. Numerical data are provided in the appendices. The conclusion of these tests was that residence time had a significant effect on calcium utilization (demonstrated by the 35 percent spread in sulfur capture at 1200°C) although the sorption reaction appears to be zero order in SO_2 at these concentrations. Conditions for further tests were selected as 600 ms residence time, 6 percent SO_2 and a nominal (mid-point) reaction zone temperature of 1100°C (2000°F). This choice of conditions was arbitrary, but, it was in a range where reasonable levels of sulfur capture could be obtained.

Test results for Vicron 45-3 under the new conditions in the reactivity probe are shown in Figure 4-14. Although the utilization efficiency does increase somewhat with decreasing calcination temperature, the effect is not as dramatic as the difference in surface areas might suggest. The scatter in the low-temperature data occurs because the ability of the sorbent to calcine effectively is more sensitive to spurious pulses in the sorbent feed rate at these conditions. The higher utilization values are considered more reliable because those samples showed extents of calcination more representative of previous data for samples collected under identical conditions.

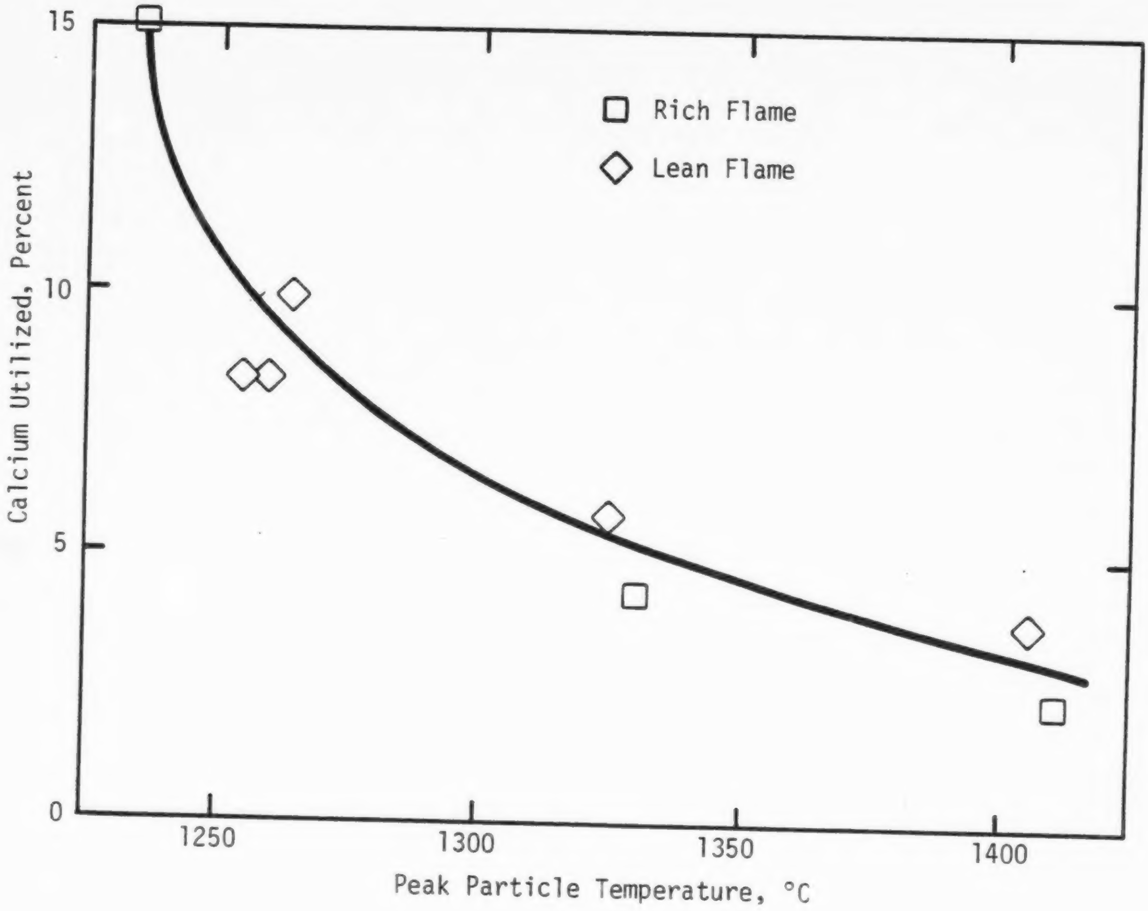

Figure 4-12. The effect of temperature on both rich and lean flame sulfur capture (residence time 150 ms).

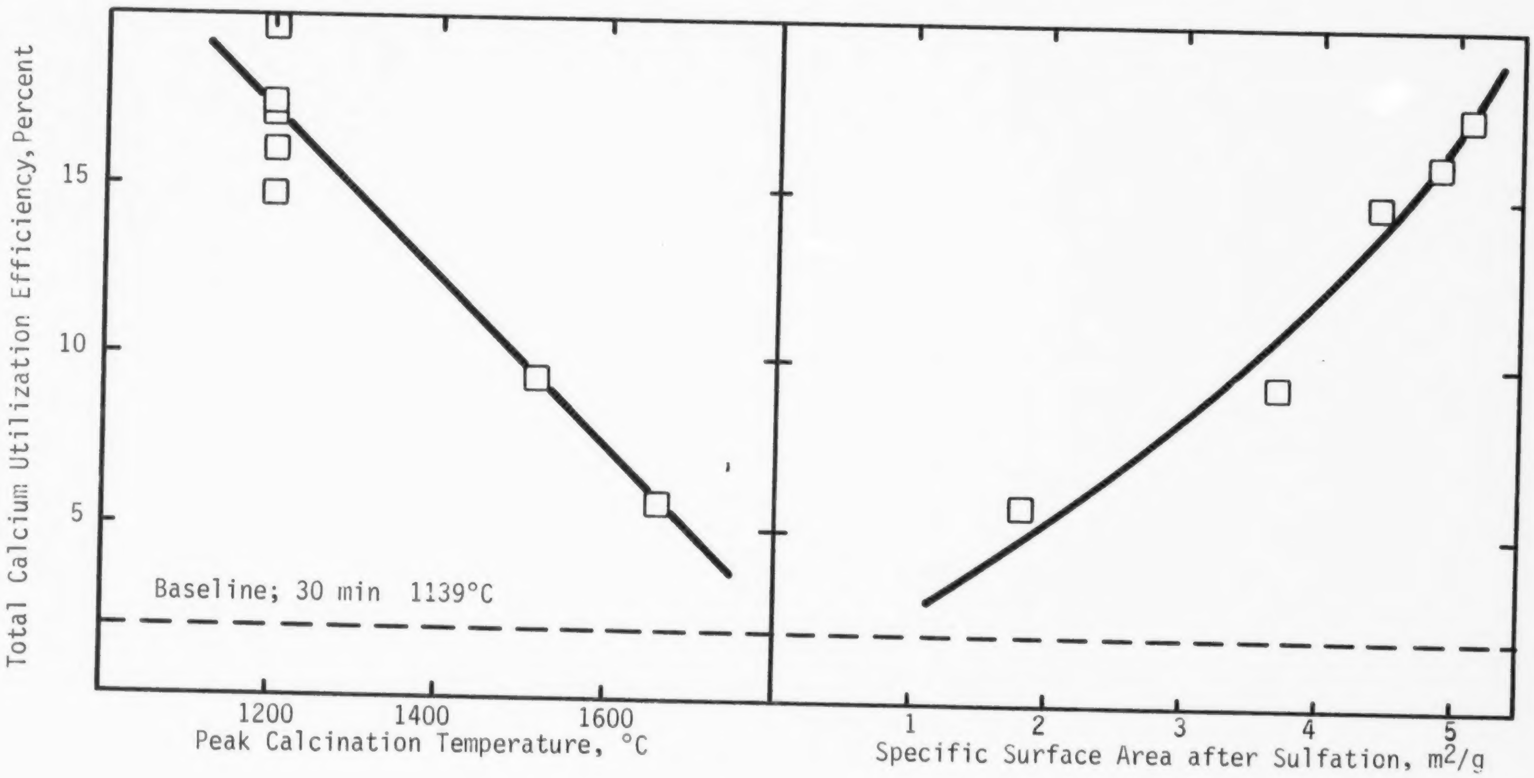

Figure 4-13. Results of scoping tests in the dispersed-phase SO_2 reactivity probe. In spite of variations in time, temperature and SO_2 concentration, calcium utilization correlates strongly with specific surface area.

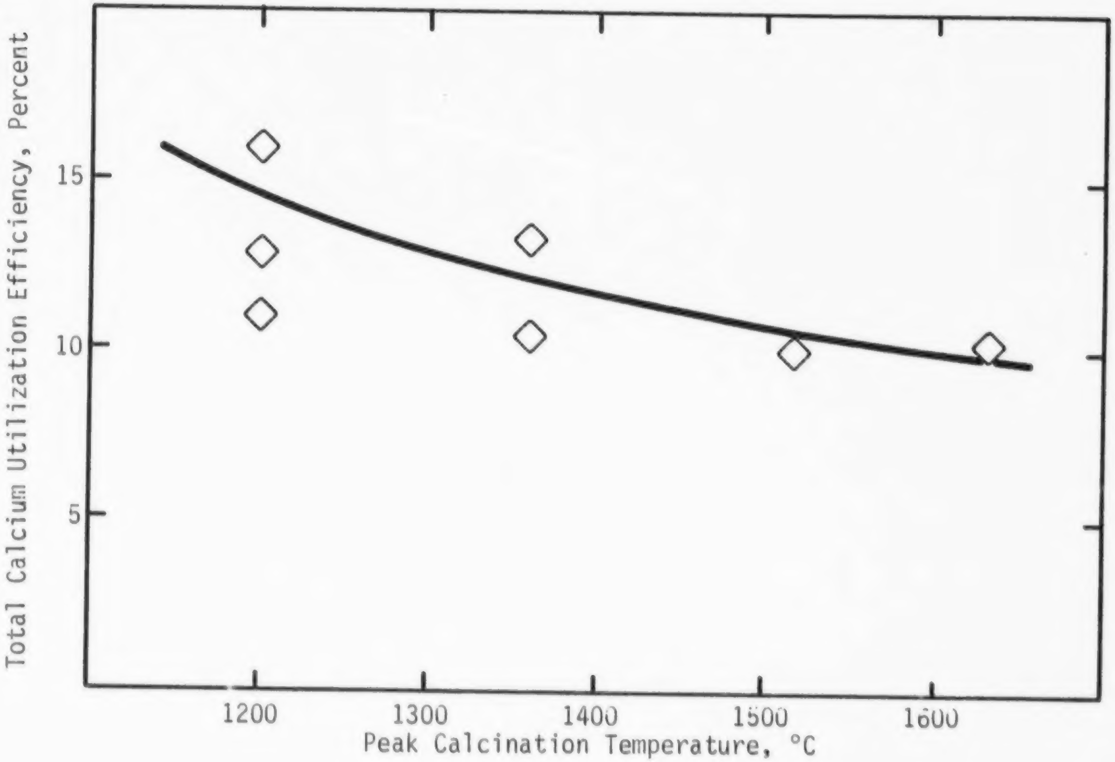

Figure 4-14. Calcium utilization efficiency of Vicron 45-3. Residence time 600 ms; nominal reaction zone temperature, 1100°C; 6% SO_2 by volume.

4.1.4 Sorbent Regeneration

As shown in the previous section, sulfur capture by limestone under fuel-rich conditions does occur with effectiveness similar to fuel-lean capture. One potential limitation, however, is the extent to which the product, calcium sulfide, might be oxidized to CaO and SO_2 in the subsequent fuel-lean region of an actual staged combustion boiler furnace. In order to test for this, a powdered calcium sulfide, similar in size to Vicron 45-3, was injected into four fuel-lean methane-air flames. Insufficient data were collected for a detailed analysis of the kinetics of the oxidation reaction but the data shown in Figure 4-15 demonstrate the rapid regeneration of the majority of the sulfide at furnace temperatures. This level of sulfide regeneration is such a short time (<100 ms) may render the fuel-rich capture process unacceptable. However, it is noteworthy that even at furnace temperatures, 20 percent of the calcium is still present as the sulfide.

The overall process of sorbent activation, sulfur capture, and possible regeneration, as it is presently understood, is summarized as follows:

- The sorbent is rapidly heated to local gas temperature.
- Parallel processes of calcination and sintering determine the ultimate specific surface area.
- Gas-phase sulfur species diffuse to the particle and react to form CaS or $CaSO_4$.
- Regeneration of CaS to CaO occurs in the fuel-lean burnout region.

4.2 Alternate Sorbents

The calcitic limestone used as a baseline (Vicron 45-3) was chosen because of its high calcium content, low cost, and the general availability of similar stones. Due to chemical reactivity, local availability, or cost, other limestones may also be of significant interest. Sorbents other than Vicron 45-3 may respond quite differently when injected into high-temperature gases. In addition, their reactivity toward SO_2 sorption may relate to specific surface area in a different way. The sorbents listed in Table 4-2

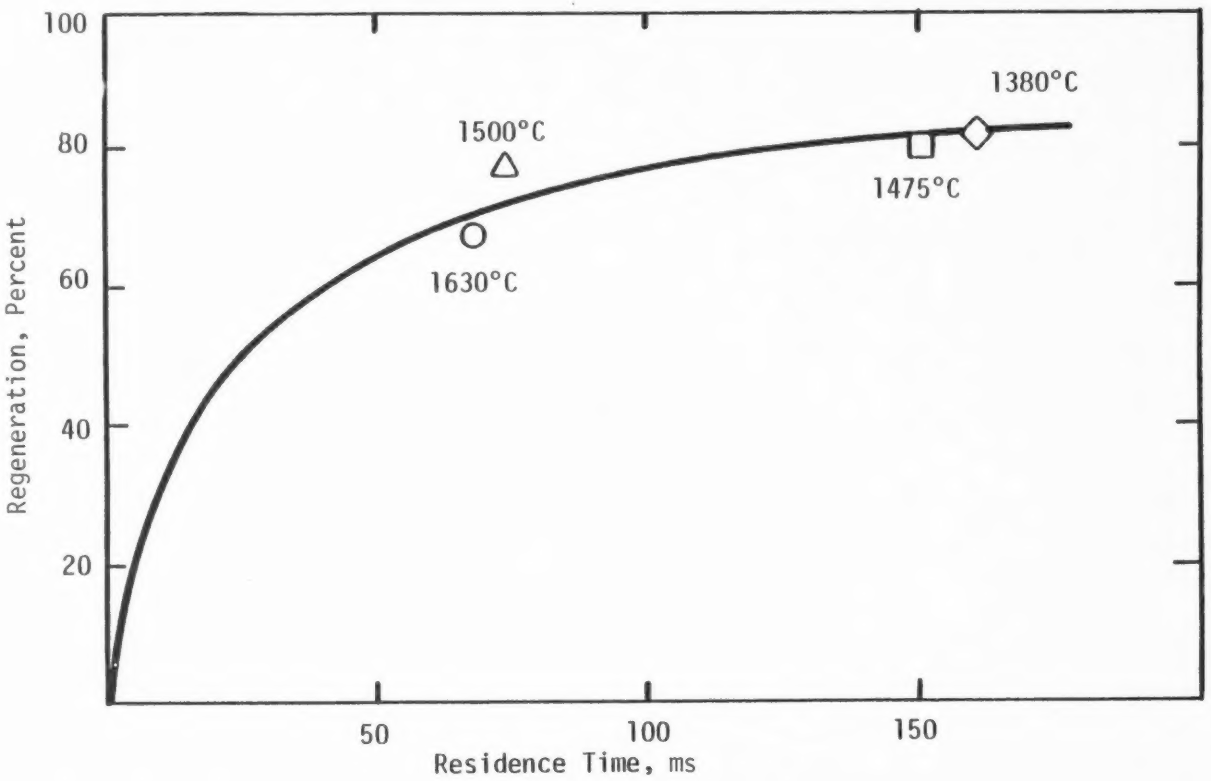

Figure 4-15. Regeneration of CaS with time in the TDR for fuel-lean methane flames.

TABLE 4-2. SORBENT CHARACTERISTICS

Sorbent	Form	Mean Size (μm)	$CaCO_3$ wt.-pct.	$MgCO_3$ wt.-pct.	Surface Area (m^2/gm)
Vicron 45-3	Calcite	11	97	1.6	0.9
Dolomite	Dolomite	34	52.5	42.5	1.6
Michigan Marl	Marl	18	62.5	3.2	2.4
Hydrated Lime	$Ca(OH)_2$	12.5	100[1]	--	14.1
Marblewhite 125	Calcite	31	97	1.7	0.5

[1] $Ca(OH)_2$

were chosen for study here because they have been utilized previously in bench- and pilot-scale studies and are representative of the major classes of limestones. In addition to the very fine Vicron 45-3, another high-purity calcite having a larger particle size, Marblewhite 125, was investigated. Other calcium-based stones; marl, dolomite, and calcium hydroxide, were tested also.

4.2.1 Calcination and Activation of Alternate Sorbents

Figure 4-16 shows the trends in surface area development and calcination for four alternate sorbents in the 1360°C methane-air flame. Also shown is the approximate curve for Vicron 45-3 taken from the previous section. In this flame the residence times were long enough in some cases that a slight decline in specific surface area is apparent for all of the sorbents except dolomite. In addition, the extent of calcination rises rapidly for all sorbents, corresponding to the initial temperature rise time of about 80 ms. After the initial rise the extent of calcination increases only slowly in the relatively cooler downstream gases.

The behavior of the dolomite surface area is likely due to the MgO which is more refractory than CaO and stabilizes the dolomitic lime (CaO·MgO) against sintering (21). Also, dolomite, as well as marl, calcines faster and, in general, displays higher extents of calcination than the other sorbents. For dolomite the reason is that the $MgCO_3$ component decomposes at a much lower temperature than $CaCO_3$ and the reaction is less endothermic. It is believed that the rapid calcination of marl may be due to combustion of the organic component contained in the stone. The organic component is essentially a coal matrix which upon combustion could overheat the particles. Visual observation suggests also that this may be the case as the marl appears to burn in a fashion similar to coal when injected into a flame.

Calcium hydroxide initially has a relatively high surface area (14.1 m^2/g). The mechanism by which it loses surface area during calcination is unknown. It may be due only to sintering of individual particles but could be augmented by other unidentified mechanisms. Marblewhite 125 is

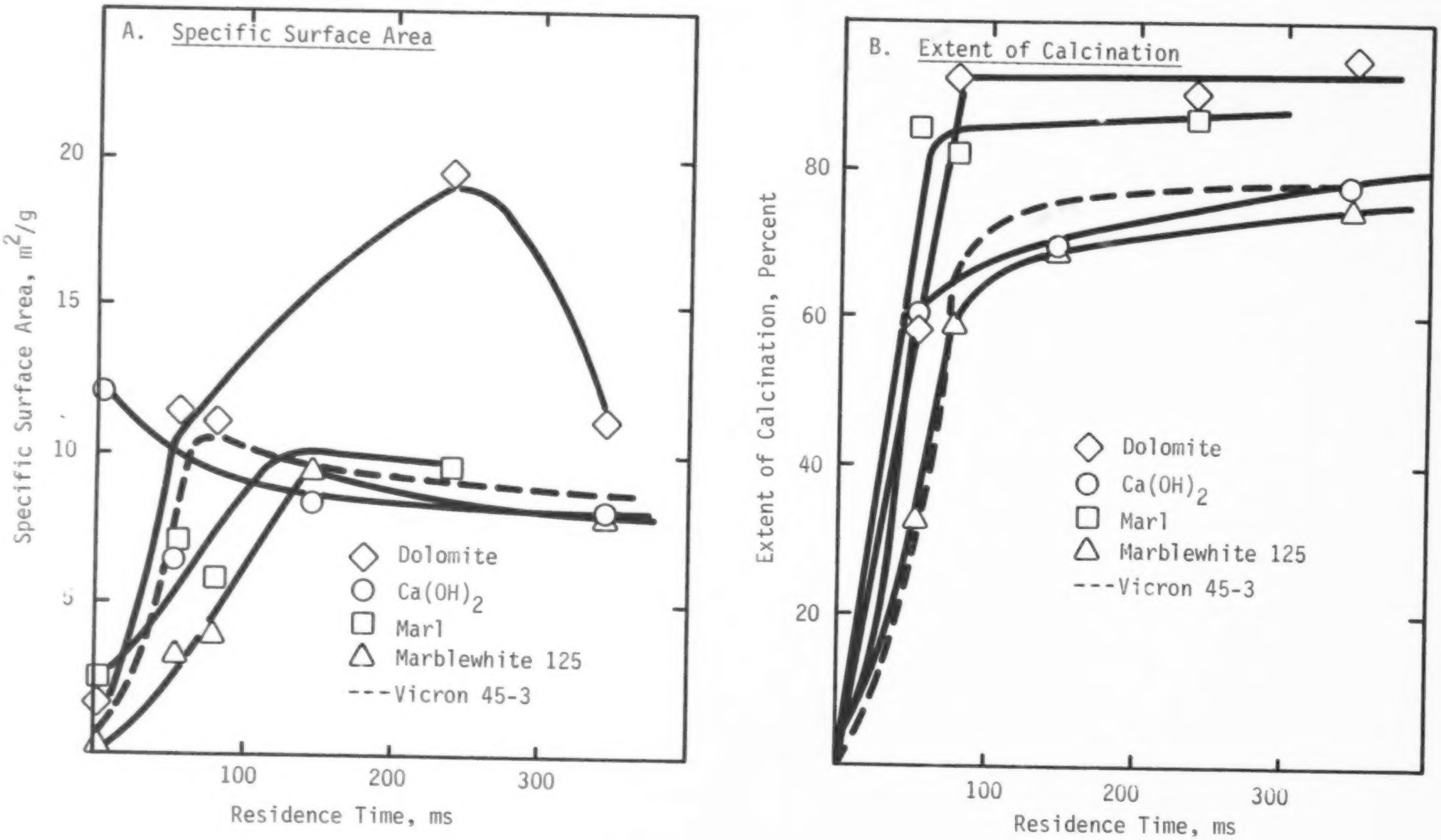

Figure 4-16. A. Specific surface area and B. Extent of calcination of alternate sorbents. Peak calcination temperature 1360°C.

essentially identical to Vicron 45-3 except for the particle size distribution. Both are crushed from the same rock. The response of Marblewhite 125 roughly parallels that of Vicron 45-3. Because of the larger particle size, however, Marblewhite 125 is often difficult to calcine completely. This fact contributed to increased scatter in the data for Marblewhite 125.

In Figures 4-17 and 4-18 additional data are shown for these four sorbents calcined at 1515°C and 1630°C. The Vicron 45-3 curves are shown for comparison. In general these data show the same trends as for the 1360°C case except that the extents of calcination are higher and the ultimate surface areas are lower at higher temperatures. In every case, however, the specific surface area of dolomite monotonically increased with increased residence time.

SEM photographs of sorbents before and after flame injection yielded further information on the processes of calcination and surface area development. One mechanism of surface area growth in limestone appears to be fragmentation. Vicron 45-3 has been found to fragment severely with rapid heating. Similar behavior has been demonstrated for a large number of sorbents in other studies (5, 24, 25). Figures 4-19 A through F show before-and-after SEM photographs of dolomite, Michigan marl, and calcium hydroxide which have been calcined at a peak temperature of approximately 1515°C. The fragmentation of the Vicron is comparable to that of the dolomite, although Vicron both starts out and ends up with smaller particles. Table 4-3 provides a brief summary of the SEM analyses and observations.

Figure 4-19 A and B demonstrate the effect of flame calcination on dolomite. The full range of particle sizes is not shown in Figure 4-19A because many of the larger particles would more than fill the micrograph. This does give an idea, however, of the typical particle size. The micrograph also shows that dolomite has a distinct crystal structure and no evidence of porosity. After calcination (Figure 4-19B) the mean particle size is significantly reduced indicating severe fragmentation. In addition, the calcined particles have acrystalline, globular surfaces (cauliflower-

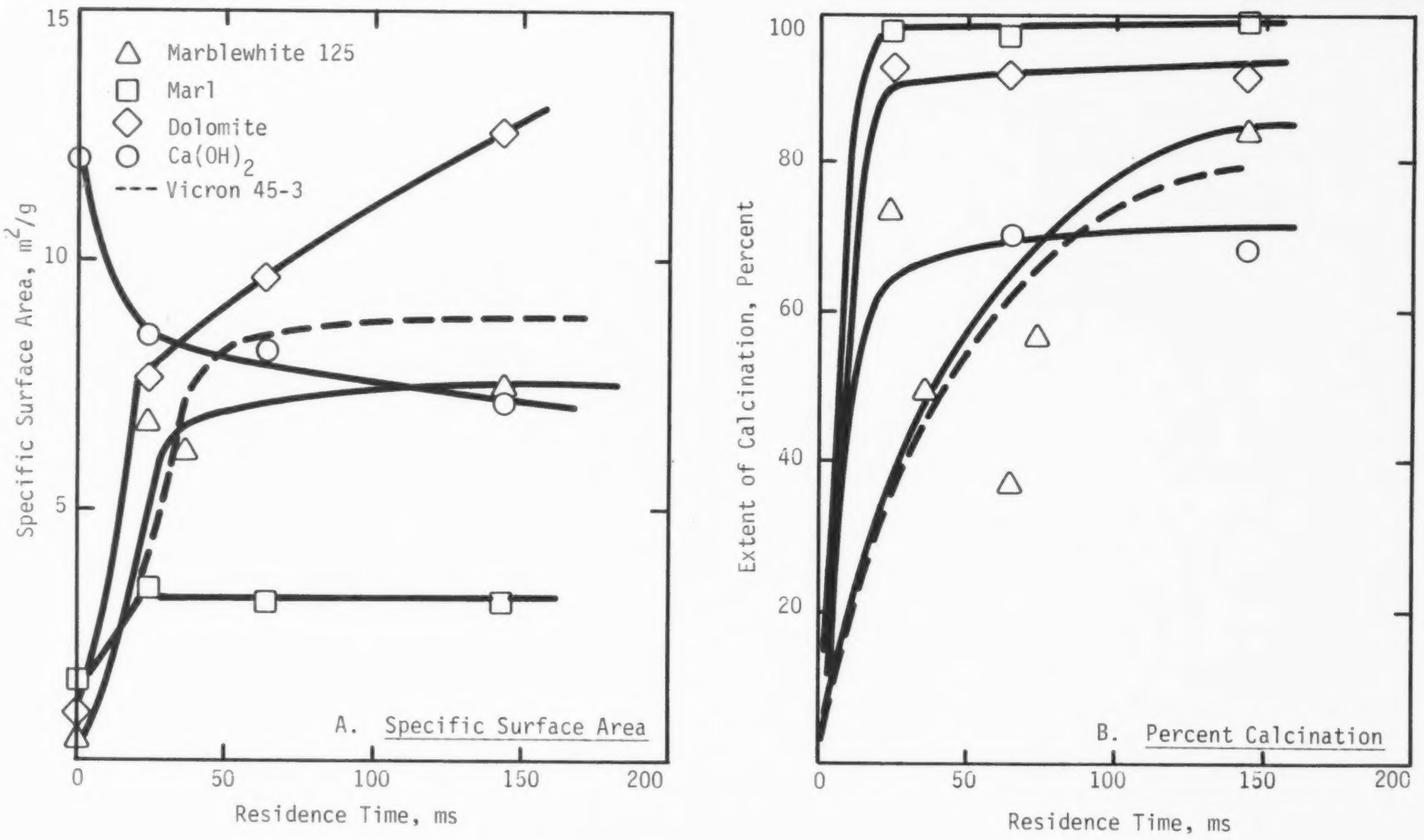

Figure 4-17. A. Specific surface area and B. Percent calcination of alternate sorbents. Peak calcination temperature 1515°C.

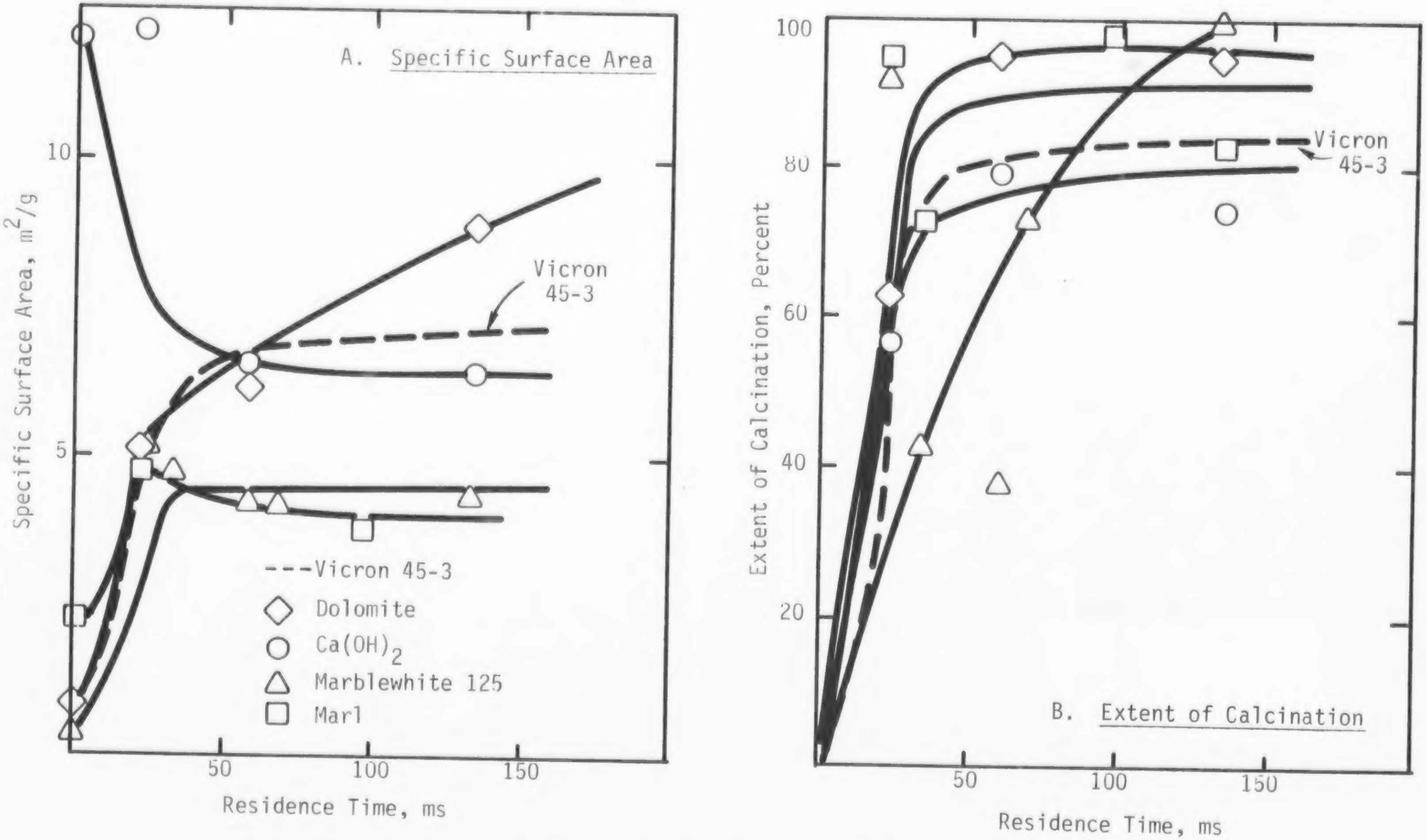

Figure 4-18. A. Specific surface area and B. Extent of calcination of alternate sorbents. Peak calcination temperature = 1630°C.

Dolomite

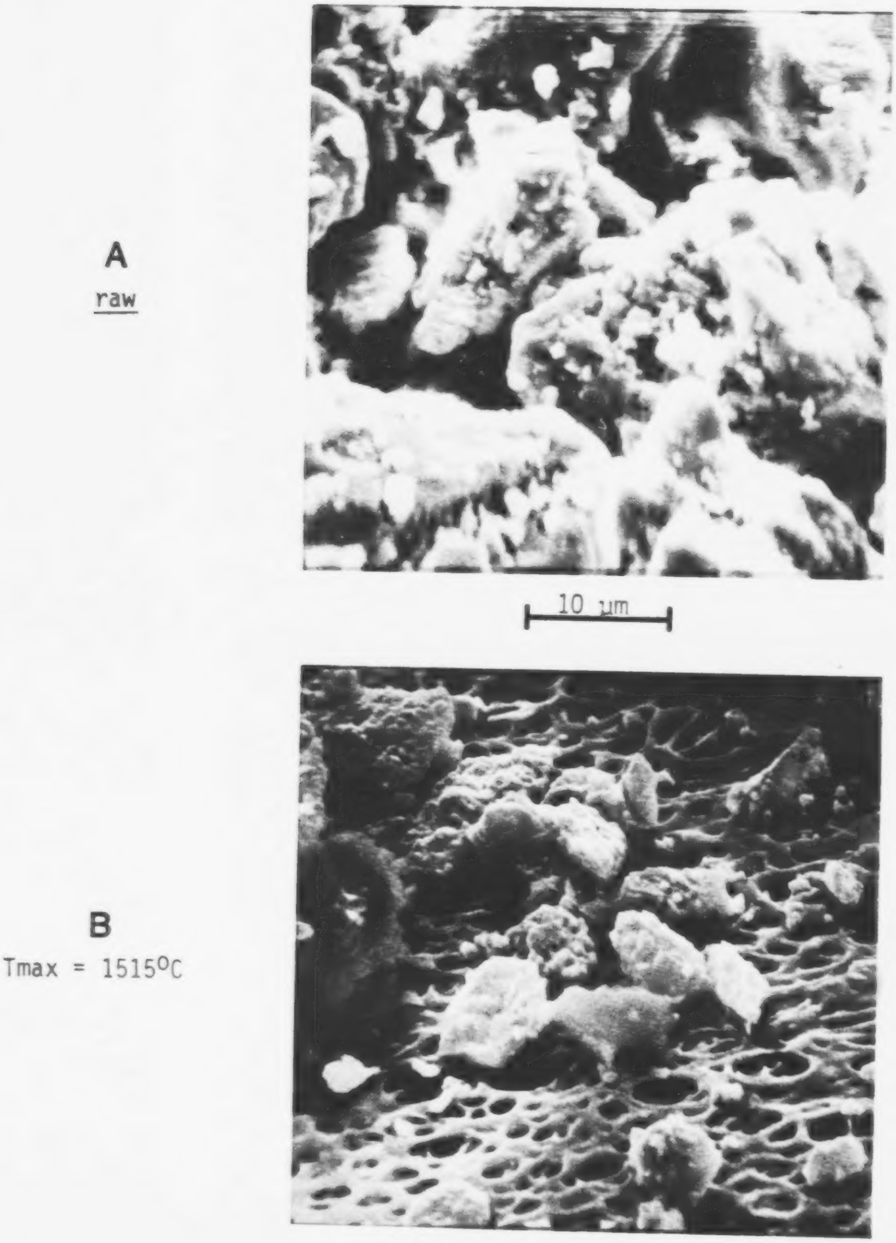

Figure 4-19. (A & B) SEM analysis of dolomite. A - raw; B - calcined in a CH_4-air flame, T_{max} = 1515°C.

Michigan Marl

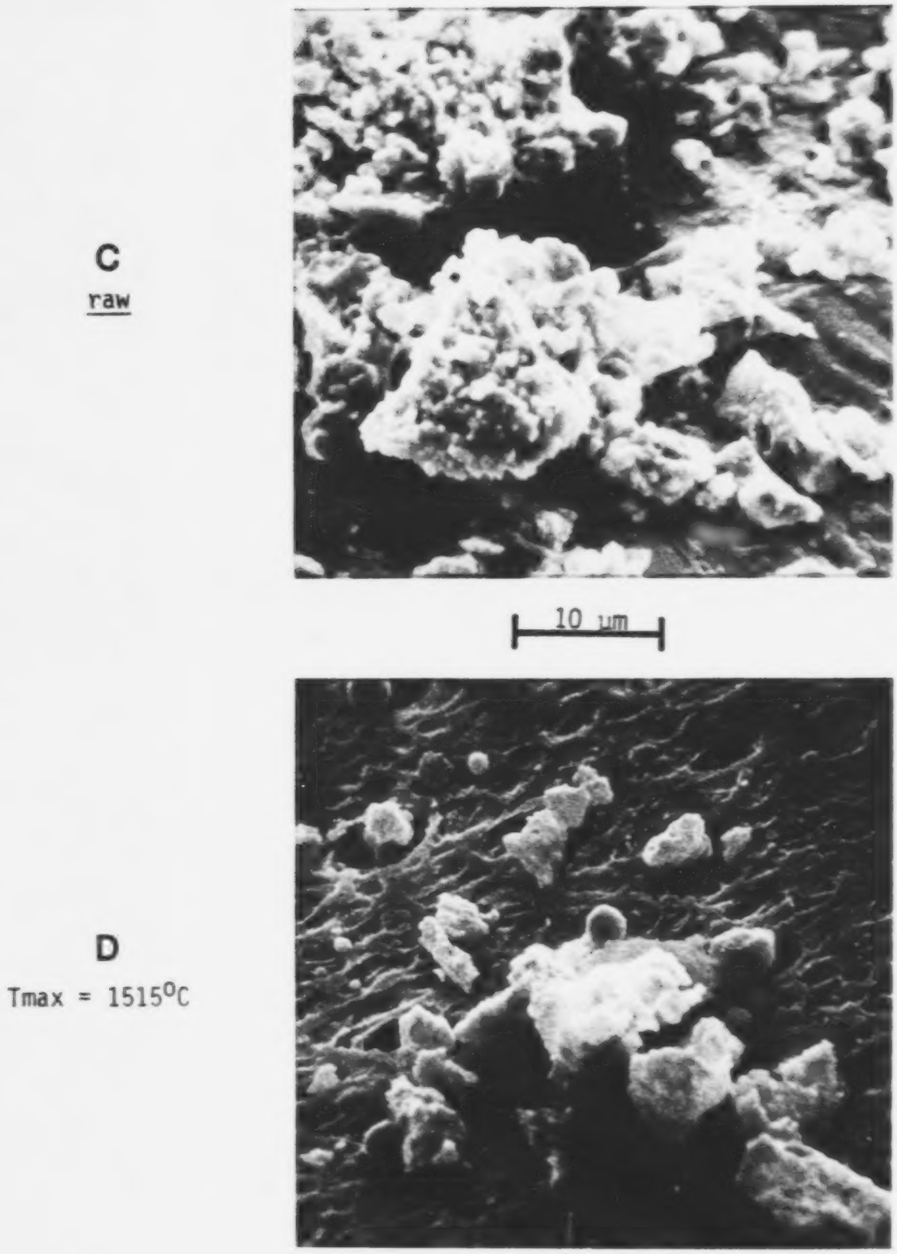

Figure 4-19. (C & D) SEM analysis of Michigan marl. C - raw; D - calcined in a CH_4-air flame, T_{max} = 1515°C.

Calcium Hydroxide

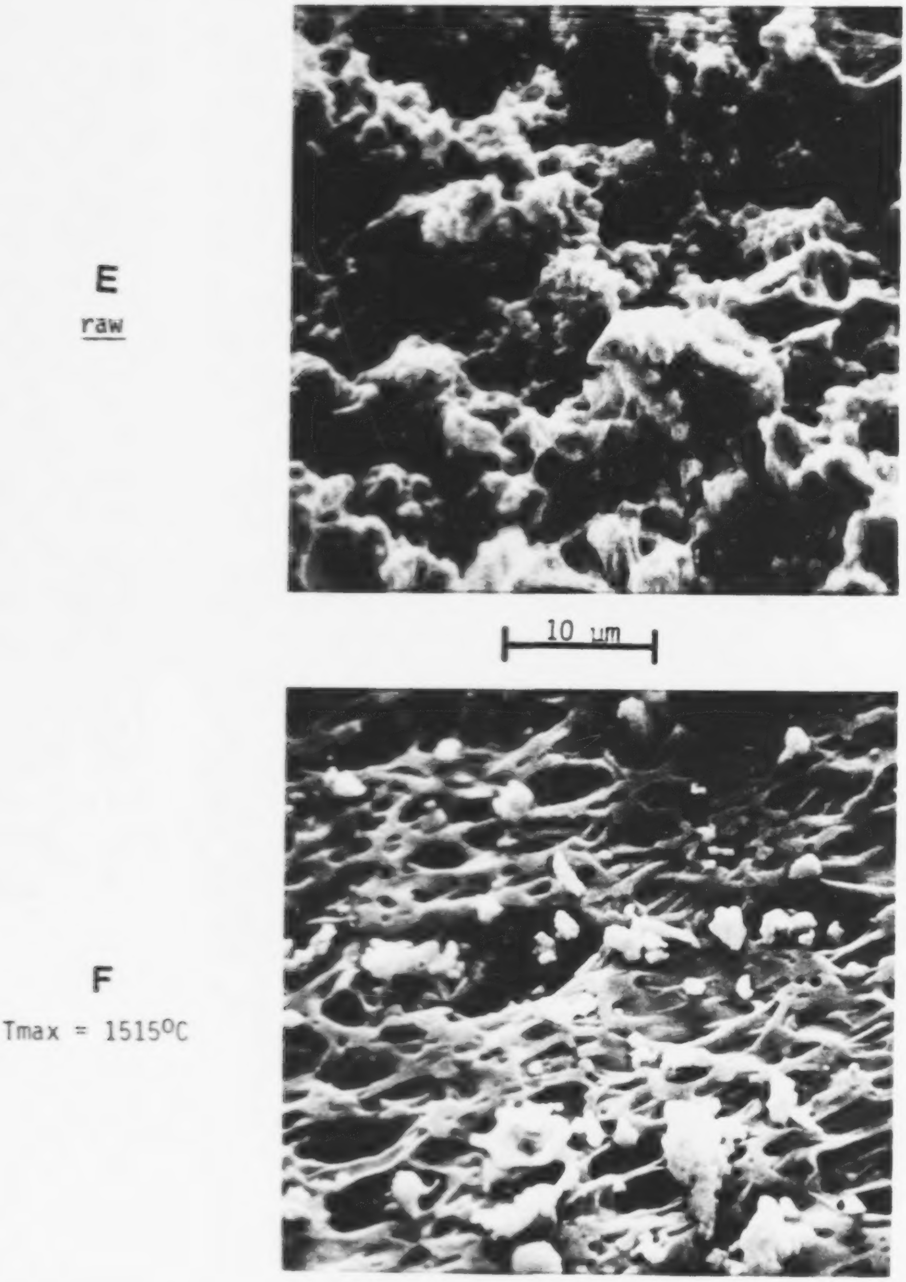

Figure 4-19. (E & F) SEM analysis of calcium hydroxide. E - raw; F - calcine in a CH_4-air flame, T_{max} = 1515°C.

TABLE 4-3. SEM EXAMINATION OF FRAGMENTATION

Sorbent	Peak Temperature °C (°F)	Fragmentation	Size Range µm	Visual Mean µm	Size Reduction Factor
Vicron 45-3	1500 (2750)	Severe	0.1-10	1-2	4-5
Dolomite	1500 (2750)	Severe	0.5-25	5-10	5-6
Michigan Marl	1500 (2750)	Not Evident	0.5-30	5	1
Calcium Hydroxide	1500 (2750)	Mild	0.5-30	3	2

like). This surface structure results in an enhanced external surface area and may indicate internal pore structure.

Michigan marl is shown in Figure 4-19C and D. The particles appear either to be very irregular or the sample shown is merely a large particle with a vast number of smaller particles adhering to the surface. Several clean stones are also evident in Figure 4-19C. The flame calcined sample does not have the high level of fragmentation which was apparent with dolomite. The mean particle diameter of the raw stone is only one-third that of dolomite yet the average particle size after calcination is comparable or larger. The spherical particles in Figure 4-19D are quite like fly-ash in appearance. This is evidence that the combination of mineral matter and organic carbonaceous impurities make up a coal-like matrix in the marl and probably accounts for the low surface areas measured.

The calcium hydroxide used for this study has a bimodal size distribution with maxima around 5 μm and 30-40 μm; the mean size being close to 12.5 μm. When observed by SEM, however, the larger particles appear to be merely agglomerates of the smaller ones (Figure 4-19E), with few truly large individual particles. This appearance is partly due to the lack of definite crystal structure. After calcination the calcium hydroxide appears to have fused (Figure 4-19F). The individual particles are smaller than those of the raw sample but the apparent grain size is similar. Sintering of these particles is enhanced by the presence of H_2O and that may account for the monotonic loss of surface area upon calcination which is unique to $Ca(OH)_2$.

4.2.2 Alternate Sorbents Reactivity to Sulfation

Two of the alternate sorbents, dolomite and calcium hydroxide, have been studied in the dispersed phase reactivity probe. Reaction zone conditions were six percent SO_2 and 600 ms residence time at a nominal temperature of 1100°C. In Figure 4-20 the results of these tests are compared with Vicron 45-3 data and with the surface areas measured when the sorbents were calcined under similar conditions of residence time and temperature.

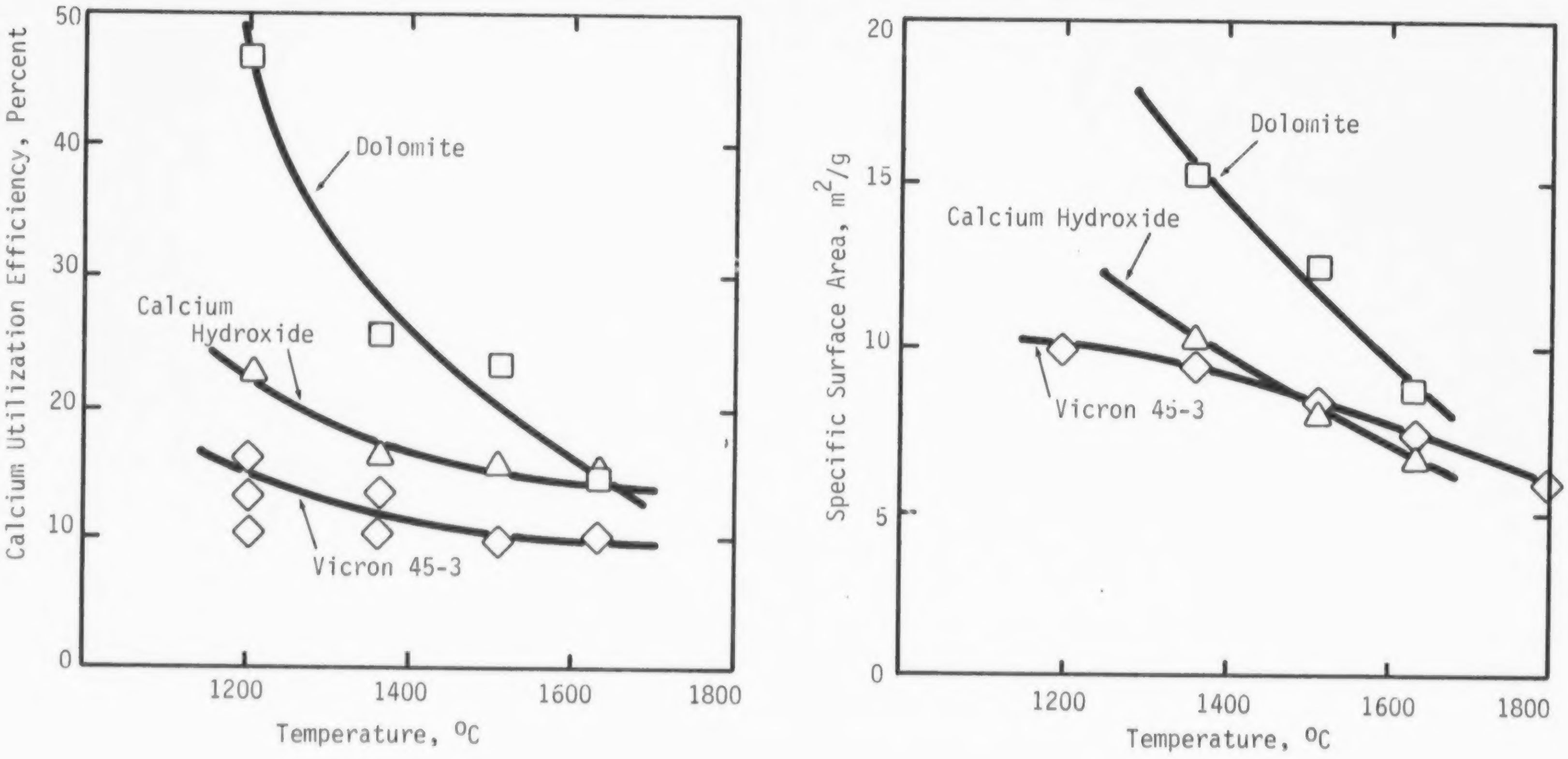

Figure 4-20. Comparison of surface area development and calcium utilization efficiency as a function of calcination temperature for three sorbents.

For each of these sorbents, both specific surface area and calcium utilization efficiency increase monotonically with decreasing calcination temperature. However, although $Ca(OH)_2$ and Vicron 45-3 had very similar surface areas over the range of study, $Ca(OH)_2$ had a significantly higher calcium utilization efficiency. The reason for this is probably because $Ca(OH)_2$ had more available calcium. Unlike $CaCO_3$, $Ca(OH)_2$ is capable of reacting with SO_2. In addition, it has been found that during the long time spent in the reactivity probe (600 ms) $Ca(OH)_2$ calcines almost completely while Vicron 45-3 does not.

4.2.3 Summary

Measurements of the specific surface area and ability to capture sulfur (reactivity) of heat-treated sorbents have indicated the following:

- The physical structure of sorbents (particle size, extent of calcination, specific surface area) after high-temperature heat treatment depends on the sorbent type and peak calcination temperature.

- The specific surface area as measured by BET techniques provides a reasonable indication of the ability of the calcined sorbent to capture sulfur.

- The specific surface areas measured for different sorbents calcined under furnace conditions (1200-1800°C) are relatively low (4-15 m^2/g) and are inversely related to the maximum temperature that the sorbent has experienced.

- There are differences in reactivity between different sorbents which cannot be adequately accounted for by surface area differences.

These findings indicate that each sorbent may have to be optimized individually for a given application and will likely require low-temperature injection to achieve high capture levels.

4.3 Sorbent Deactivation

Sorbent deactivation is any process which inhibits the ability of the sorbent to react with sulfur species. In a boiler furnace, two modes of deactivation are important:

1. Sintering or deadburning.
2. Physical or chemical interaction with other material.

The first of these, sintering, is a time-temperature dependent phenomenon. This process apparently competes with the generation of surface area during the calcination process. As such, it has been considered already in the discussion of sorbent activation.

Physical and chemical interactions may come about as a result of collisions with walls or dispersed solid/liquid matter or as a result of chemical reaction with gaseous species. This study has concentrated on determining the effects that coal-fly-ash components may have on sorbent deactivation.

The approach followed in this study was first to investigate the effects of fly ash by co-feeding it with sorbent into the flame reactor and determining the surface area of the heat-treated mixture. The extent of deactivation was taken as the decrease in specific surface area attributable to the presence of fly-ash. Second, minerals known to be constituents of fly ash were tested for their sorbent deactivation ability. Third, specific chemical compounds contained in ash and in the minerals were tested. Finally, the dispersed-phase reactivity probe was employed to correlate measurable deactivation (loss of surface area) with decreased ability to capture sulfur.

4.3.1 Effect of Coal Ash Minerals on Limestone Activation

A mixture of an Indiana coal fly ash with Vicron 45-3 (75:25 by weight) was injected into a methane-air flame with a peak particle temperature of 1515°C. Samples were collected at varying residence times and analyzed for surface area. The results are shown in Figure 4-21 along with the data for pure vicron 45-3 injected and sampled at the same conditions. It is clear from these data that the ash component itself has a significant specific surface area. This obscures any conclusion which might otherwise have been drawn from these tests. Nonetheless, Vicron 45-3 undergoes an increase in surface area from about 1.0 m^2/g to about 10 m^2/g, a factor of 10, while the Vicron/fly-ash mixture shows an increase of only a factor of 2.5.

Further tests involved the preparation of mixtures of Vicron 45-3 with two mineral compounds which have been identified as components of coal mineral matter (26). These compounds, kaolinite and bentonite (montmorillonite) are primarily aluminosilicates but contain impurities such as iron, calcium and sodium at levels as high as several percent. One of these, kaolinite, has been identified as a major inorganic component in a broad spectrum of coal types (27) which makes it especially attractive for this study.

Mixtures of 5-, 10- and 25-percent bentonite in Vicron 45-3 were injected into flames with peak temperatures of 1200°C, 1360°C, 1515°C and 1630°C. Samples were collected and analyzed for specific surface area. The results are shown in Figure 4-22. Interaction between bentonite and limestone was indicated for both the 5 percent and 10 percent mixtures by a sharp decrease in surface area even at the relatively low temperature of 1200°C. The results are somewhat less clear with higher proportions, however, because bentonite itself has a significant surface area even after high temperature calcination. The initial specific surface area of bentonite is 140 m^2/g and even after calcination at 1630°C this is reduced only to 5 m^2/g.

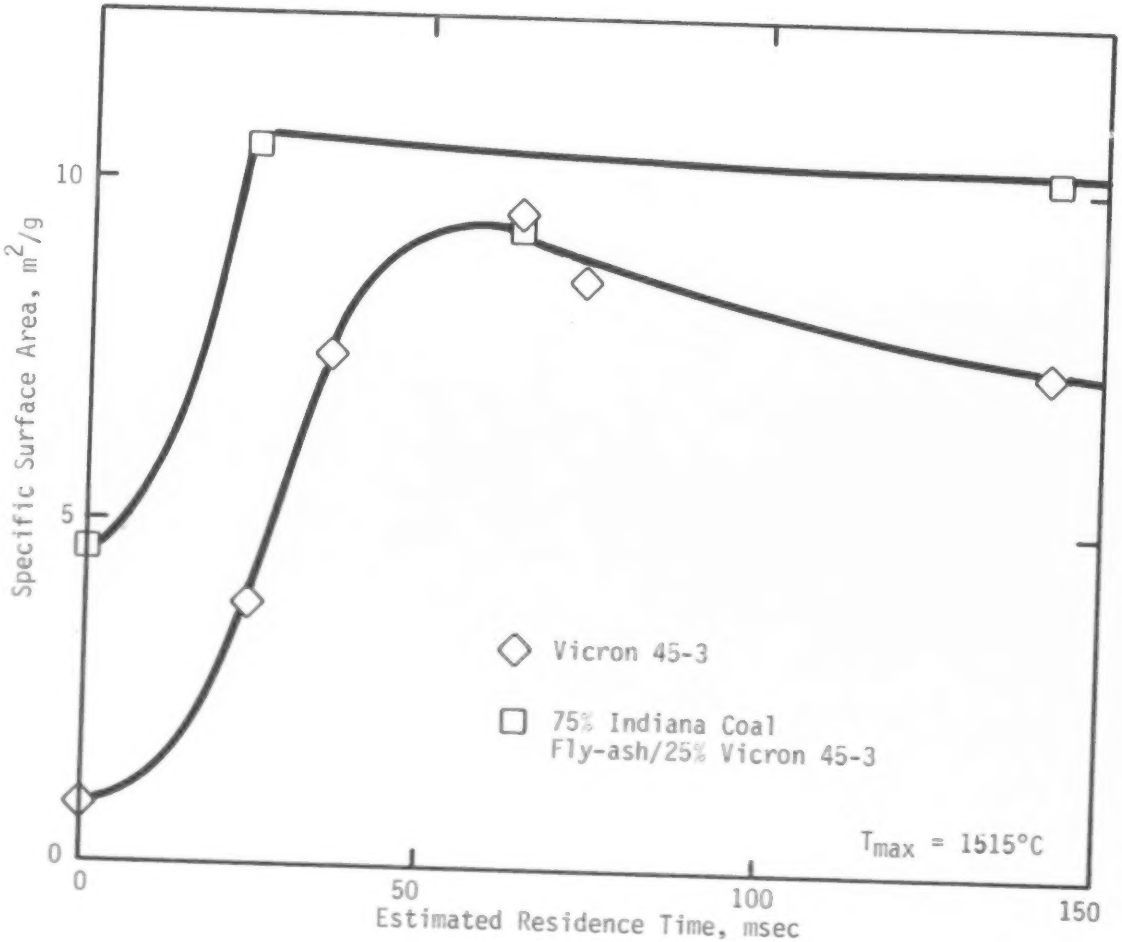

Figure 4-21. Comparison of surface area development for Vicron 45-3 and a Vicron/fly ash mixture. T_{max} = 1515°C.

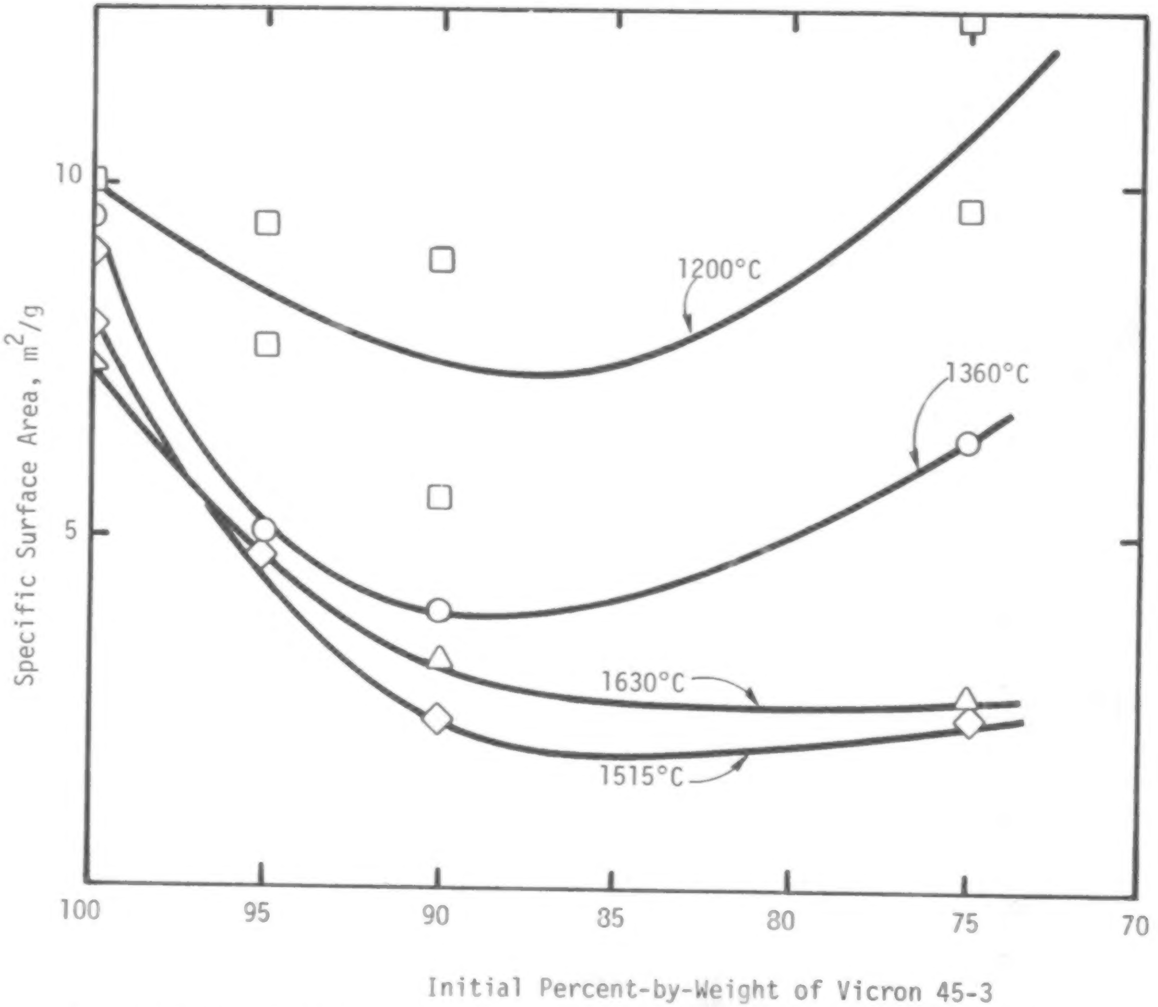

Figure 4-22. Ultimate specific surface area of Vicron 45-3/Bentonite mixtures for different peak calcination temperatures.

The experiment was duplicated with a kaolinite-containing clay, Georgia kaolin, and the results are shown in Figure 4-23. Kaolin severely reduced the specific surface area of Vicron 45-3 at every condition studied. The kaolin used for this study had an initial specific surface area of 14 m^2/g which, after calcination at 1200°C, was reduced 2.5 m^2/g.

The sample of 5 percent kaolin in Vicron 45-3 calcined at 1200°C was examined by scanning electron microscopy. The micrographs are shown in Figures 4-24 and 4-25. Spherical particles, evident in both figures, provide evidence that at least some of the kaolin mixture had melted. Further examination of the spheres by electron microprobing indicated that the spheres contained approximately the one-to-one ratio of Si-to-Al which is characteristic of kaolin but, in addition, they contained significant amounts of calcium. This strongly suggests that kaolin deactivates sorbent, at least in part, by scavenging and absorbing sorbent particles. There is evidence of this in Figure 4-25 which shows crystalline material imbedded in the sphere.

Testing with the 5 percent kaolin mixture was carried further by collecting samples from the 1200°C and 1630°C flames for particle size analysis. The distributions are shown in Figures 4-26 and 4-27 along with distribution curves for pure Vicron 45-3 samples collected under identical conditions. In both cases the smaller particle mass fraction (indicated by the slopes of the curves) had been reduced by 50 percent. This test indicated a preferential loss of finer particles when mineral matter was present. Thus, the loss of smaller particles resulted in a large change in specific surface area and suggests that the smaller particles in the sample were responsible for a large portion of the specific surface area.

In the experiments discussed so far, the sorbent-mineral mixtures were prepared beforehand and were well-mixed in order to provide the maximum opportunity for any sort of interaction. In practical systems with staged combustion burners it is more likely that sorbent and minerals will contact only after injection into the radiant zone of the furnace. In order to examine the differences in interaction, an additional set of experiments was performed in which the sorbent (Vicron 45-3) and mineral (kaolin) were

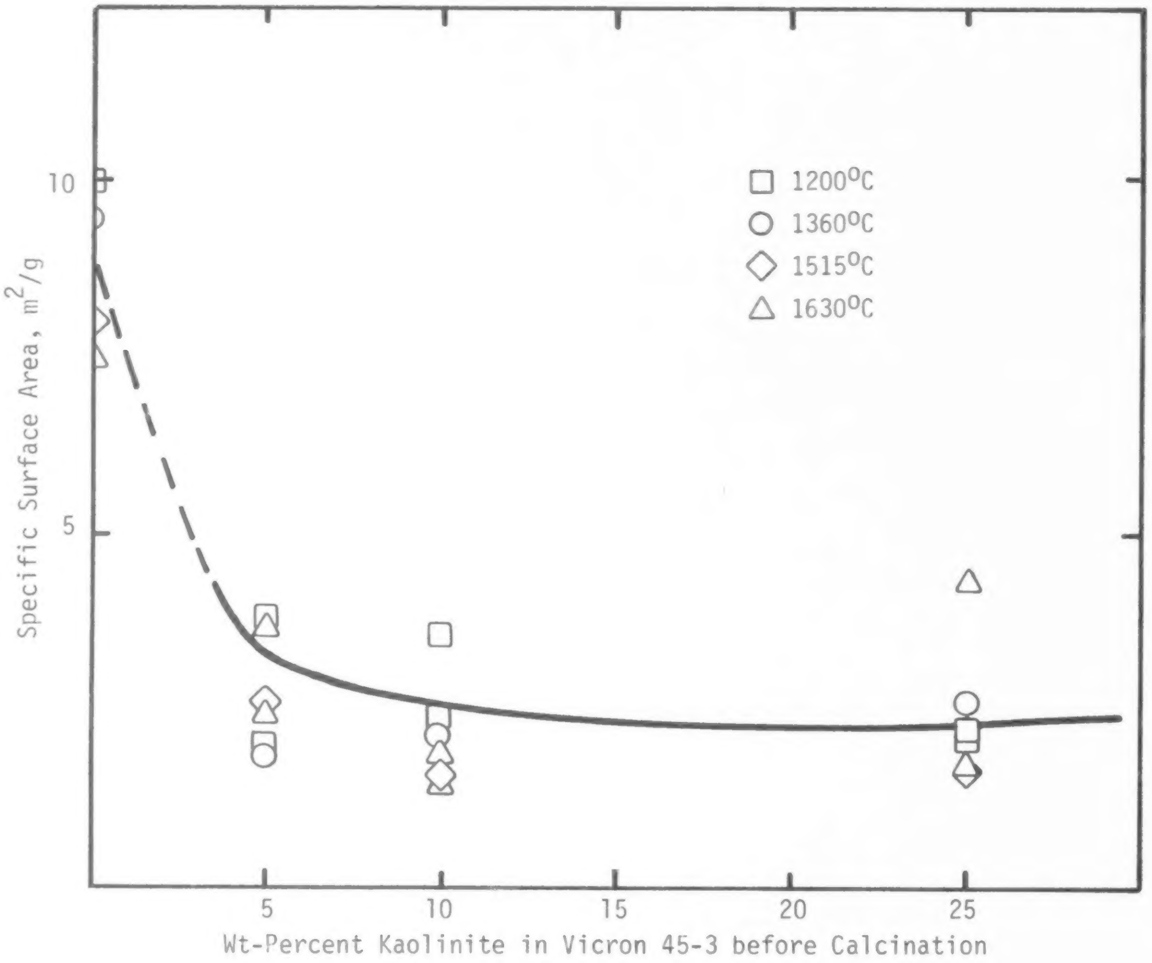

Figure 4-23. Effect of temperature on the ultimate specific surface area of calcined Vicron 45-3/Kaolin mixtures.

5% Kaolinite in Vicron 45-3

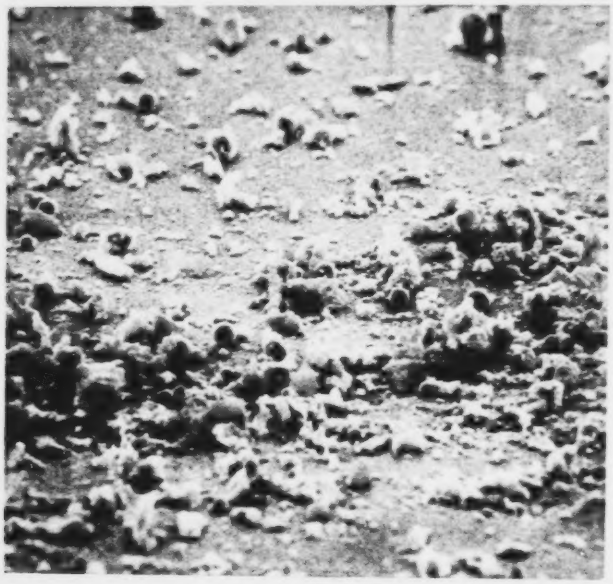

500 X

T_{max} = 1200°C

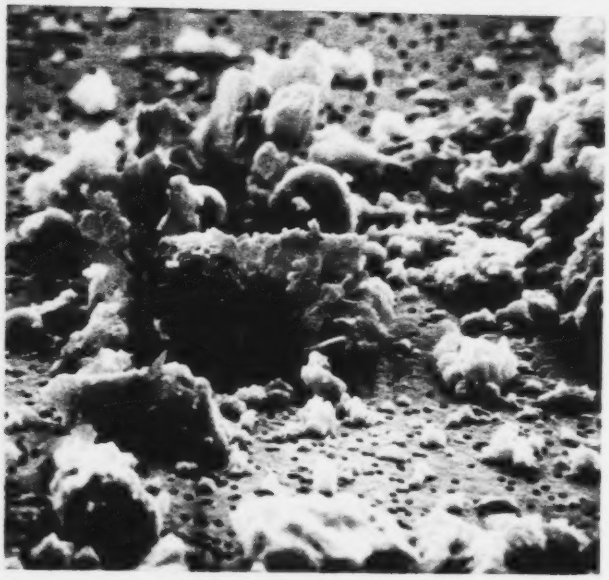

2000 X

Figure 4-24. SEM analysis of a Vicron 45-3/5% Kaolin mixture calcined in an H_2-air flame, T_{max} = 1200°C.

5% Kaolinite in Vicron 45-3

10,000 X

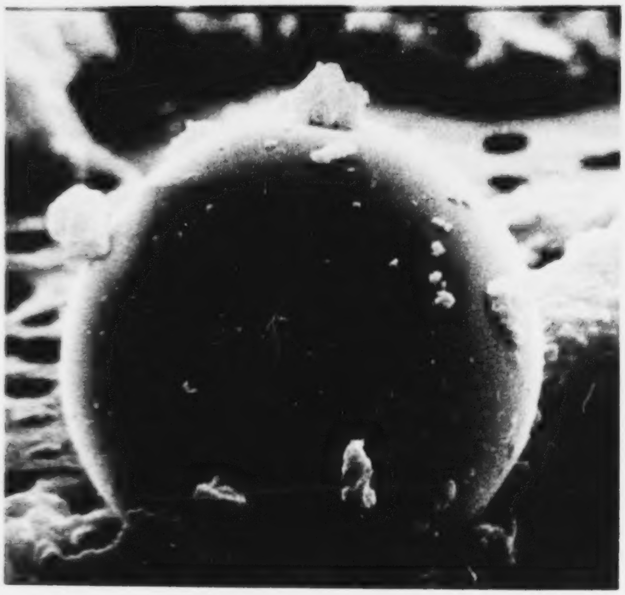

T_{max} = 1200°C

Figure 4-25. SEM analysis of a Vicron 45-3/5% Kaolin mixture calcined in an H_2-air flame, T_{max} = 1200°C.

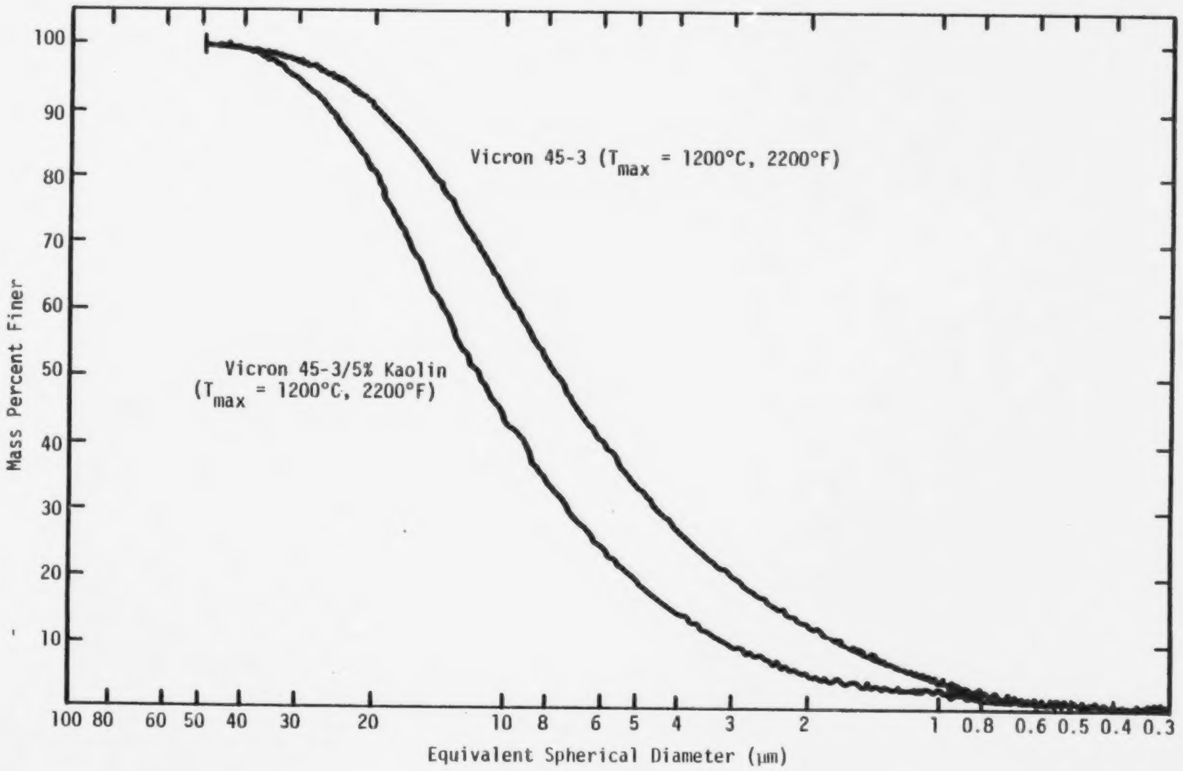

Figure4-26.Effect of 5% kaolin addition on the particle size distribution of limestone injected into a flame with a peak calcination temperature of 1200°C.

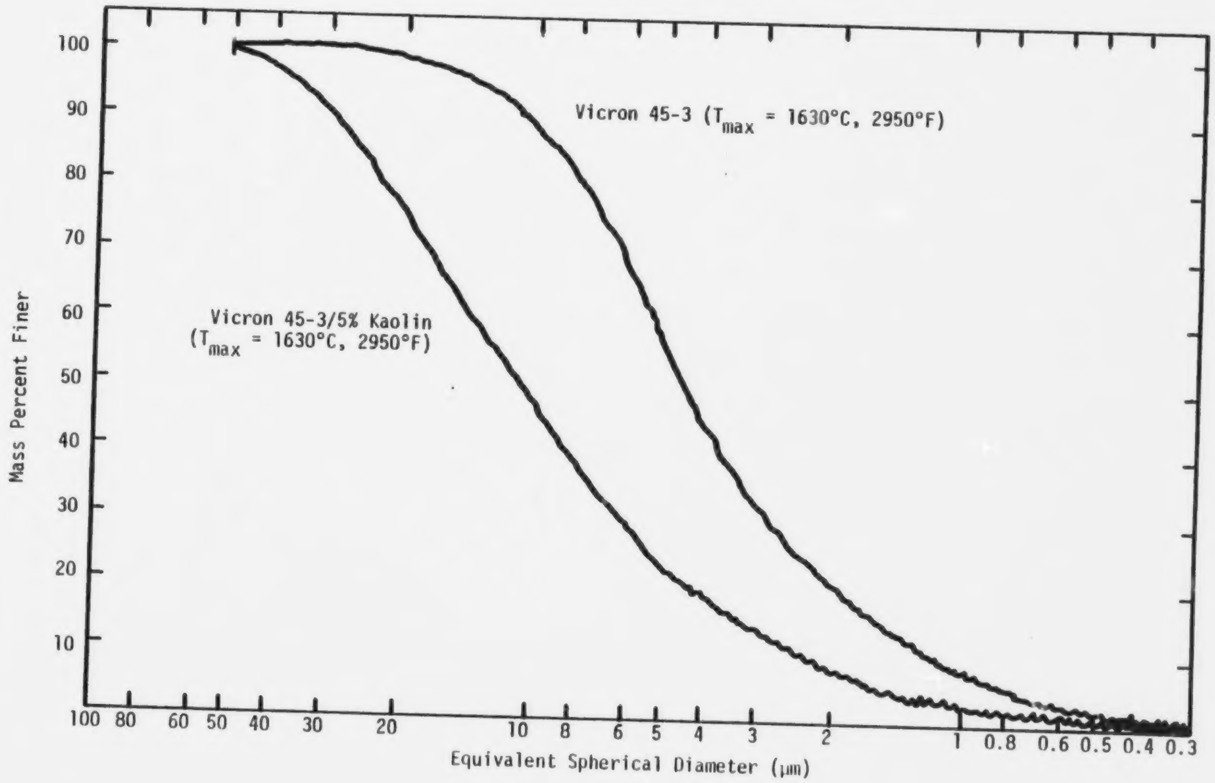

Figure 4-27. Effect of 5% kaolin addition on the particle size distribution of limestone injected into a flame with a peak calcination temperature of 1630°C.

injected separately into the TDR. Three separate injection configurations were tested. These configurations are represented diagramatically along with the standard injection mode (technique I) in Figure 4-28.

In injection technique II, coaxial mixing, kaolin was dispersed into a 0.95 cm (3/8-in.) tube. About 10 cm (4 in.) downstream, Vicron 45-3 was injected along the axis of the tube about 10 cm (4 in.) from the flame front. In injection technique III, the sorbent and mineral were injected in parallel streams into a 0.95-cm (0.37-in.) tube 10 cm (4 in.) before the flame front. In these two configurations, contacting was expected before the mixture entered the flame but the intimacy of mixing was presumed to be lower than in the previous tests. Injection technique IV permitted contacting (5 cm into the flame) only after the mineral matter had been heated to the flame temperature. This was closer to being representative of downstream sorbent injection.

The results of these tests are presented by the histograms in Figure 4-29. The data for techniques II and III indicate that a significant interaction between sorbent and mineral matter occurs even when contacting of the two is minimized before flame treatment. The results of technique IV, however, are less clear. Samples were collected with and without mineral matter since no comparable injection technique had been previously tried. Chemical analysis of all four samples indicated that the limestone had been poorly calcined. This may indicate that the limestone did not spend enough time in the flame to be heated completely.

4.3.2 Effect of Pure Compounds on Limestone Activation

Additional experiments were conducted to determine whether there are specific compounds in coal ash which are detrimental to limestone surface area development. The major compounds in kaolinite and bentonite (and in coal mineral matter) are alumina and silica. In general substantial amounts of iron oxides, alkali and alkaline carbonates, titanates, and transition metal oxides are also present.

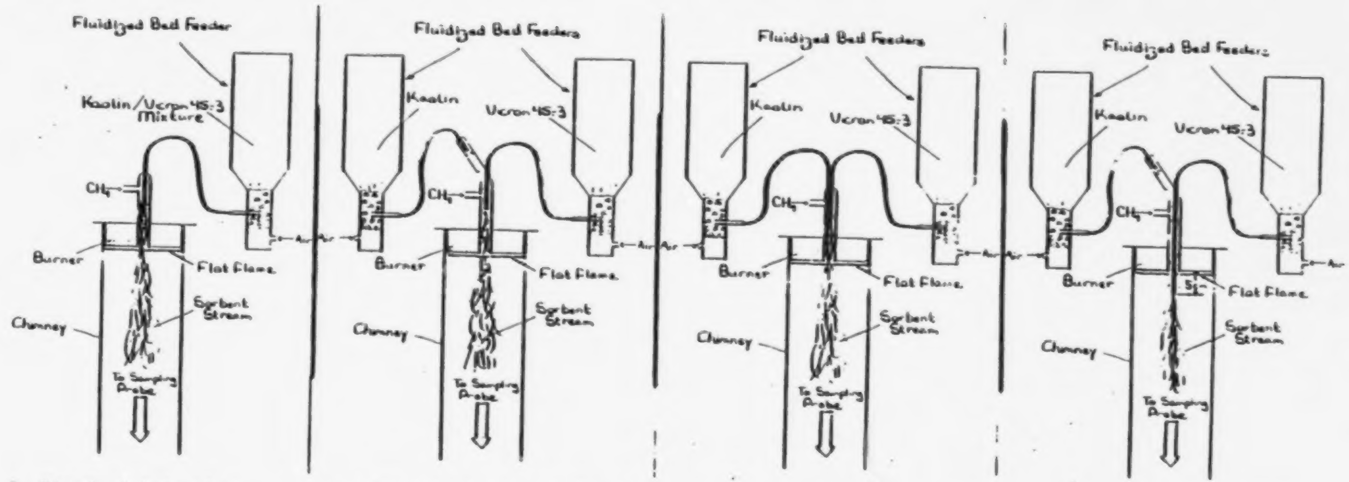

I. Standard injection. 25%-by-weight kaolin is mixed with sorbent for co-injection from F.B.

II. Coaxial mixing. 1:3 ratio of kaolin:sorbent. Kaolin initially dispersed in 3/8" i.d. tube. Sorbent is injected along tube axis downstream but prior to burner.

III. Parallel mixing. 1:3 ratio kaolin:sorbent. Simultaneous injection followed by dispersion and mixing in eight inch length of 3/8" i.d. tube.

IV. Delayed injection. Sorbent is injected two inches into the flame zone. Contacting occurs after kaolin is already hot and decomposed.

Figure 4-28. Sorbent/mineral co-injection techniques.

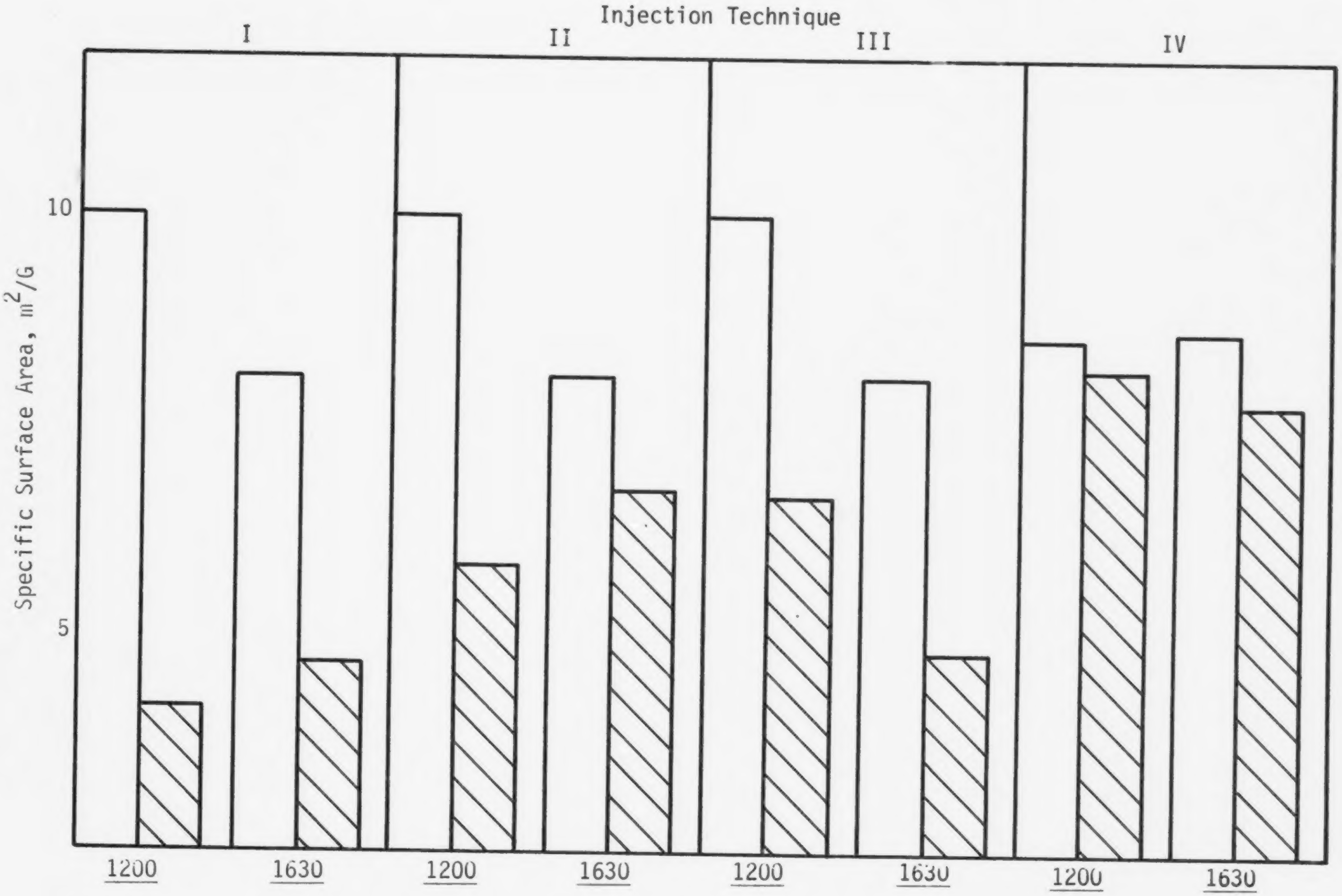

Figure 4-29. Surface area of Vicron 45-3 after injection into flames at peak temperatures of 1200°C and 1630°C. Open bars indicate surface areas observed for pure Vicron 45-3; shaded bars are for samples with Kaolin co-injection. There were no previous data to provide typical values for Vicron 45-3 in Injection Technique IV, but samples were collected with and without mineral matter.

Mixtures of Al_2O_3, SiO_2 (two size cuts), Na_2CO_3, and Fe_2O_3 with Vicron 45-3 were prepared by mixing 5 percent by weight with the limestone. Each of the mixtures was calcined at 1200°C, 1360°C, 1515°C and 1630°C in the flames described earlier. Samples were collected at a distance of 20 cm from the burner and analyzed to determine their effect on the surface area development of Vicron 45-3. The results of these experiments are shown in Figures 4-30 through 4-32. The data for Na_2CO_3, Fe_2O_3 and SiO_2 were averaged for clarity. Kaolin and bentonite mixture data are included for comparison. The shaded band in each figure indicates the range of values obtained for pure Vicron 45-3 at several residence times.

Figure 4-30 presents the data for the Na_2CO_3 and Fe_2O_3 mixtures. It is clear that both of these materials interact with limestone to some degree at all temperatures. In addition the effect of increased residence time at 1630°C has been to further decrease the surface area. The data shown are average values, the level of scatter increased from ± 1.5 m^2/g at 1630°C to ± 3 m^2/g at 1200°C.

The effects of Fe_2O_3 and Na_2CO_3 are not surprising. Both of these materials undergo chemical and physical changes at these temperatures. Sodium carbonate converts to the oxide and reacts with lime to form low melting mixtures. Ferric oxide, as well as other transition metal oxides, experiences a change in oxidation state at these temperatures. The change is known to be affected by the presence of lime or alkali oxides.

Data for the alumina mixture and the two silica mixtures are shown in Figure 4-31. The silica has a significantly greater effect than the alumina. It is uncertain whether the difference between the two size cuts of SiO_2 is significant. Also, the effect is lessened at lower temperatures. The alumina has only a small effect on the Vicron surface area at high temperatures and the result is negligible at 1200°C. The difference between silica and alumina is also understandable. Silica has a much lower melting point than alumina, and these samples were heated above the softening temperature of silica--except in the lowest temperature condition.

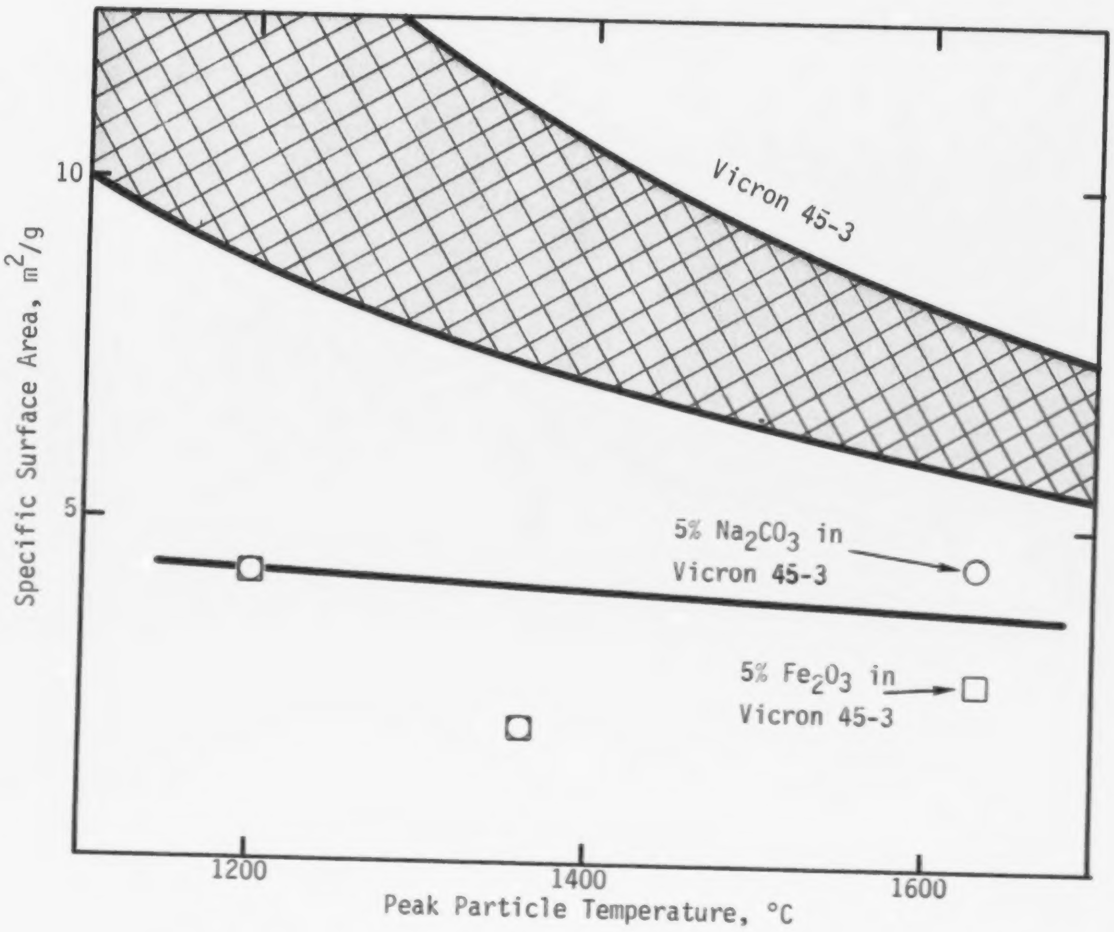

Figure 4-30. Effect of Na_2CO_3 and Fe_2O_3 addition on the ultimate surface area of Vicron 45̄-3 after calcination.

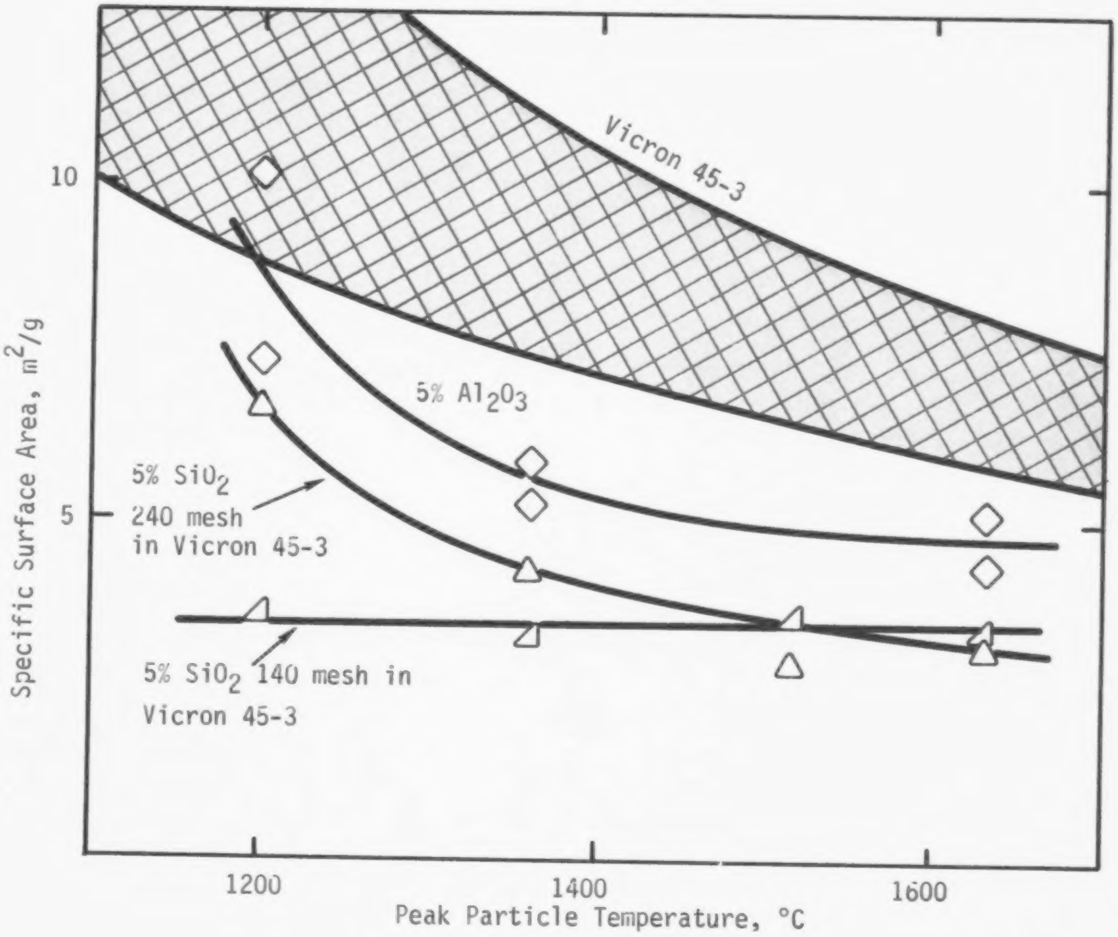

Figure 4-31. Effect of Al_2O_3 and SiO_2 addition on the ultimate surface area of Vicron 45-3 after calcination. A particle-size effect for SiO_2 is also indicated.

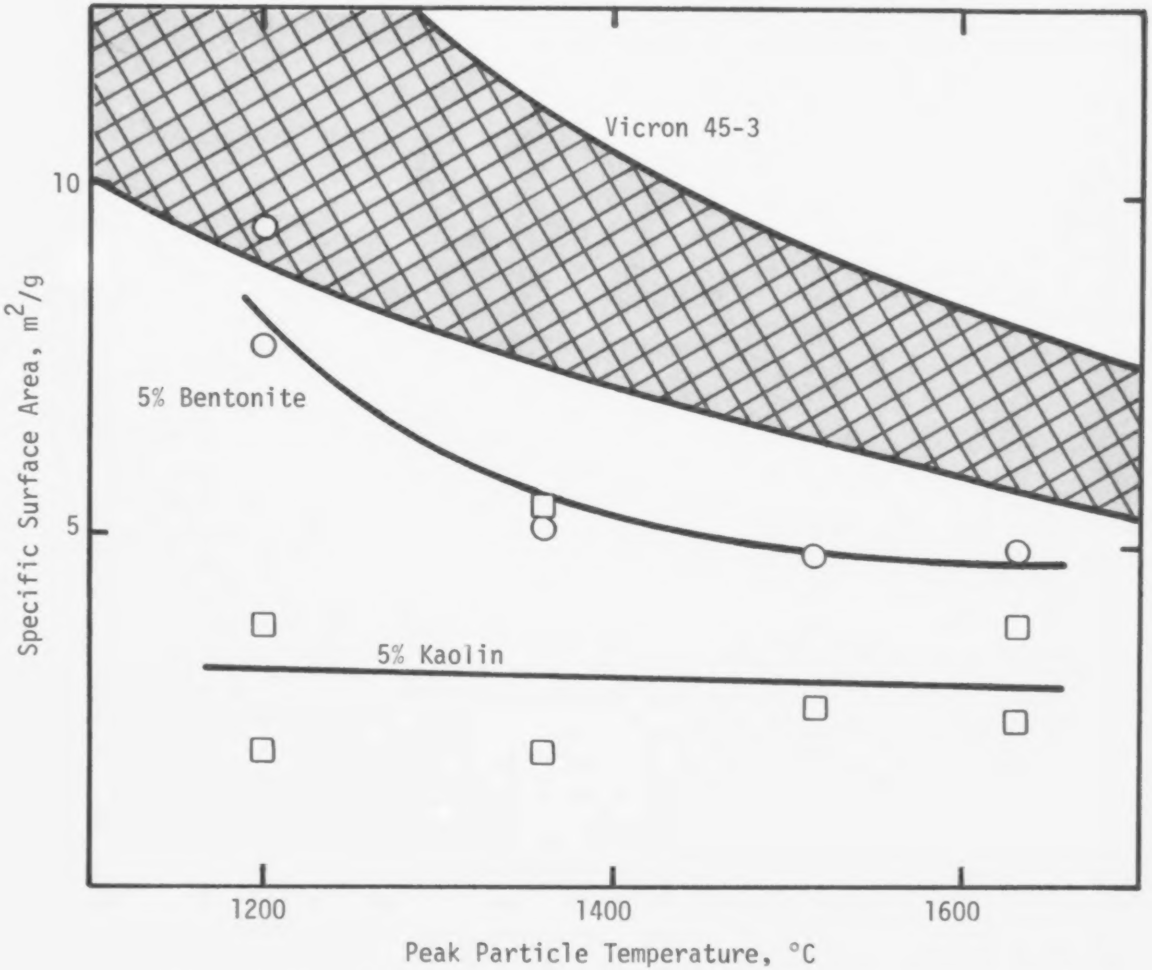

Figure 4-32. Effect of Bentonite and Kaolin on the ultimate surface area of Vicron 45-3 after calcination.

Data from the five percent-by-weight mixtures of kaolin and bentonite with Vicron 45-3 are replotted in Figure 4-32 for comparison with the SiO_2, Al_2O_3 and Na_2CO_3 mixture tests. Again, the effect of kaolin is much more severe than that of bentonite. Furthermore, kaolin interacts even at lower temperatures. The effect of bentonite is lessened at 1200°C but, again, this may be due to the intrinsic specific surface area of the mineral itself.

In order to estimate the potential for interaction between different sorbents and different minerals, several sorbents and sorbent-mineral mixtures were placed in iron crucibles and fired in an electric furnace for 12 hours at 950°C. The temperature, (950°C) was the limit of the available furnace so a long time of 12 hours was used to ensure that reaction would be observed. The furnace was cooled and then the samples were removed and evaluated subjectively. The observations are presented in Table 4-4. Overall, the limestone-containing samples hardened. Dolomite and calcium hydroxide mixtures did not. The latter result is surprising since it would be expected that $Ca(OH)_2$ and $CaCO_3$ would decompose identically to CaO when heated to 950°C in air.

4.3.3 Effect of Mineral Matter on Sorbent Reactivity

Several sorbent-mineral mixtures were tested in the dispersed-phase SO_2 reactivity probe. Figure 4-33 compares the reactivity of Vicron/kaolin mixtures with the surface area development for calcination at 1200°C. In Figure 4-34 specific surface area and calcium utilization efficiency are presented as a function of calcination temperature for pure Vicron 45-3 and for mixtures with 240-mesh SiO_2 and kaolin. Again, the data for SiO_2 have been averaged for clarity. In each case, there is a general correspondence between specific surface area and reactivity toward SO_2.

Figure 4-35 compares the effect of kaolin on the reactivities of dolomite, calcium hydroxide and Vicron 45-3. The data are plotted alongside of the reactivity test results for the pure sorbents. It is obvious that kaolin has essentially no effect on dolomite and $Ca(OH)_2$. This is a bit surprising but agrees with the physical observations presented in Table 4-4.

TABLE 4-4. APPEARANCE OF SORBENTS, MINERALS, AND MIXTURES AFTER HEATING AT 950°C FOR 12 HOURS

Compound	Appearance
Vicron 45-3	White, hard crust, clumps of material
Dolomite	Off-white, sandy appearance, no clumps
Kaolinite	Gold reflection, flaky appearance, light
Bentonite	Yellow-brown, hard crust
5% Kaolin in Vicron 45-3	White, clumps, granular
10% Kaolin in Vicron 45-3	White, light powder, some clumping
25% Kaolin in Vicron 45-3	White, flaky powder, some clumping
5% Bentonite in Vicron 45-3	Off-white, hard crust, clumpy, clumps decay into powder when broken
10% Bentonite in Vicron 45-3	Tan-white, large clumps
25% Bentonite in Vicron 45-3	Tan, small clumps
5% Kaolin in Marblewhite 125	White, sandy, granular, no powder
5% Fe_2O_3 in Vicron 45-3	Light brown, clumpy, granular
5% Na_2CO_3 in Vicron 45-3	White, Yellow-green shading, clumpy
5% 140 mesh SiO_2 in Vicron 45-3	White, hard crust, granular
5% 240 mesh SiO_2 in Vicron 45-3	White, hard crust, clumpy
5% Al_2O_3 in Vicron 45-3	White, hard crust, small clumps
5% Kaolin in Dolimite	Off-white, sandy appearance, loose
10% Kaolinite in $Ca(OH)_2$	White, powdery, no clumps or grains

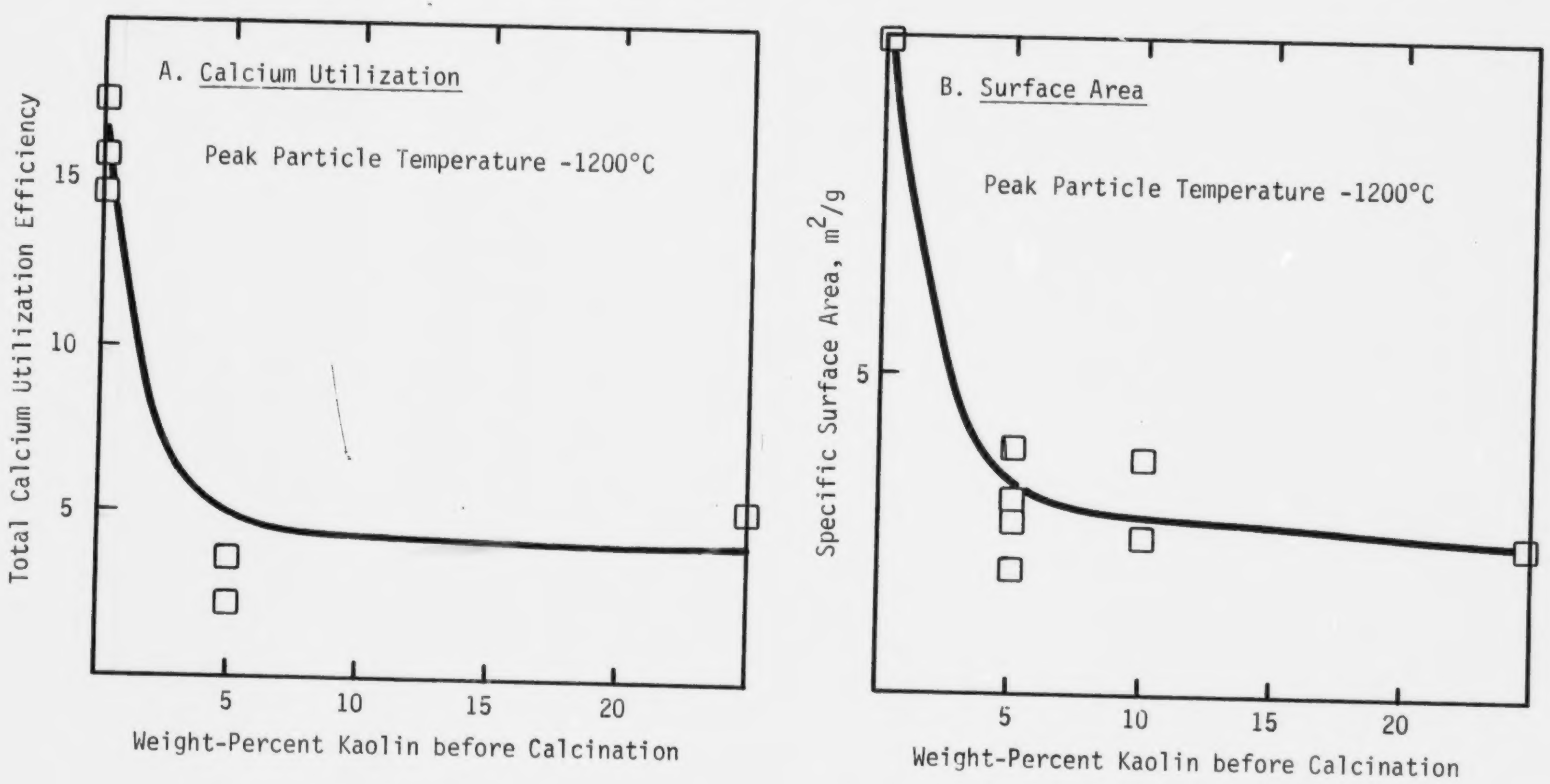

Figure 4-33. Effect of kaolin concentration on, A. Calcium utilization efficiency and, B. Specific surface area of Vicron 45-3/Kaolin mixtures. Tmax = 1200°C.

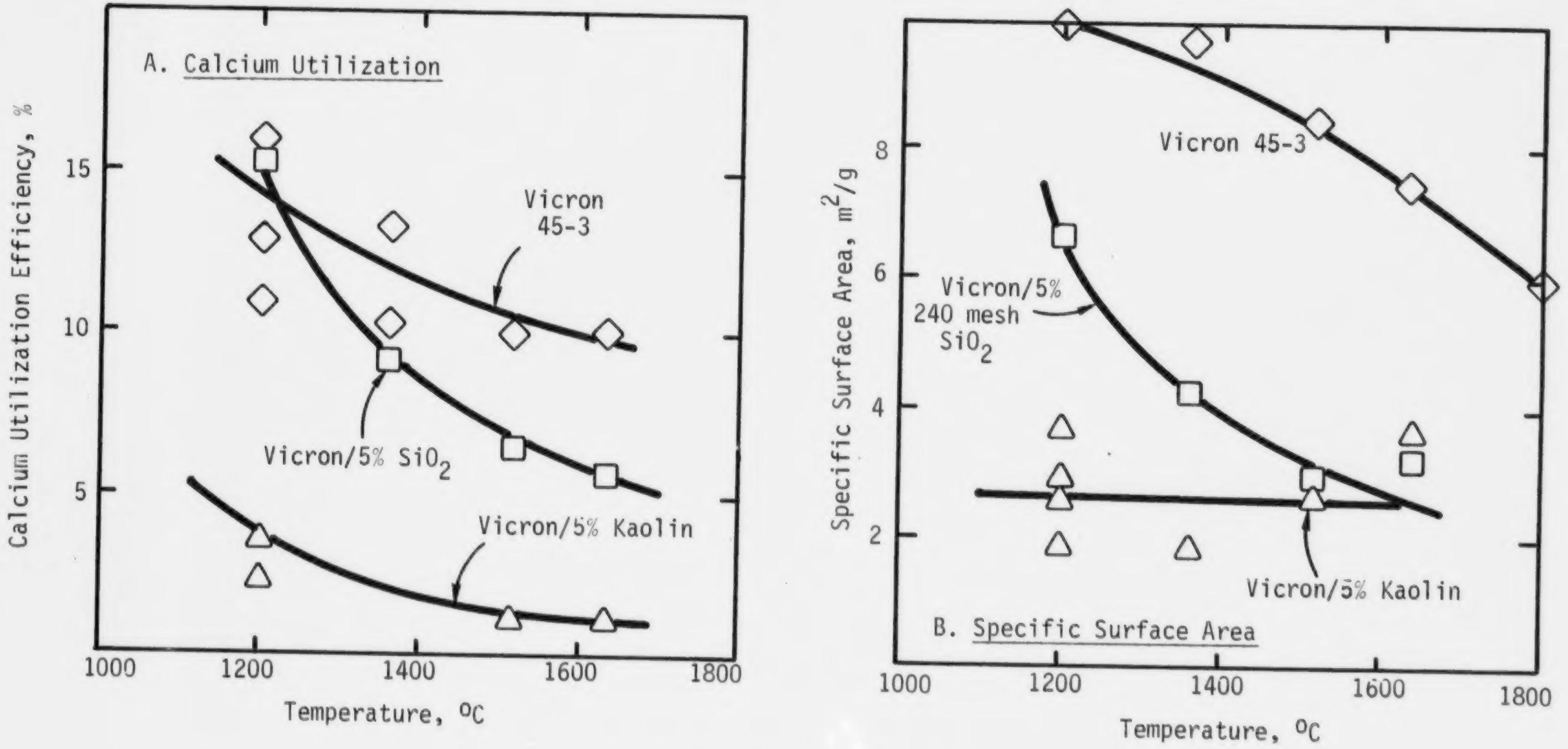

Figure 4-34. Comparison of A. Calcium utilization efficiency and B. Surface area development of limestone in the presence of mineral matter as a function of peak calcination temperature.

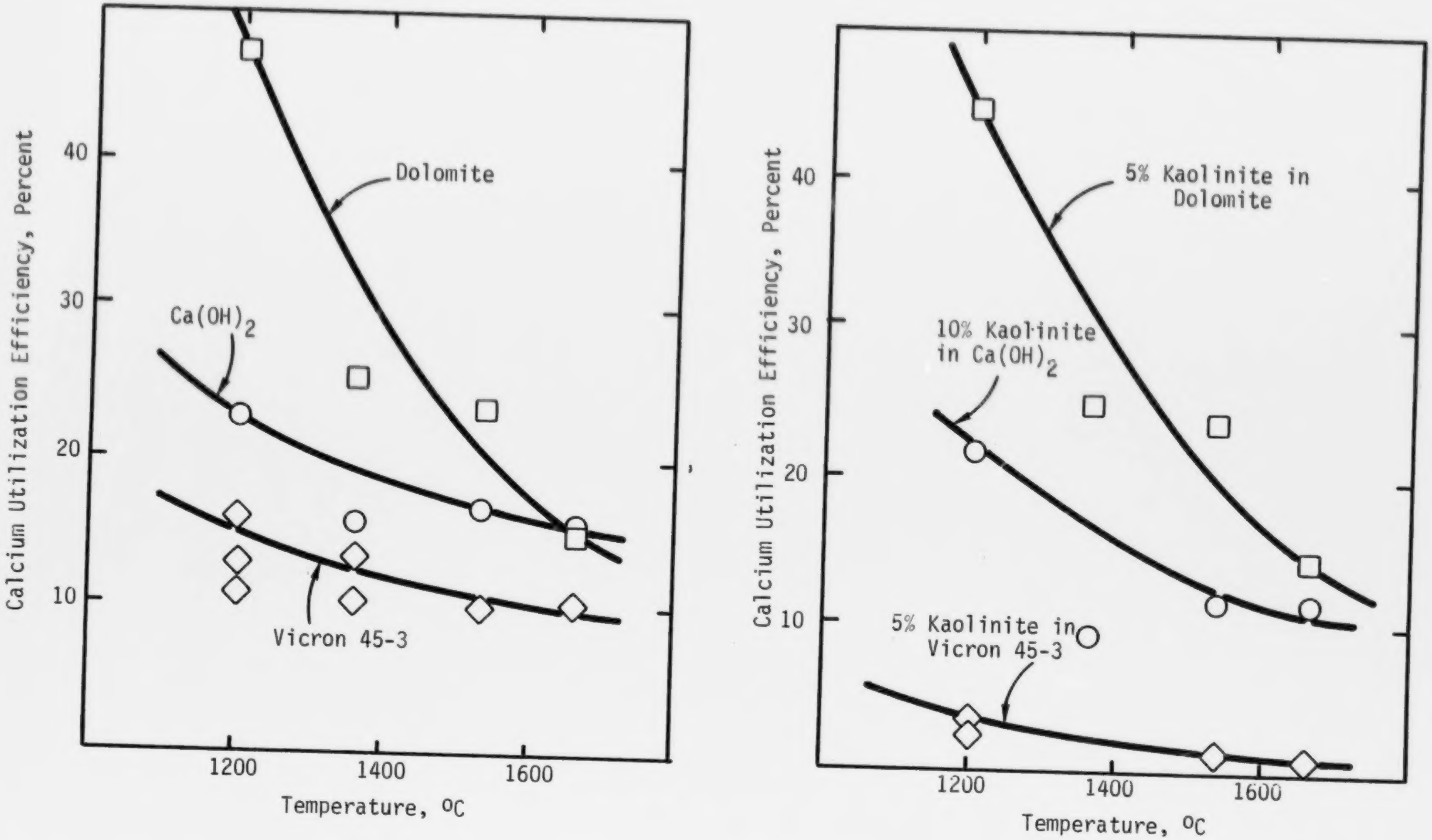

Figure 4-35. Effect of Kaolin on the calcium utilization efficiency of three sorbents. Data on left is for pure sorbents, data on right is for sorbent/Kaolin mixtures.

These results suggest that different sorbents are likely to have strikingly different degrees of interaction with coal mineral matter. The physical/chemical mechanisms that result in such differences are unclear but may result from different particle sizes after calcination and the refractory nature of MgO.

4.3.4 Summary of Mineral Matter Interactions

All of the minerals tested demonstrated some degree of interaction with the sorbents. The interactions all resulted in a loss of sorbent specific surface area and a corresponding decline in reactivity toward SO_2. It was generally observed that materials which soften, or melt, or those with a chemical potential for reaction with CaO, evoked the greatest effects. The level of this effect was fairly uniform across the range of temperatures studied, although there was some indication that the impact of SiO_2 on Vicron 45-3 might lessen if peak temperatures were lowered further.

An important observation is that there are differences between different sorbents. Dolomite and $Ca(OH)_2$ were both affected by kaolin but the effects of kaolin were slight compared to its effect on Vicron 45-3. Although the reason for this resistance to mineral matter is not known, the implication is that it may be possible to choose sorbents for their ability to stay reactive in the presence of different coal fly-ash minerals.

5.0 CONCLUSIONS AND IMPLICATIONS

In this study, the high-temperature, short-time behaviors of calcium containing sorbents were investigated in an environment which simulated the radiant zone of a pulverized coal furnace. Measurements on the physical and chemical changes which influence the ability of the heat-treated sorbents to capture sulfur were made. A new technique was developed to make direct measurements on the ability of the heat-treated sorbent to capture sulfur without the need to quench the sample to ambient conditions. This technique utilized a reactivity probe which allowed the sorbent to be subjected to sulfur dioxide under well-controlled, dispersed-phase conditions. A variety of calcium-containing sorbents and mixtures of sorbent and mineral matter were investigated.

The important conclusions which have been reached are as follows:

Particle Heatup and Calcination. Pulverized sorbent particles heat rapidly to the local gas temperature and calcination times are short (<100 ms) at typical furnace temperatures (1200-1800°C). These processes are not rate limiting in the overall process of sorbent utilization after injection into the furnace radiant zone. However, the application of the calcination model discussed in Appendix D indicates that for the lower temperatures that might exist in the furnace convective passages, or for larger particles (>50 μm) the time required for calcination may be a significant fraction of the time available.

Surface Area Generation. The growth of surface area for the limestones tested occurred in the same time frame as calcination. The sorbent type and the peak calcination temperature were the most important parameters which determined the ultimate surface area achieved with heat treatment. The gas phase composition (O_2, CO_2, H_2O) appeared to have a negligible effect on the ultimate surface area.

Sintering. Sintering reactions occur as a process competing with surface area development. As the peak calcination temperature was increased, the rate of sintering increased so that the ultimate surface area achieved decreased with temperature. The effect of temperature was largest at lower temperatures (<1300°C) and the surface areas approached asymptotic values at higher temperatures. The surface areas measured for all sorbents tested under furnace temperatures were relatively low (5-25 m^2/gm). The surface areas of different sorbents had strikingly different temperature responses, with dolomite having the strongest temperature dependence.

Fragmentation. Many of the sorbents severely fragmented when injected into the flame. In particular, the Vicron 45-3 (a large-crystal, pure, calcitic limestone) and the dolomite tested decreased in mean diameter by more than a factor of two. This fragmentation process may be responsible for a significant portion of the surface area increase during calcination. The size after calcination must be adequately accounted for in any subsequent modeling of sulfation of the sorbent.

Surface Area and Sulfation. Surface area after calcination provides an indication of the ability of the sorbent to subsequently capture sulfur. In Figure 5-1 is shown the calcium utilization as determined by the reactivity probe versus the specific surface area measured after calcination for all of the sorbent and sorbent/mineral matter mixtures and conditions tested. The surface area appears to be the most important single parameter determining reactivity. However, there are additional differences in reactivity between sorbents that cannot be completely accounted for by surface area. These may be associated with inherent chemical reactivity, degree of fragmentation, or details of the pore structure.

Mineral Matter Interactions. The decrease in SO_2 capture efficiency when small amounts of fly ash or mineral matter are present during calcination is attributable to a reduction in surface area. This loss of surface area is only slightly temperature-dependent, having lesser impact at lower temperatures. The loss is strongly dependent on the sorbent type. The surface areas of dolomite and calcium hydroxide are very insensitive to the presence of impurities while Vicron 45-3 limestone is extremely sensitive even to small amounts of mineral matter. The loss of surface area apparently

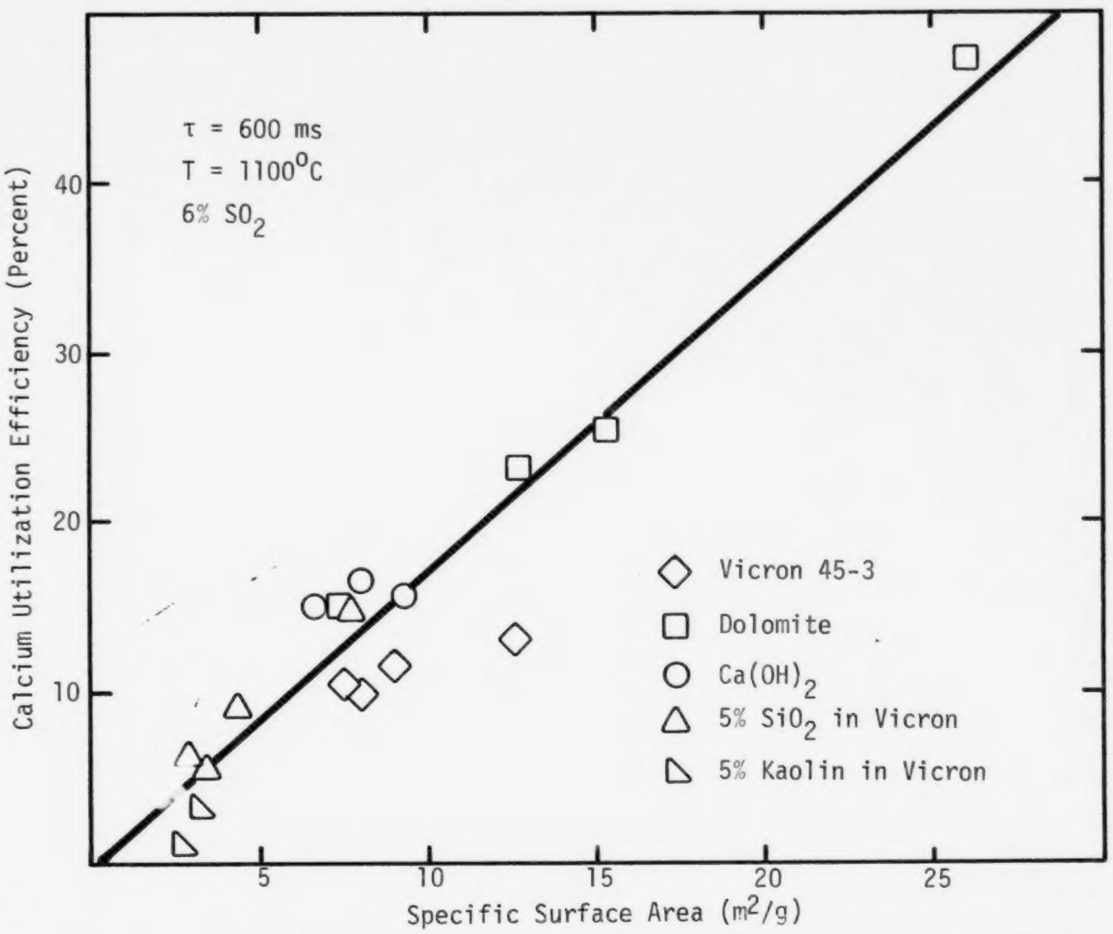

Figure 5-1. Calcium utilization efficiency of sorbents and sorbent-mineral mixtures as a function of specific surface area of sample calcined under identical conditions. Increasing specific surface area corresponds to decreasing peak calcination temperature for a given sorbent.

results from accelerated sintering or formation of low-melting-point mixtures. These mixtures contain spherical particles which scavenge other sorbent particles.

Future FCR activities (contract 68-02-3633) will involve more detailed studies of techniques for generating the high surface area and, hence, high reactivity sorbents that are required to optimize the process. Particular emphasis will be placed on low-temperature calcination in post-flame gases and external calcination in inert environments. The behavior of high reactivity sorbents will be investigated when injected into high-temperature flames containing mineral matter and also during sulfation.

REFERENCES

1. Attig, R. C. and P. Sedor. Additive Injection for sulfur dioxide Control. A Pilot Plant Study. APTD-1176. NTIS No. PB226761, 1970.

2. Kelly, M. E. and S. A. Shareef. Second Survey of Dry SO_2 Control Systems. EPA-600/7-81-018 NTIS No. PB81-157919, 1981.

3. Bellot, J. A., G. M. Drissel, C. J. Royce, L. J. Scott, and A. G. Sliger. Review of Dry Limestone Injection Process. APTD-1136. NTIS No. PB-211-431. 1972.

4. Borgwardt, R. H., G. R. Gillis and N. F. Roache. IERL-RTP Research on Sulfur Capture in LIMB. EPRI CWS-3182, V. 1., 1983.

5. Coutant, R. W., R. Simon, B. Campbell, and R. E. Barrett. Investigation of the Reactivity of Limestone and Dolomite for Capturing SO_2 from Flue Gas. APTD-0802, 1971.

6. Gordon, S. and B. J. McBride. Computer Program for Calculation of Complex Chemical Equilibrium Compositions, Rocket Performance, Incident and Reflected Shocks and Chapman-Jouquet Detonations. NASA SP-273, 1976.

7. JANAF Thermochemical Tables. 2nd ed. Stull, D. R. and H. Prophet, Eds. NSRDS-NBS-37, 1971.

   1974 Supplement. J. Phys. Chem. Ref. Data, 1974, 3 (2) 311-480.
   1975 Supplement. J. Phys. Chem. Ref. Data, 1975, 4 (1) 1-175.
   1978 Supplement. J. Phys. Chem. Ref. Data, 1978, 7 (3) 793-940.
   1982 Supplement. J. Phys. Chem. Ref. Data, 1982, 11 (3) 695-940.

8. Case, P. L., L. Ho, W. D. Clark, E. Kau, D. W. Pershing, R. Payne and M. P. Heap. Testing and Evaluation of Experimental Wall-Fired Furnaces to Determine Optimum Means to Reduce Emissions of Nitrogen and Sulfur Oxides: Final Report, EPA Contract No. 68-02-3921. Energy and Environmental Research Corp., Irvine, CA; 1984.

9. Ruth, L. A., A. M. Squires and R. A. Graff. Desulfurization of Fuels with Half-Calcined Dolomite: First Kinetic Data. Environ. Sci. and Technology. 1972, 6 (12), 1009-14.

10. Pell, M. Reaction of Hydrogen Sulfide with Fully Calcined Dolomite. Ph.D. Thesis, City University of New York, New York, N.Y. 1976.

11. Levy, A. and E. L. Merryman. CaO Interaction in the Staged Combustion of Coal. DOE/PC/30301-9. NTIS No. PB83-006630, 1983.

12. Field, M. A., D. W. Gill, B. B. Morgan and P. G. W. Hawksley. Combustion of Pulverized Coal. British Coal Utilization Research Association. Leatherhead, England, 1967.

REFERENCES

13. Seeker, W. R., G. S. Samuelsen, J. C. Kramlich, and M. P. Heap. Fundamental Combustion Research Applied to Pollution Formation. Volume II. Physics and Chemistry of Two Phase Flames. EPA Final Report Contract 68-02-3633.

14. Hamor, R. J. and I. W. Smith. Fluidizing Feeders for Fine Particles at Low Stable Flows. Fuel, 1971, 50 394-404.

15. Altenkirch, R. A., R. E. Peck and S. L. Chen. Fluidized Bed Feeding of Pulverized Coal. Powder Technology, 1978, 20 189-96.

16. Beer, J. M. and N. A. Chigier. Combustion Aerodynamics. p. 18. Applied Science Publishers, LTD, London, 1972.

17. Hildebrand, Lundell, Bright, and Hoffman. Applied Inorganic Analysis, 2nd ed., 1953.

18. Payne, R., P. L. Case, M. P. Heap, J. Lee, C. N. McKinnon, P. Nelson, and D. W. Pershing. Development of Criteria for Extension of Applicability of Low-Emission, High-Efficiency Coal Burners. Fourth Annual Report, EPA Contract 68-02-2667. Energy and Environmental Research Corporation, Irvine, Calif. 1981.

19. Gaydon, A. G. and I. R. Hurle. The Shock Tube in High-Temperature Chemical Physics. p. 177, Reinhold Publ., N. Y., 1963.

20. Borgwardt, R. H. Kinetics of the Reaction of SO_2 with Calcined Limestone. Environ. Sci. and Technology. 1970, 4 (1), 59-63.

21. Boynton, R. S. Chemistry and Technology of Limestone, 2nd ed. J. Wiley and Sons, N.Y., 1980.

22. Gregg, S. J. and K. S. W. Sing. Adsorption Surface Area and Porosity. Academic Press, N.Y., 1967.

23. Borgwardt, R. H. and R. D. Harvey. Properties of Carbonate Rocks Related to SO_2 Reactivity. Environ. Sci. and Technology. 1972, 6 (4), 350-360.

24. McClellan, G. H. Physical Characterization of Calcined and Sulfated Limestones. Presented at the Fourth Dry Limestone Process Symposium. Gilbertsville KY, June 1970.

25. Harvey, R. D. Petrographic and Mineralogical Characteristics of Carbonate Rocks Related to Sorption of Sulfur Oxides in Flue Gases. EPA APTD-0920, July 1970.

26. Kuhn, L. and H. Plogman. Reaction of Catalysts with Mineral Matter During Coal Gasification. Fuel, 1983, 62 (2) 205-208.

REFERENCES

27. Mitchell, R. S. and H. J. Gluskoter. Minerology of Ash of Some American Coals: Variations with Temperature and Source. Fuel, 1976, 55 (1) 90-96.

28. Bhatia, S. K. and D. D. Perlmutter. The Effect of Pore Structure on Fluid-Solid Reactions: Application to the SO_2-Lime Reaction. AICHE. J. 1981, 27 (2), 226-234.

29. Gallagher, P. K. and D. W. Johnson, Jr. The Effects of Sample Size and Heating Rate on the Kinetics of the Thermal Decomposition of $CaCO_3$. Thermochimica Acta, 1973, 6, 67.

APPENDIX A

FLAME GAS TEMPERATURE MEASUREMENTS

Figure No.	Title	Page
A-1	Gas temperature profile in a CH_4-air flame. SR = 0.92, V_o = 38.0 $cm \cdot s^{-1}$	107
A-2	Gas temperature profile in a CH_4-air flame. SR = 1.03, V_o = 38.0 $cm \cdot s^{-1}$	108
A-3	Gas temperature profile in a CH_4-air flame. SR = 1.16, V_o = 37.0 $cm \cdot s^{-1}$	109
A-4	Gas temperature profile in a CH_4-air flame. SR = 1.0, V_o = 77.8 $cm \cdot s^{-1}$	110
A-5	Gas temperature profile in a CH_4-air flame. SR = 0.96, V_o = 50.2 $cm \cdot s^{-1}$	111
A-6	Gas temperature profile in a CH_4-air flame. SR = 1.58, V_o = 45.2 $cm \cdot s^{-1}$	112
A-7	Gas temperature profile in a CH_4-air flame. SR = 1.01, V_o = 48.0 $cm \cdot s^{-1}$	113
A-8	Gas temperature profile in a CH_4-air flame. SR = 1.18, V_o = 47.3 $cm \cdot s^{-1}$	114
A-9	Gas temperature profile in a CH_4-air flame. SR = 1.30, V_o = 47.0 $cm \cdot s^{-1}$	115
A-10	Gas temperature profile in a CH_4-air flame. SR = 1.52, V_o = 23.2 $cm \cdot s^{-1}$	116
A-11	Gas temperature profile in a CH_4-air flame. SR = 2.09, V_o = 49.8 $cm \cdot s^{-1}$	117
A-12	Gas temperature profile in a CH_4-air flame. SR = 0.98, V_o = 47.6 $cm \cdot s^{-1}$	118
A-13	Gas temperature profile in a CH_4-air flame. SR = 0.98, V_o = 45.8 $cm \cdot s^{-1}$	119
A-14	Gas temperature profile in a CH_4-air flame. SR = 1.67, V_o = 49.0 $cm \cdot s^{-1}$	120

Gas Temperature Profiles

Flame-gas temperatures were measured with a type S (Pt/Pt-10 percent Rh) thermocouple and readout with an Omega 199 thermocouple thermometer. Correction of the measured temperature for radiation losses from the thermocouple junction to the surroundings (assumed to be at 300K) was made with the relation:

$$T_g = \frac{\epsilon \sigma}{h}[(T + 273)^4 - (300)^4] + T \tag{A-1}$$

where

T_g = true gas temperature, ^oC

T = thermocouple temperature, ^oC

σ = Stefan-Boltzmann constant = 1.355×10^{-12} $cal \cdot s^{-1} \cdot cm^{-2} \cdot K^{-4}$

ϵ = emissivity of platinum = f (T)

h = heat transfer coefficient 1.4×10^{-2} $cal \cdot cm^{-2} \cdot s^{-1}$

Gas flow rates, stoichiometric ratio and cold-gas velocity for each flame is provided in Table A-1.

TABLE A-1. FLAME CONDITIONS

No.	Feed Gas Flow Rates, L/s						S.R.[1]	To,[2] °C	T_{max}℄,[3] °C	Vo,[4] m/s
	CH_4	H_2	N_2	CO_2	O_2	Air				
1	0.227	0	0	0	0	1.99	0.92	1820	1680	0.38
2	0.203	0	0	0	0	1.99	1.03	1820	1680	0.38
3	0.180	0	0	0	0	1.99	1.16	1630	1540	0.37
4	0	1.29	0	0	0	3.04	1.0	1882	1805	0.78
5	0	0.85	0	0	0	1.94	0.96	1680	1600	0.50
6	0	0.53	0	0	0	1.98	1.58	1315	1280	0.45
7	0.252	0	0	0	0	2.42	1.01	1954	1850	0.48
8	0.215	0	0	0	0	2.42	1.18	1727	1630	0.47
9	0.195	0	0	0	0	2.42	1.30	1602	1515	0.47
10	0.083	0	0	0	0	1.21	1.52	1478	1360	0.23
11	0.221	0	0	0	0.49	2.05	2.09	1734	1670	0.50
12	0.221	0	0.37	0	0	2.05	0.98	1729	1640	0.48
13	0.221	0	0	0.26	0	2.05	0.98	1730	1670	0.46
14	0	0.61	0	0	0	2.42	1.67	1260	1200	0.49

[1] Stoichiometric Ratio

[2] Peak Flame Temperature

[3] Peak Centerline Temperature

[4] Face Velocity

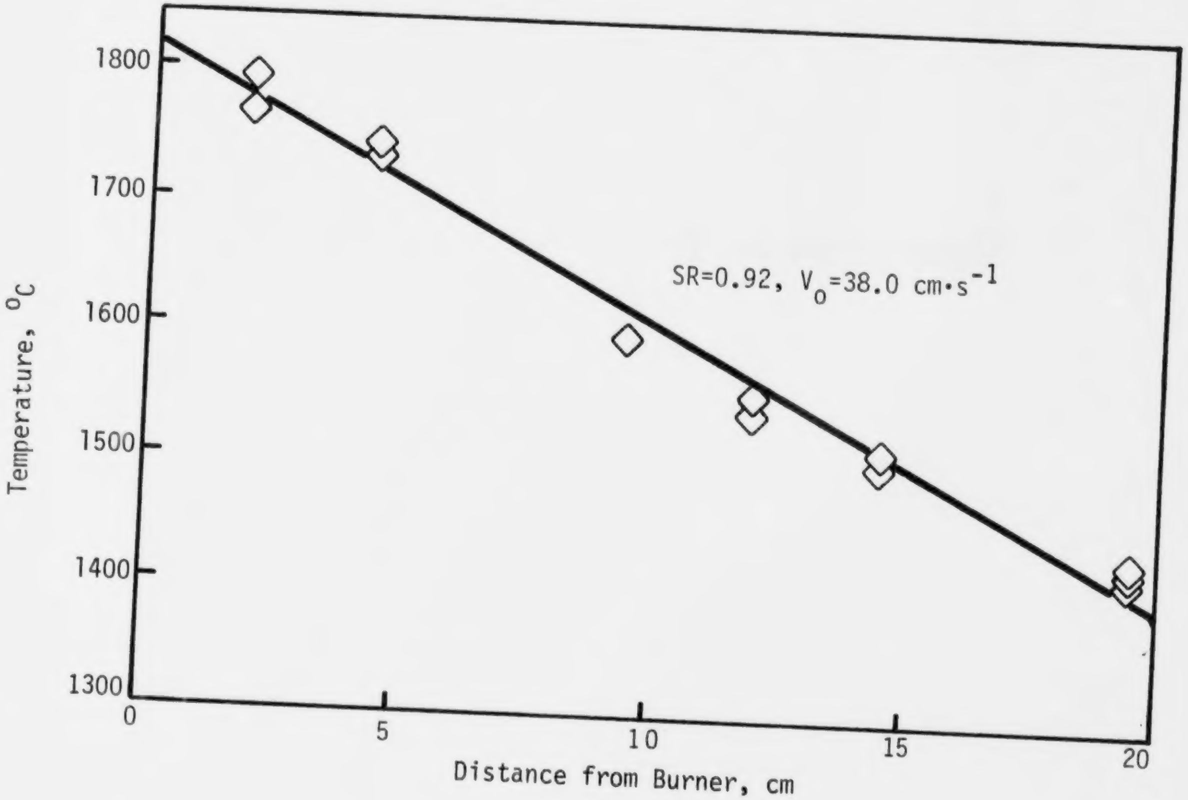

Figure A-1. Gas temperature profile in a CH_4-air flame.

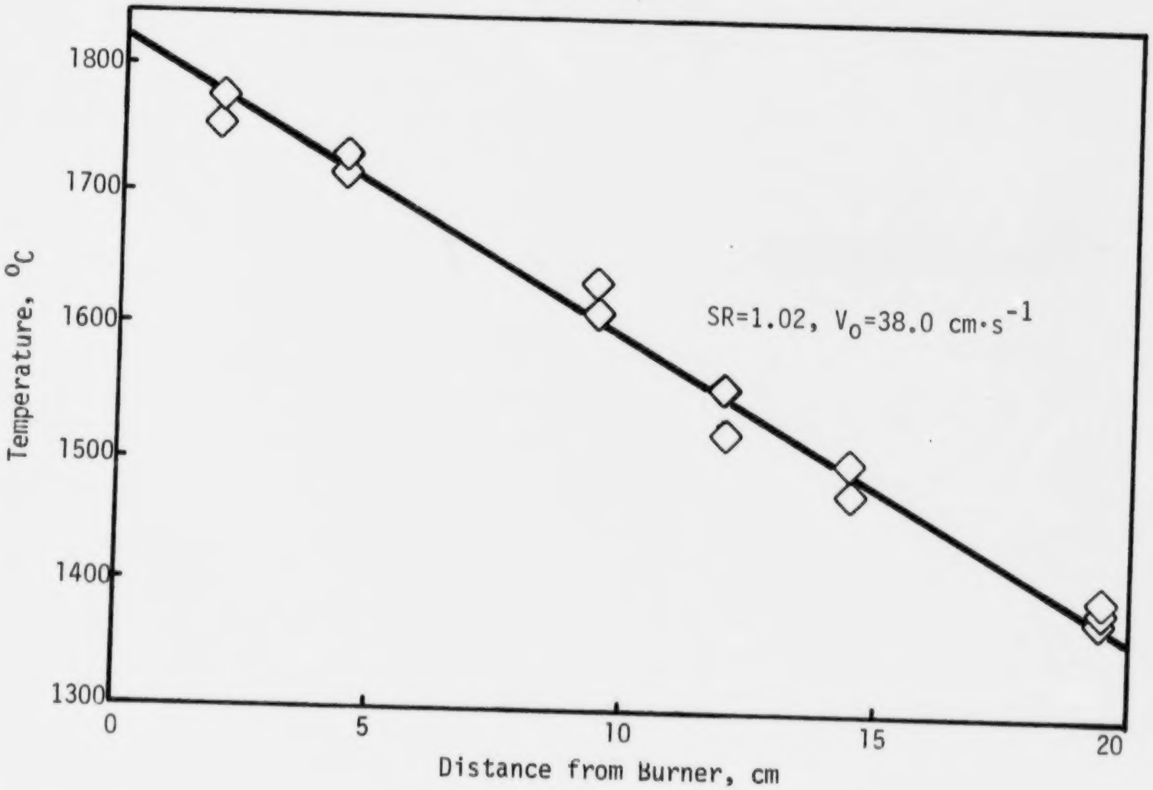

Figure A-2. Gas temperature profile in a CH_4-air flame.

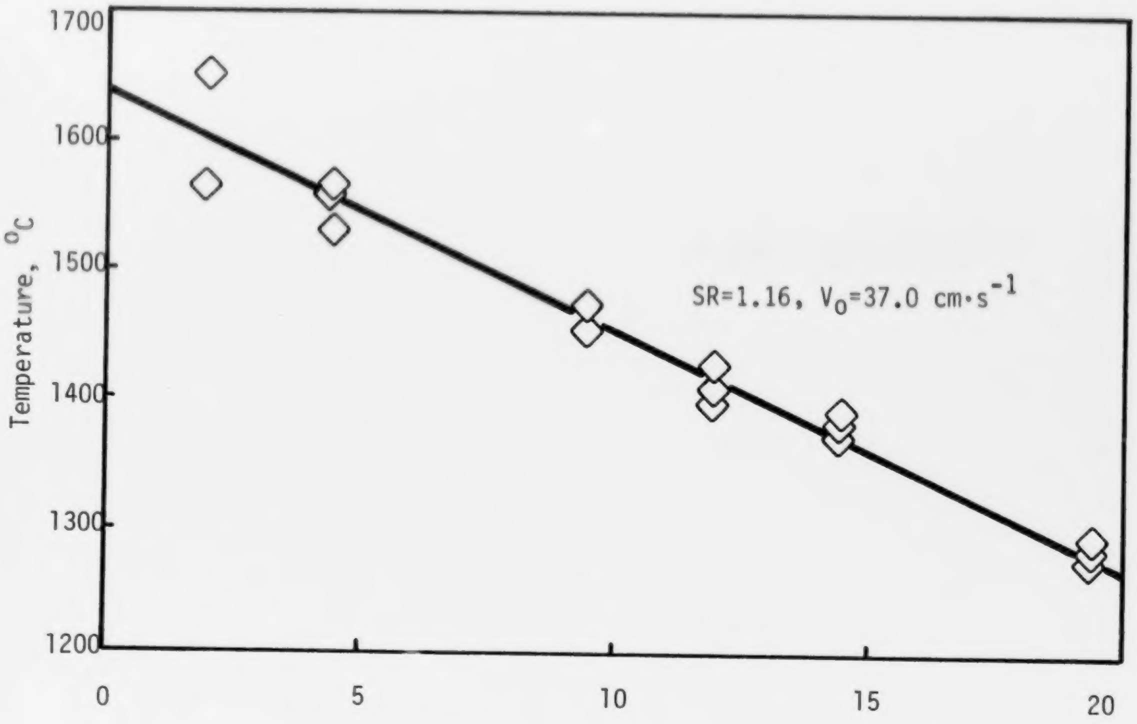

Figure A-3. Gas temperature profile in a CH_4-air flame.

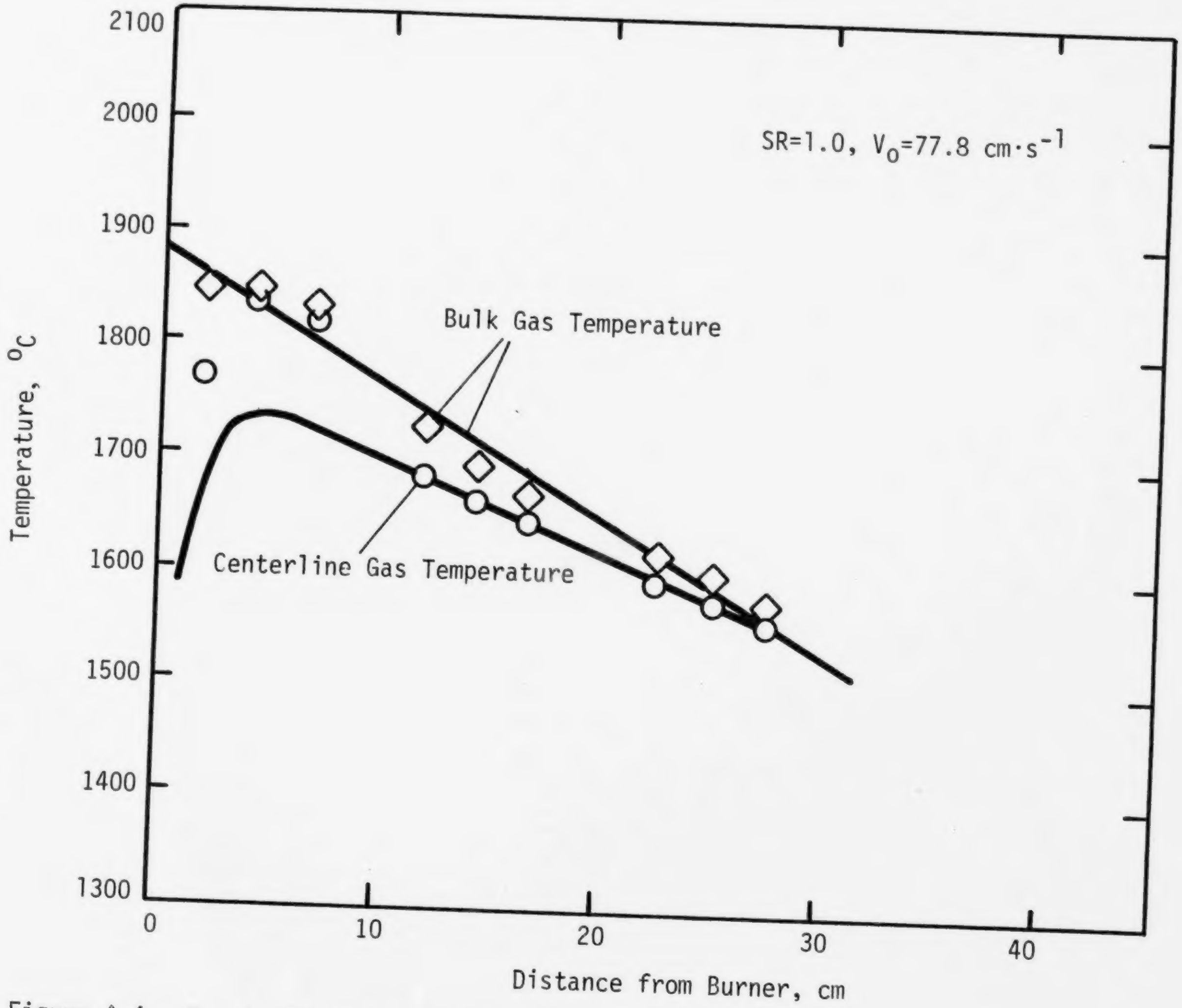

Figure A-4. Gas temperature profile in an H_2-air flame.

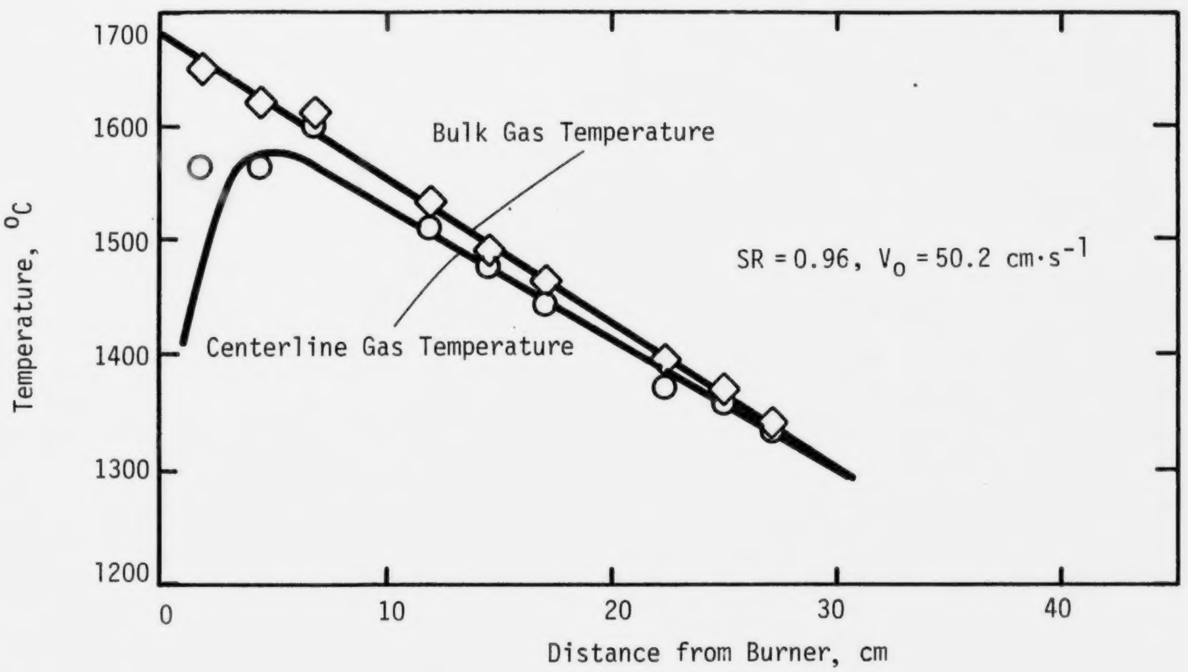

Figure A-5. Gas temperature profile in an H_2-air flame

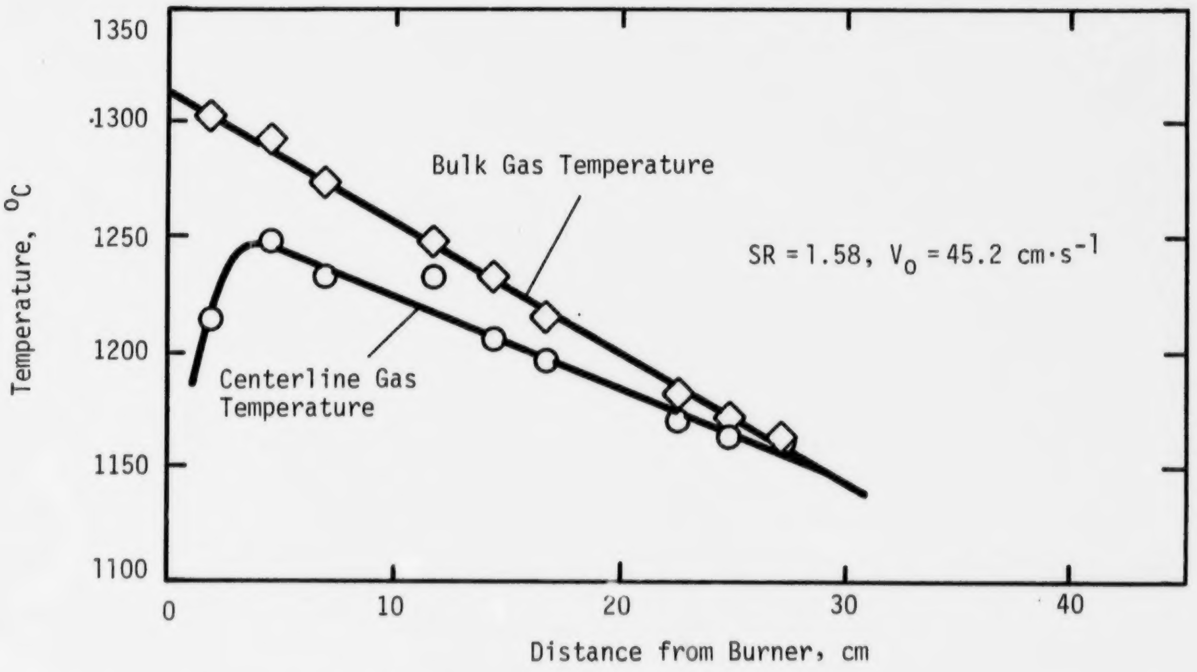

Figure A-6. Gas temperature profiles in an H_2-air flame.

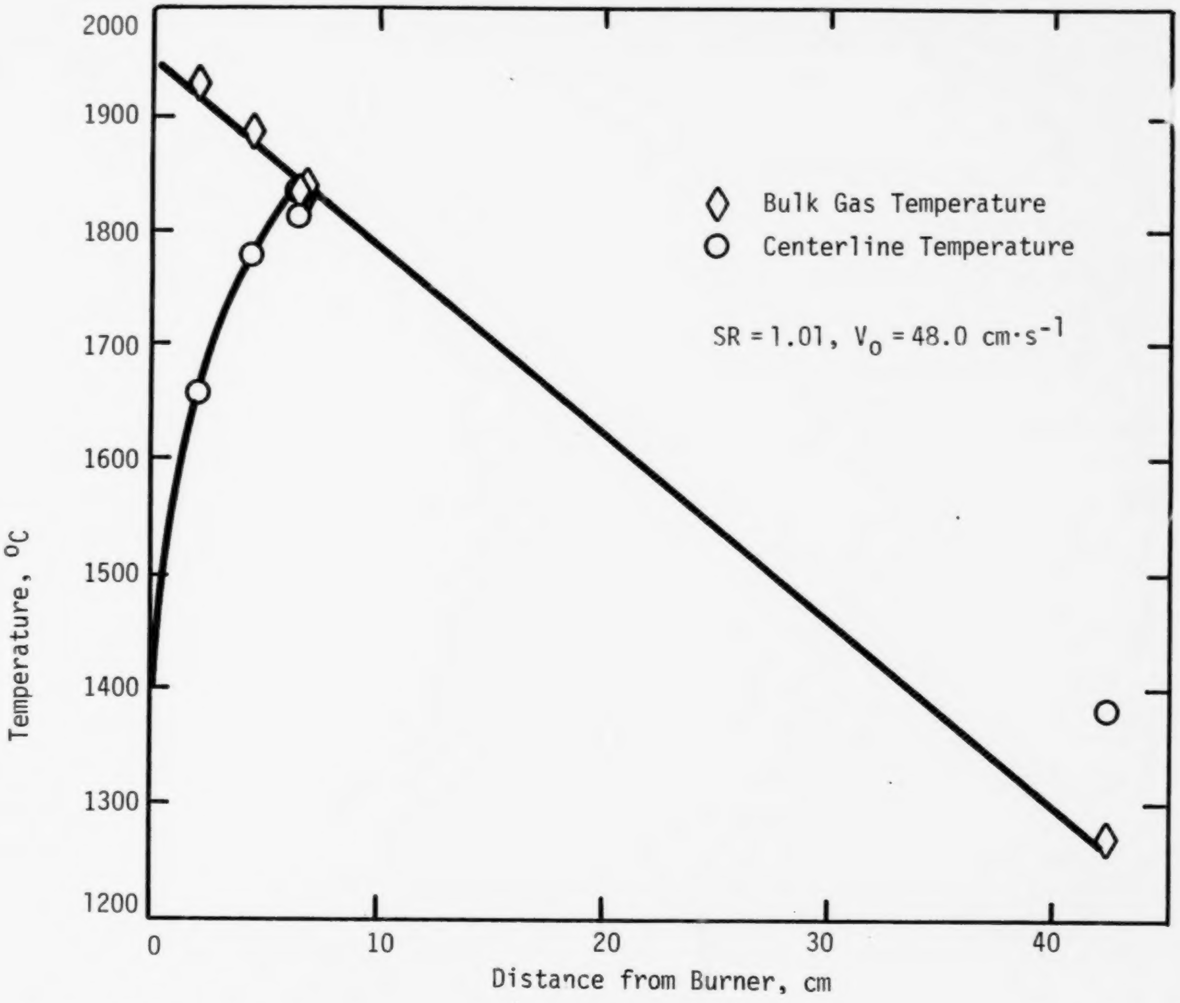

Figure A-7. Gas temperature profile in a CH_4-air flame.

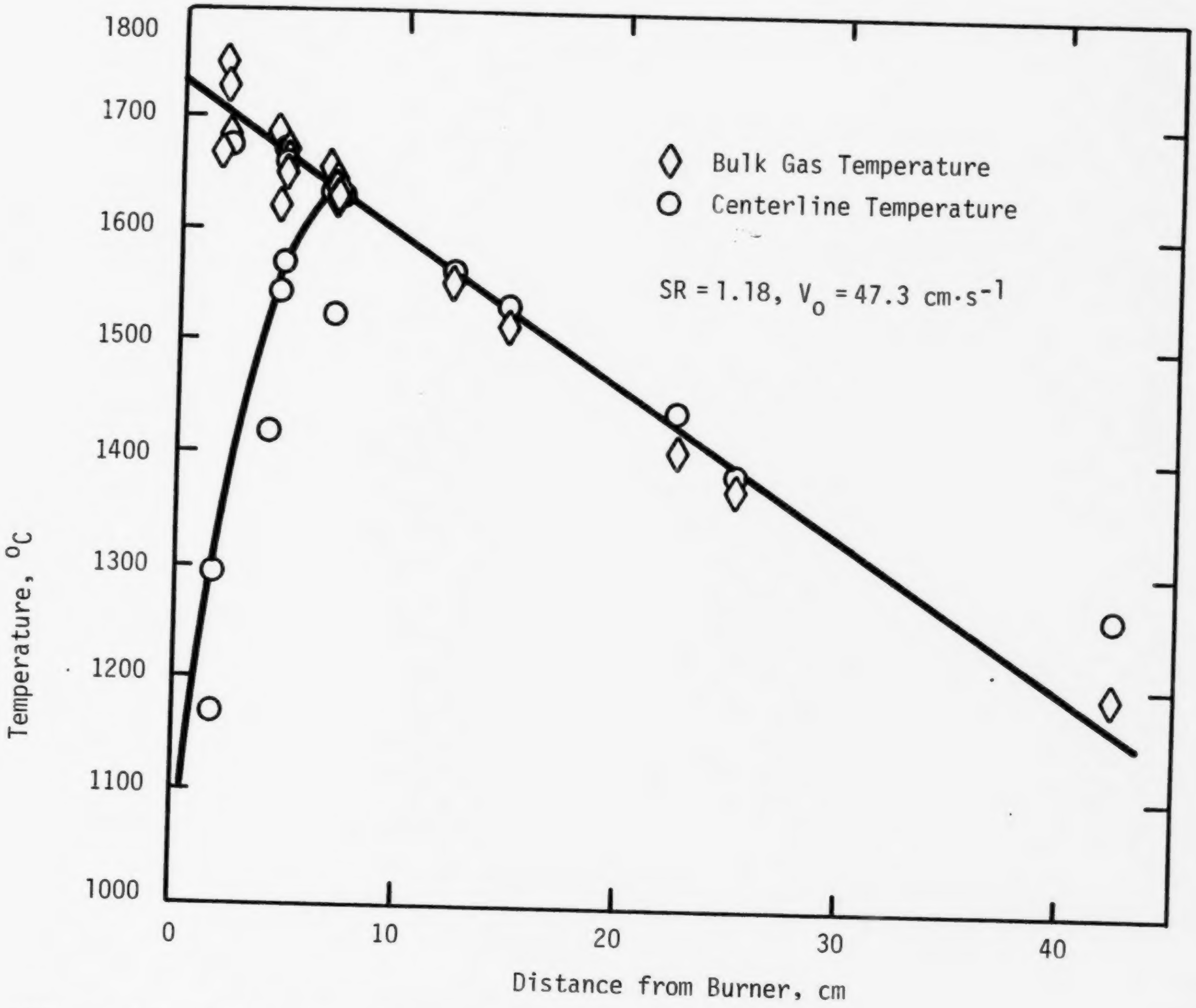

Figure A-8. Gas temperature profile in a CH_4-air flame.

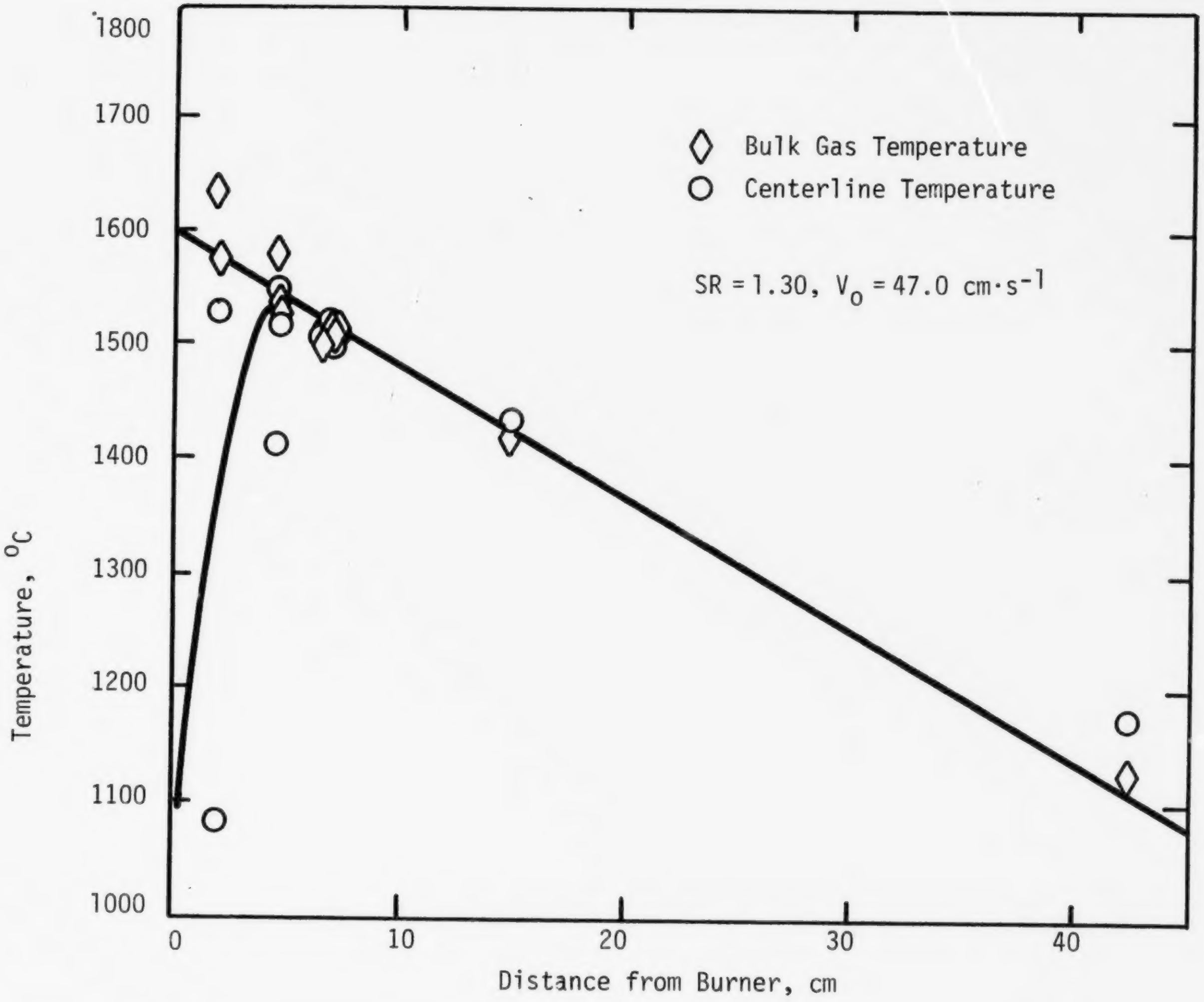

Figure A-9. Gas temperature profile in a CH_4-air flame.

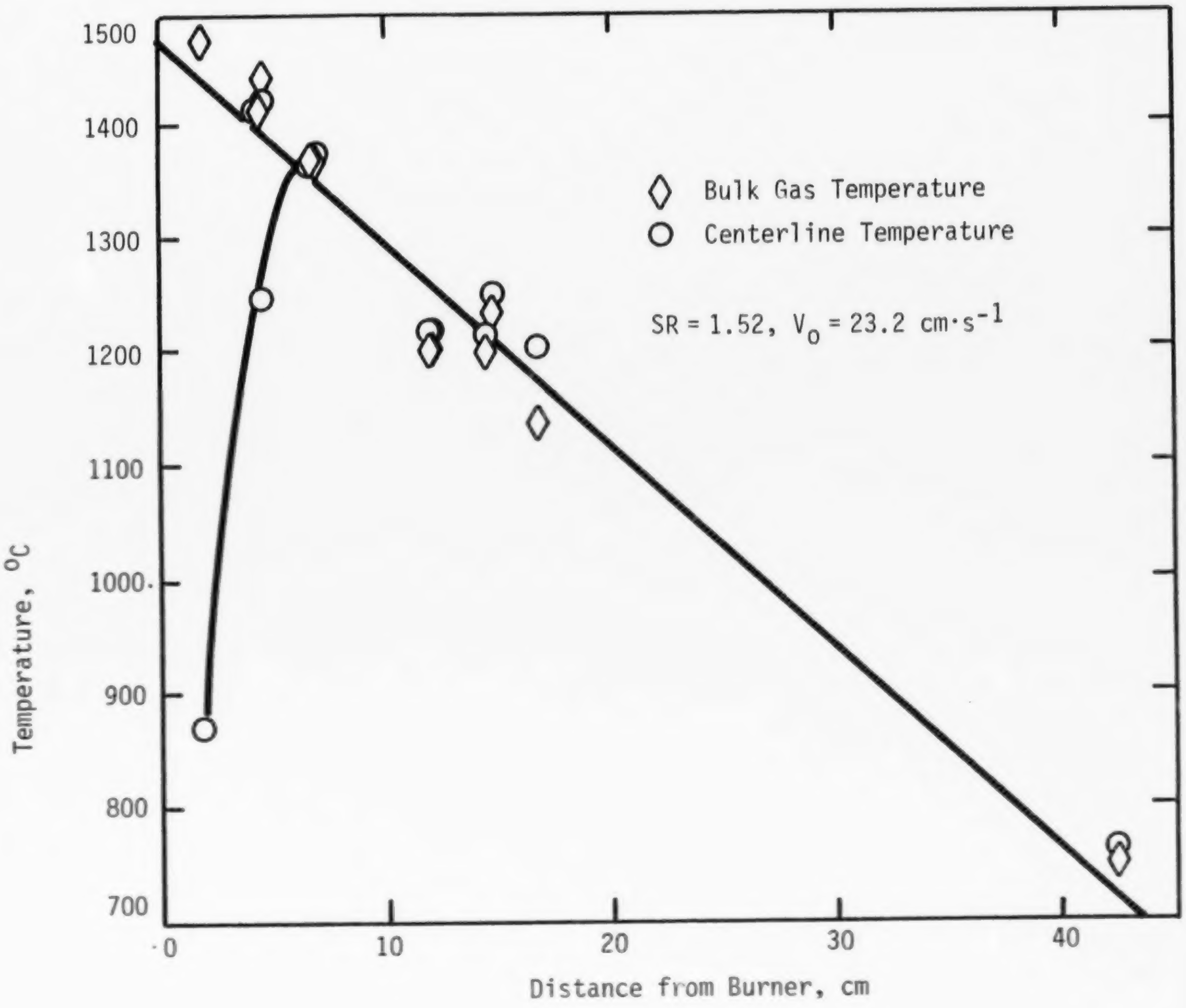

Figure A-10. Gas temperature profile in a CH_4-air flame.

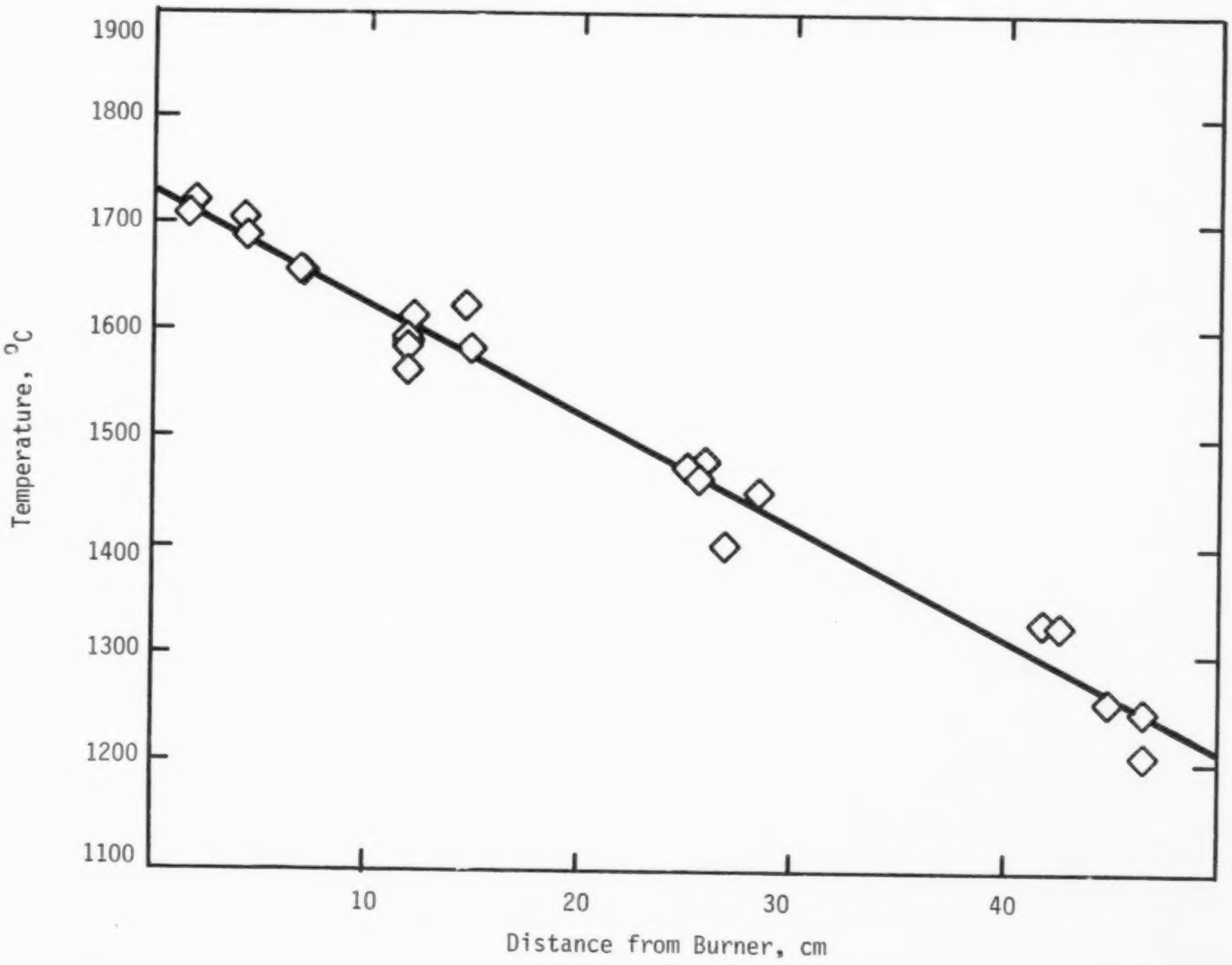

Figure A-11. Gas temperature profile in a CH_4-air flame.

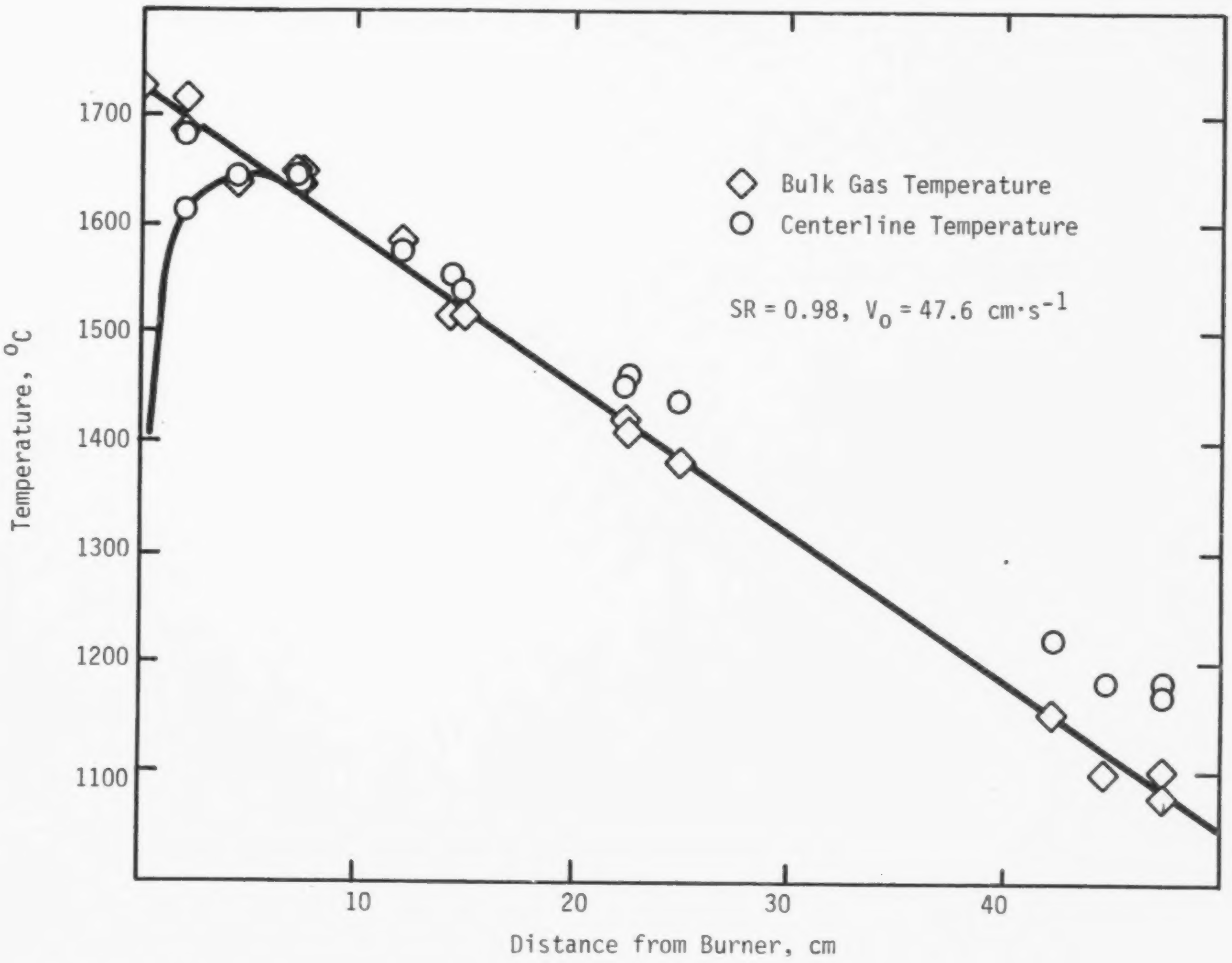

Figure A-12. Gas temperature profile in a CH_4-air-N_2 flame.

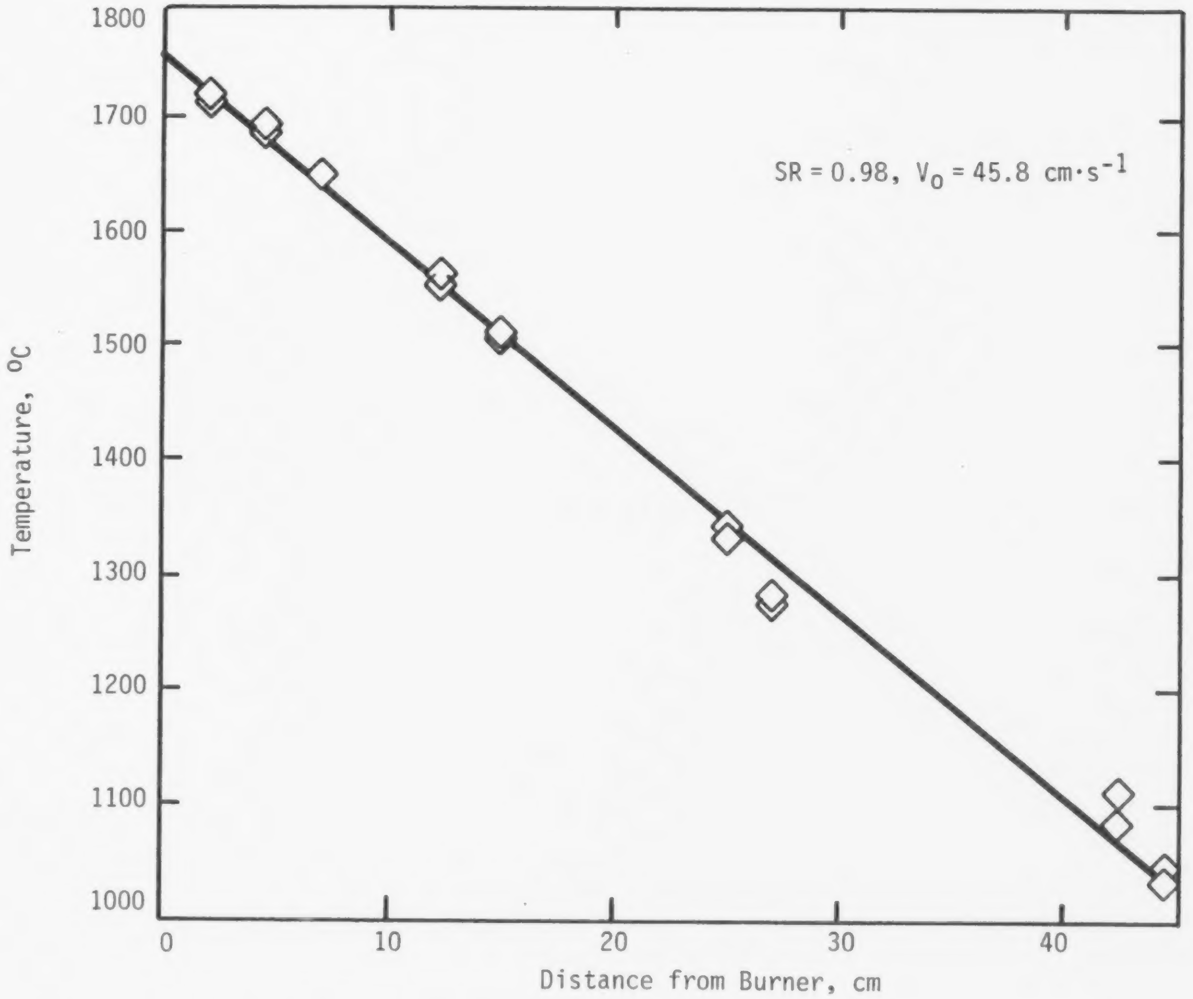

Figure A-13. Gas temperature profile in a CH_4-air-CO_2 flame.

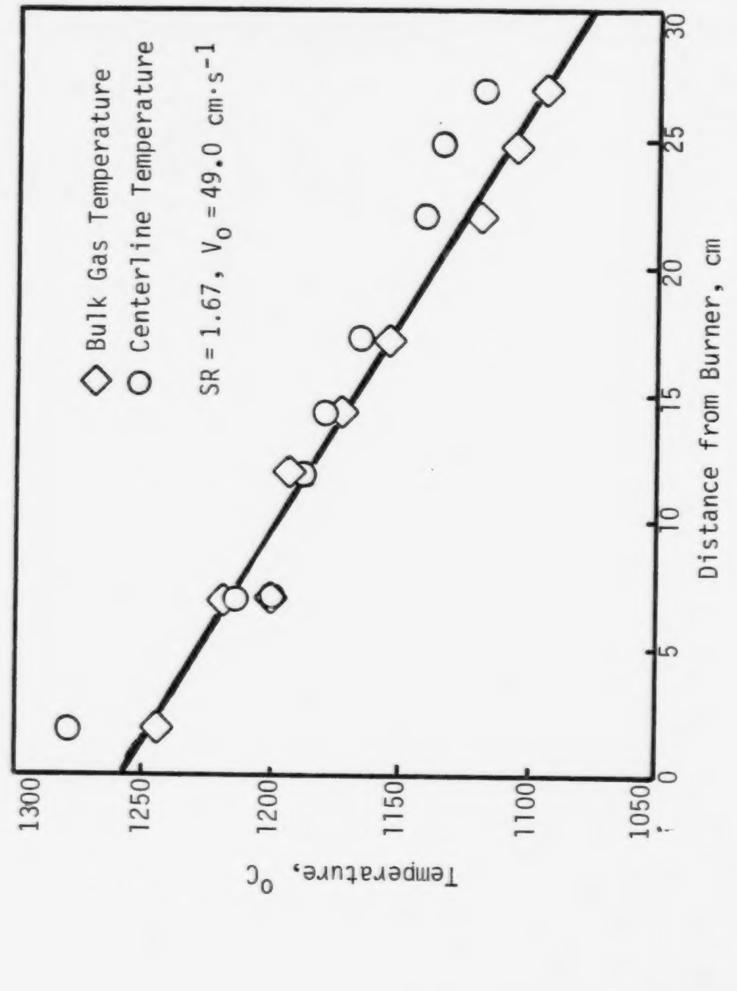

Figure A-14. Gas temperature profile in an H_2-air flame.

APPENDIX B

SORBENT MATERIAL AND MINERAL DATA

Limestone sorbents were generally selected from those employed previously in pilot-scale or bench-scale sorbent study programs. With one exception, the sorbents were taken from the same lots as those used in the boiler-simulator furnace (BSF) program. The exception was calcium hydroxide (hydrated lime) for which Fisher A.C.S. reagent grade material was used.

A high-calcium limestone, Vicron 45-3, was used as the base-case sorbent for the program. Also, employed were calcium hydroxide, a fertilizer grade dolomite, Marblewhite 125 (essentially a larger size cut of Vicron) and a Michigan marl, an impure limestone containing metal oxides and an organic component (approximately $CH_{0.8}N_{0.041}$) which accounts for nearly 5 percent of the sorbent mass.

Table B-1 lists the approximate chemical properties of the sorbents as determined by an outside laboratory (Hazen; Golden, CO). The N_2-BET surface area and loss-on-ignition (LOI) were measured in-house while the mean-size and density data were determined by a second outside laboratory (Micron-Data Lab; Mission Viejo, CA). The data presented in Table B-1 are accurate only for the analyzed sample. Both physical and chemical properties varied slightly from batch to batch. However, the data in Table B-1 are representative.

TABLE B-1. PHYSICAL AND CHEMICAL PROPERTIES OF SORBENTS AND MINERALS

Sorbent	Theoretical Composition	Physical Properties				Chemical Analysis (% Weight [Hazen])						
		Mean Size (μm)	Density (gm/cm^3)	Surface Area (m^2/gm)	Loss on Ignition (950^{o}C), wt-pct.	Ca	Fe	Al	Na	Mg	K	Si
Vicron 45-3	$CaCO_3$	11.0	2.757	0.9	44.0	39.2	0.037	0.07	0.022	0.485	0.11	0.07
Michigan Marl	$CaCO_3$	18.0	2.533	1.52	42.0	25.0	0.873	1.09	0.188	0.931	0.444	9.29
Dolomite	$CaCO_3$ $MgCO_3$	34.0	2.855	0.64	47.1	21.0	0.102	0.09	0.033	12.1	0.039	0.37
Hydrated Lime	$Ca(OH)_2$	12.5	2.24[1]	14.1	25.6	54.0[1]	0.02	--	--	0.3	--	--
Marblewhite 125	$CaCO_3$	30.0	2.71	0.45	42.8	38.8[1]	0.03	0.26	--	0.48	--	0.47
25% Vicron 45-3/ 75% Indiana Ash	--	--		4.61	19.9	--	--	--	--	--	--	--
Calcium Sulfide	CaS	Pwdr	2.5	1.09	21.0	55.5[1]	--	--	--	--	--	--
Kaolinite	$Al_4Si_4O_{10}$ $(OH)_8$	5.0[1]	2.58[1]	9.39	15.02	0.36	0.21	20.3	0.20	0.154	.03	21.14
Bentonite	$(Al_3,Fe_5,mg)\cdot Si_{12}O_{30}(OH)_6$ Na_3 Ca	45.0[3]	--	140.0	22.2	0.65[1]	3.60	21.08	2.57	2.67	--	63.02
Alumina	Al_2O_3	Pwdr	3.97	0.54	0.51	--	0.001	52.9[1]	0.1	--	--	.001
Silica	SiO_2	+240[2]	2.3	0.85	--	--	--	--	--	--	--	45.7[1]
Silica	SiO_2	-140[2]	2.3	0.60	--	--	--	--	--	--	--	45.7[1]
Sodium Carbonate	Na_2CO_3	Pwdr	2.53	--	--	--	--	--	43.4[1]	--	--	--
Ferric Oxide	Fe_2O_3	Pwdr	5.24	9.87	--	--	73.7[1]	--	--	--	--	--

[1] Analysis as supplied

[2] Sieve size

[3] As determined by sieve.
Sedimentation provides 2.4 μm mean size.

APPENDIX C

TWO-COLOR PYROMETRIC PARTICLE TEMPERATURE MEASUREMENTS

Table C-1. TWO-COLOR PYROMETRIC PARTICLE TEMPERATURE MEASUREMENTS FOR VICRON 45-3 CO-INJECTED WITH CH_4-AIR INTO A STOICHIOMETRIC HYDROGEN-AIR FLAME AT $T_o = 1917^oC$ AND $V_o = 77.8\ cm.s^{-1}$

Distance from Burner	0.75cm	0.9cm	1.1cm	1.3cm	1.75cm	2.3cm	3.0cm
Estimated Residence Time	1.3msec	1.6msec	1.9msec	2.3msec	3.1msec	4.1msec	5.3msec
Temperature, °C	1355 1573 1752 1725	1419 1344 1139 1211	1788 1602 1859	1388 1349	1420 1861 1795	1445 1730 1802	1263 1683 1889 1856
Mean $\pm$ σ	1601 ±182	1338 ±172	1750 ±133	1419 ±98	1692 ±238	1659 ±189	1798 ±95

APPENDIX D

CALCINATION AND SULFATION MODELS

In order to support the experimental work a random pore model has been developed at EER, based on similar work by Bhatia (25), to describe sulfation in calcined limestone. The model considers the internal structure of the particle to be given by a set of overlapping, random-sized, cylindrical pores. The reaction is initiated at the pore surface and a layer of reaction product (calcium-sulfate) forms around the pore. This reaction product layer separates the pore surface and the solid reactant surface. The gas (SO_2) must diffuse through the product layer to the surface of the solid reactant (CaO) where the sulfation reaction takes place.

Model Development

The model considers boundary layer diffusion and pore diffusion of the gas reactant. The resulting governing equations are:

$$\frac{1}{r^2}\frac{\partial}{\partial r}\left(D_e\, r^2 \frac{\partial C}{\partial r}\right) = \frac{\alpha\, \rho (1-\varepsilon_0)}{Mb}\frac{dX}{dt} \qquad \text{(D-1)}$$

$$\frac{dX}{dt} = \frac{K_s\, S_0\, C\, (1-X)\sqrt{1 - \psi \ln (1-X)}}{(1-\varepsilon_0)\, [1 + \frac{\beta z}{\psi}\sqrt{1 - \psi \ln (1-X) - 1)}]} \qquad \text{(D-2)}$$

Equation 1 describes the diffusion of gaseous reactant into the pore while Equation 2 gives the local rate of conversion (accounting for the effect of the product layer diffusional resistance).

The boundary conditions are:

$$\frac{\partial C}{\partial r} = 0 \qquad \text{at } r = o \tag{D-3}$$

and

$$D_e \frac{\partial C}{\partial r} = k_b \, (C_\infty - C) \qquad \text{at } r = R \tag{D-4}$$

where k_b is the boundary layer mass transfer coefficient and C is the concentration of gas reactant at the free stream. The governing equations, (D-1), (D-2) and the boundary condition equations (D-3) and (D-4) constitute the complete system for the pore model. These equations were nondimensionalized and solved numerically in the following manners:

- Equation (D-1) and boundary condition (D-3) and (D-4) were integrated

- Equation (D-1) and boundary condition (D-3) and (D-4) were integrated numerically by finite-difference method to give the intraparticle concentration distribution.

- Equation (D-2) was simultaneously integrated (using a fourth-order Runge-Kutta scheme) to give local conversion.

The intrinsic reaction rate for sulfation and product layer diffusion were obtained from Bhatia's (28) analysis of Borgwardt's (20) sulfation data:

$$K_s = 1890 \; \frac{\text{cm}^4}{\text{g-mol} \cdot \text{sec}} \; \exp\left(\frac{-6794\text{K}}{T}\right) \tag{D-5}$$

$$D_p = 0.0528 \; \frac{\text{cm}^2}{\text{sec}} \; \exp\left(\frac{-14092\text{K}}{T}\right) \tag{D-6}$$

This model has been used to assess the impact of loss of surface area on the rate of sulfur capture.

Thermal Interactions

The thermal response of limestones injected into any combustion system is what ultimately determines the physical and chemical interactions that will take place. Accurate interpretation of these interactions in turn requires knowledge of the thermal history of the particles.

Thermal history depends upon the heat capacity of the particle, convective heat transfer between the particle and the surrounding gas, radiative heat transfer between the particle and the walls of the combustion system, and heat consumption in the endothermic calcination process. The EER calcination model treats these according to the following equation:

$$\frac{dT_p}{dt} = \frac{6}{D^3\pi\rho_p[\alpha C_{p_1} + (1-\alpha)\frac{M_2}{M_1} C_{p_2}]} \quad x$$

$$\left\{[\pi\cdot D\cdot Nu\cdot K\cdot(Tg-Tp)] + [\pi\cdot\varepsilon_r\cdot D^2\sigma\cdot(T_w^4-T_p^4)] + \left[\frac{D^3\pi\rho_p}{6M_1}\Delta H_r \frac{d\alpha}{dt}\right]\right\} \qquad (D-7)$$

A second differential equation is used to describe the reaction kinetics. Data of Borgwardt (20) and Coutant (5) taken in differential and dispersed-phase reactors at temperatures ranging from 820 to 1360K and particle sizes ranging from 1.5 to 90 μm can be described by exponential calcination:

$$\frac{d\alpha}{dt} = -\alpha K_{rxn} \qquad (D-8)$$

for the particle size independent reaction rate constant:

$$K_{rxn} = 1.861 \times 10^8\ s^{-1}\cdot\exp\left(\frac{-23187K}{T_p}\right) \qquad (D-9)$$

Data of Gallagher and Johnson (29) taken isothermally and dynamically in a furnace at temperatures between 880 and 980K with 1- to 32-mg samples of packed 20-44 μm powder can be described by shrinking core calcination:

$$\frac{d\alpha}{dt} = -2\, K_{rxn} \sqrt{\alpha} \qquad \text{(D-10)}$$

For the particle size dependent reaction rate constant:

$$K_{rxn} = \left[\exp 2.303 \cdot \left[\left(\frac{636.7K}{T_p} - 1.3152 \right) \log \left(\frac{m}{m_g} \right) \cdot 8.4026 - \frac{10855K}{T_p} \right] \right] \qquad \text{(D-11)}$$

Figures D-1, D-2 and D-3 show the effects of assumptions about calcination kinetics, particle diameter and gas temperature on particle heatup rates. The latter two figures also include the rate of calcination as predicted by the models.

Effects of calcination kinetics and mode of heat transfer are examined in Figure D-1. Particle heatup as predicted by the EER model is shown utilizing Borgwardt exponential kinetics, Gallagher and Johnson shrinking core kinetics, and instantaneous kinetics (heat transfer controlled calcination). Also shown is a model which only allows for radiation heating of the particles.

The fast-kinetics model is the simplest. It assumes that at a fixed temperature (780°C) the calcination reaction is "switched on". Heat is then consumed by the endothermic calcination reaction as fast as it is transferred to the particle by convection. When the calcination reaction is complete, the temperature rise resumes.

The Gallagher and Johnson kinetics are based on the shrinking-core concept and the calcination data of Gallagher and Johnson. In this model it is assumed that the calcination occurs at an interface which moves toward the center of the particle, leaving a product layer of CaO around the outside. Heat must then diffuse across the product layer to the calcination interface. Calcination occurs between 780°C and 930°C in this model.

The Borgwardt kinetics model is derived from dispersed-phase reactors and differential reactor data for calcination of 1.5- to 90-μm particles between 530°C and 1130°C. Figure D-4 shows that those data extrapolate quite

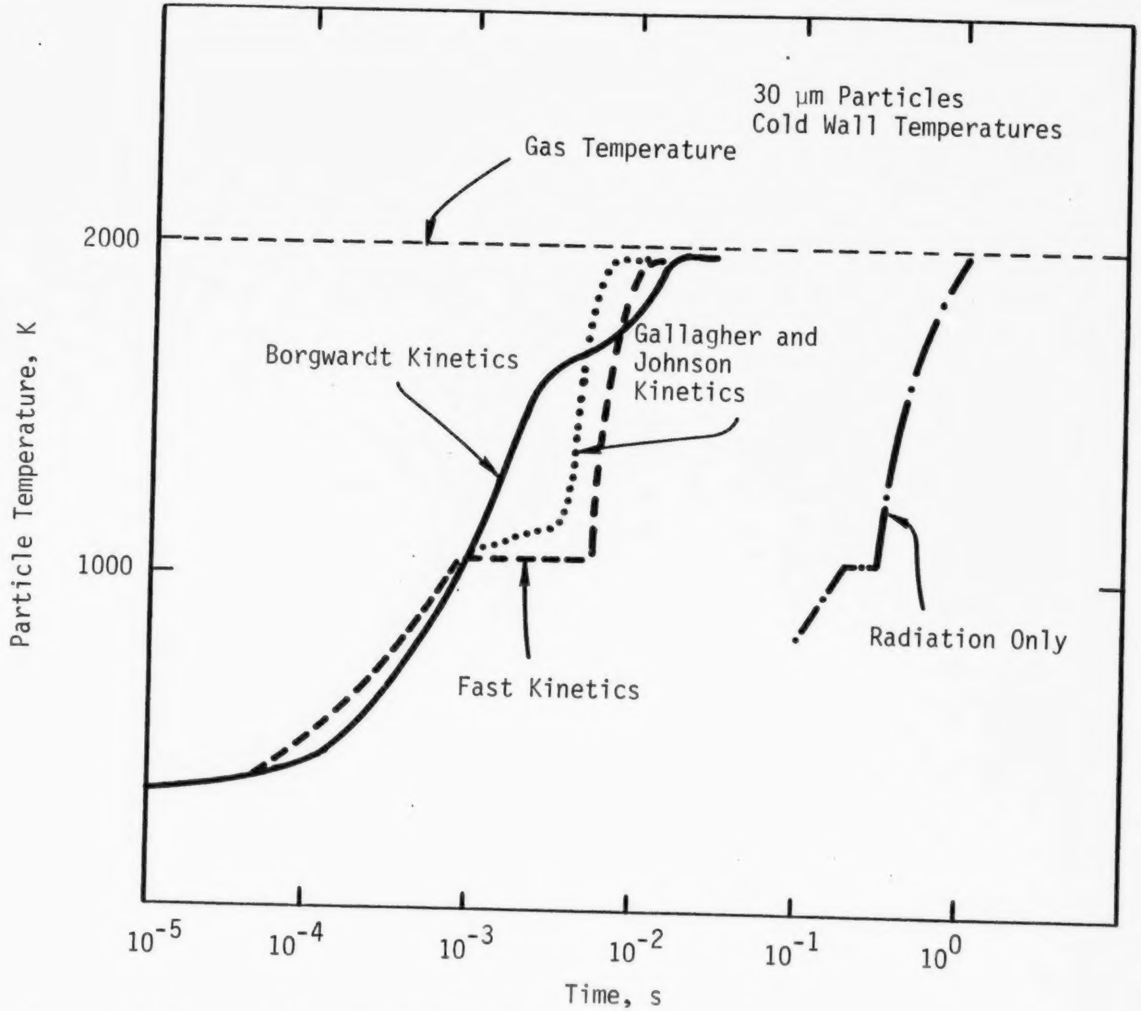

Figure D-1. Comparison of different kinetic models for calcination of 30μm limestone particles at 1730° C.

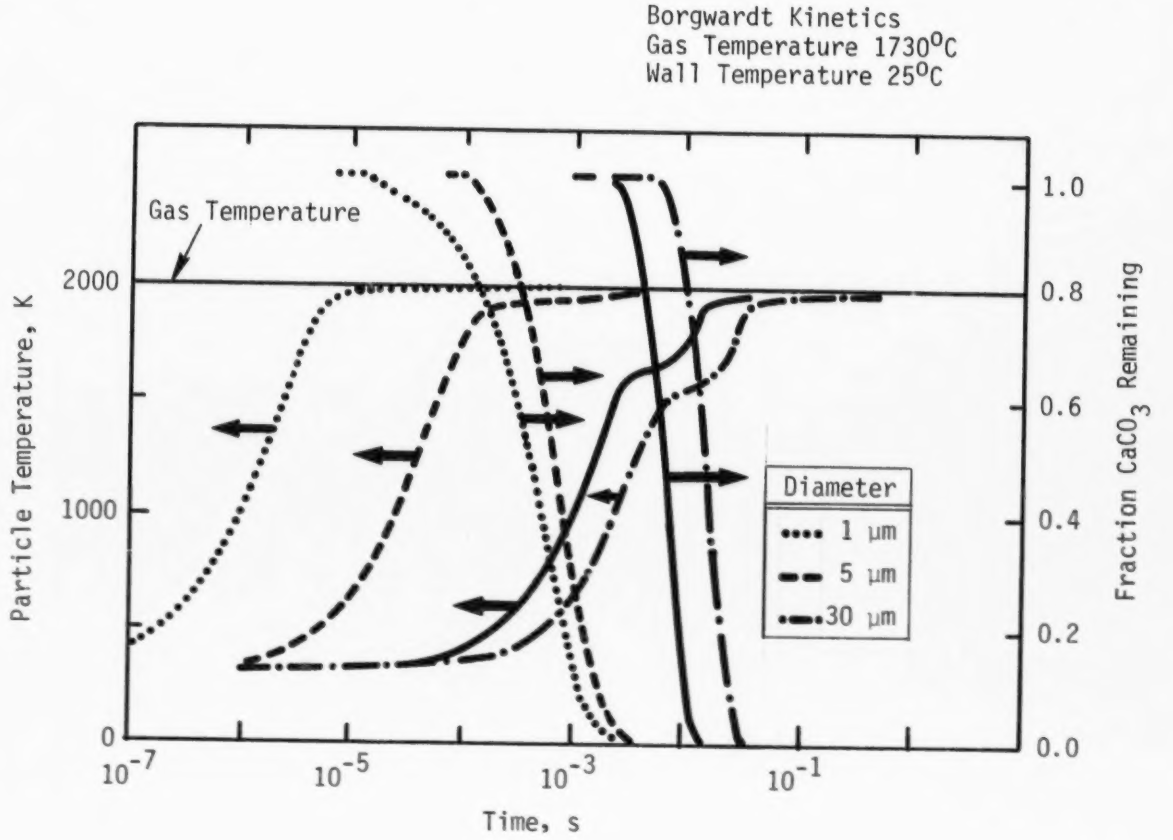

Figure D-2. The effect of particle size assumptions on the heating and calcination rates of limestone.

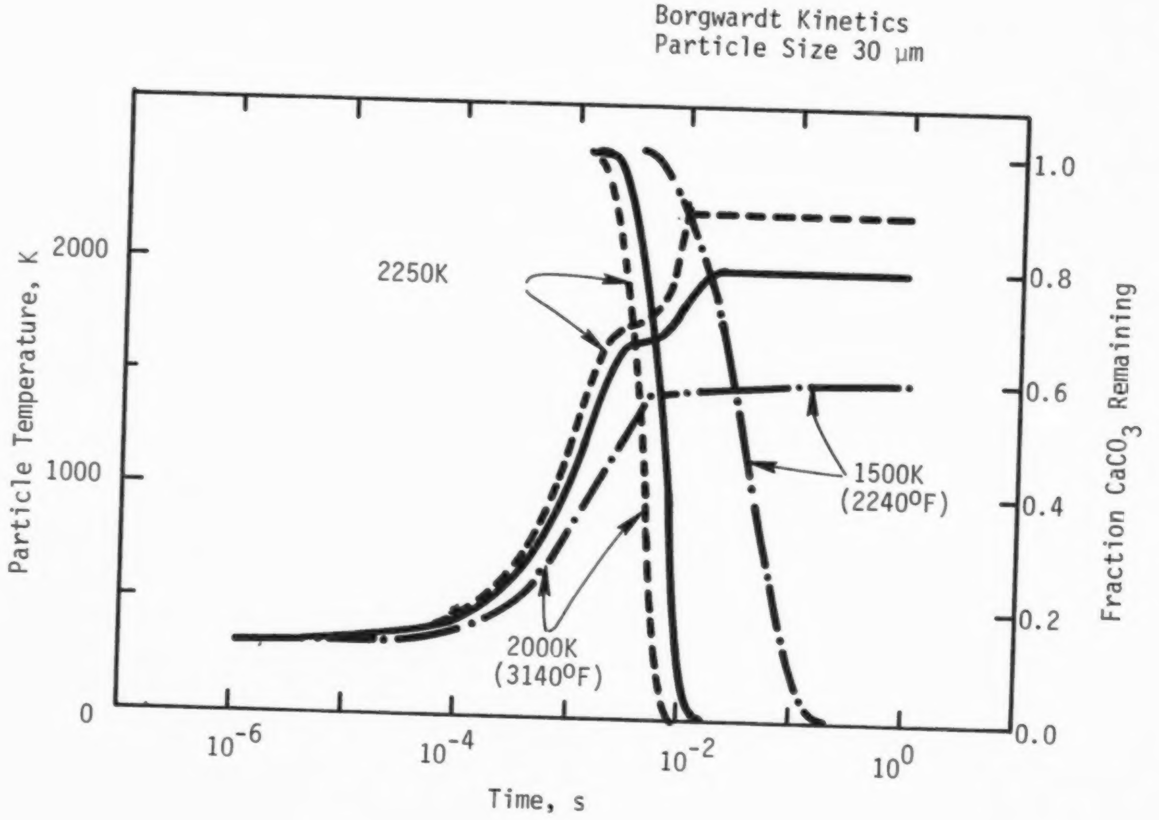

Figure D-3. The effect of gas temperature on model assumptions for 30 μm limestone particle heating and calcination.

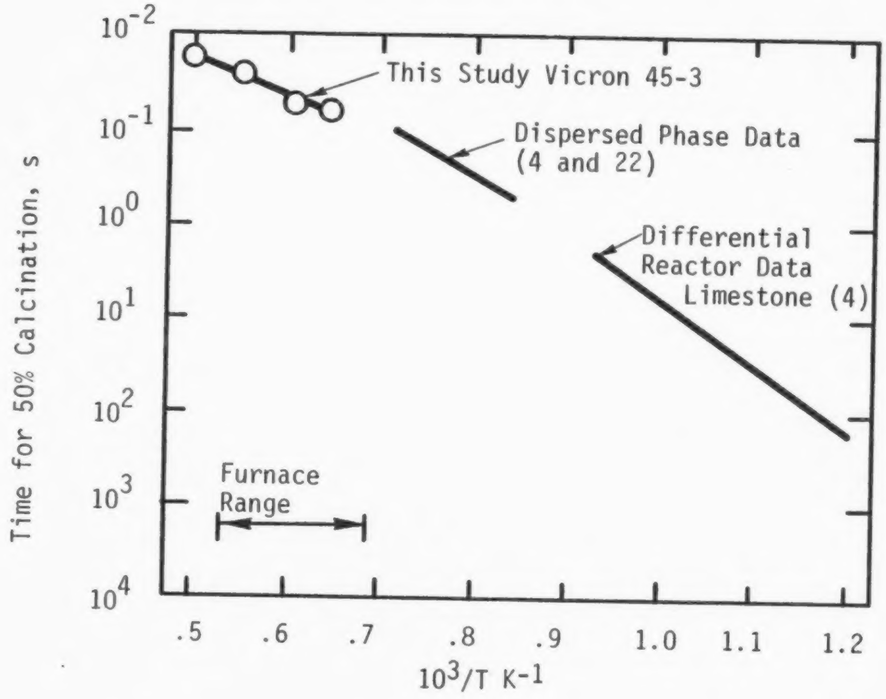

Figure D-4. Times for 50 percent calcination of Vicron 45-3 (this work) and similar limestones over the temperature range of 500°C-1750°C.

well to the results of this study. In this model the calcination reaction affects the particle temperature rise only slightly prior to 1130°C. At temperatures greater than 1130°C the reaction rate (fitted to an exponential temperature-dependent rate equation) is still somewhat slower than predicted by the previous models.

It should be noted that the differences between predictions utilizing Borgwardt kinetics and Gallagher and Johnson kinetics is due mainly to the differences in reaction rate constants. Because the Borgwardt data requires less extrapolation and because it agrees fairly well with EER data, Borgwardt kinetics has been chosen for further modeling studies. However, this does not necessarily mean that exponential decay kinetics are superior to shrinking core kinetics, especially at high temperature where mass transfer effects are expected to become increasingly significant.

The EER convective heatup model with Borgwardt calcination kinetics is tested in Figure D-2 for the effects of particle size. Not surprisingly, the heatup rate increases dramatically with decrease in particle diameter. For the smallest particles (1 μm), however, the heatup is much faster than the calcination reaction which then occurs nearly isothermally at about 1730°C (3150°F). Even for 5 μm particles the calcination reaction does not significantly perturb the heatup rate. In Figure D-3, the effect of gas temperature is taken into account and it is shown that both calcination and heatup are significant.

In reality, the particles do not encounter a step change in temperature. Even when sorbent is co-fired with a fuel-air mixture there is a measurable rise in the injection gas temperature for 25 to 50 ms depending on the flame. Furthermore, the flame-gas temperature is rapidly declining with time. When this variable gas temperature is taken into account, the model prediction closely matches the measured calcination rate (Figure D-5) for 11 μm mean diameter particles. A discrepancy between data and prediction arises because a maximum extent of calcination of only 80 percent is experimentally obtained.

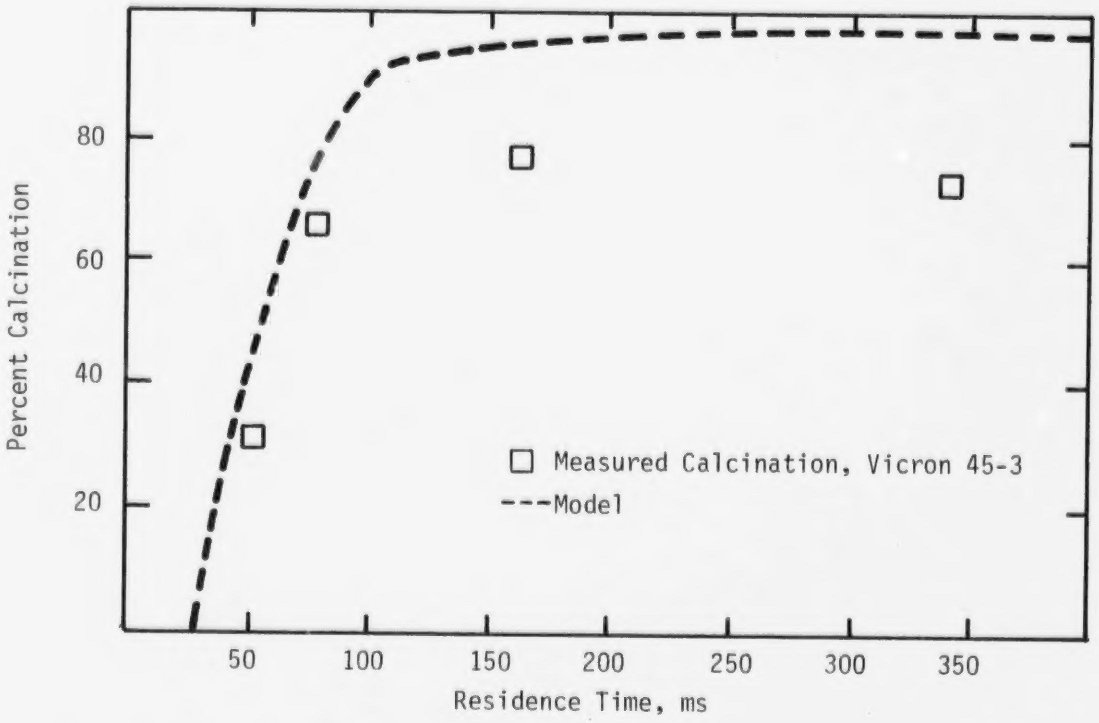

Figure D-5. Comparison of measured data for Vicron 45-3 with the calcination model using the measured gas temperature profile.

For the same particle size, although at a higher peak temperature, the particle heatup prediction has been compared with particle temperature measurements by two-color pyrometry (Figure D-6). The gas temperature experienced by the particles, and used for the modeling predictions, is labeled in the figure as the centerline temperature. The model prediction, shown as the dashed curve, agrees with the measured data quite well.

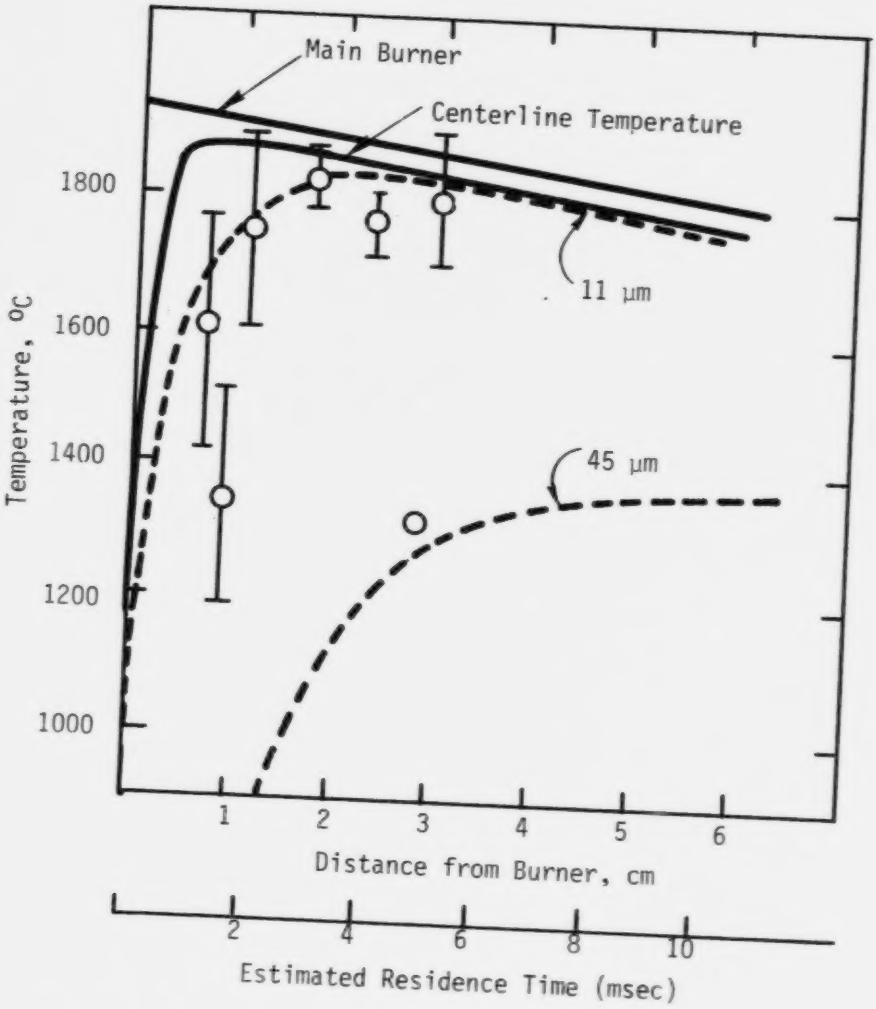

Figure D-6. Measured gas and Vicron 45-3 particle temperatures compared with model predictions for 11μm and 30μm limestone particles at 1830°C.

APPENDIX E

Limestone Samples Data

Table E-1 BET Surface Area Samples Data 139

Table E-2 Vicron 45-3/Kaolin Separate Injection Results . . 148

Table E-3 Sulfur Capture Data (Reactivity Probe) 149

Table E-4 In-Flame Sulfur Capture Data 151

The following abbreviations are used in the tables to improve readability:

V - Vicron 45-3
D - Pfizer Dolomite
Ca - Calcium hydroxide
K - Kaolin
MW, MW125 - Marblewhite 125
B - Bentonite
Al - Al_2O_3
Na - Na_2CO_3
Fe - Fe_2O_3
Si140 - SiO_2, -140 mesh
Si240 - SiO_2, +240 mesh
4A - Union Carbide Type 4A molecular sieve

In addition, an abbreviated notation is used to describe mixtures of materials. For example, a mixture of five percent-by-weight of kaolin in Vicron 45-3 is written as 5K95V.

TABLE E-1. BET SURFACE AREA SAMPLES DATA

Test No.	Sorbent	Fuel	Diluent	Peak Temperature °C	Residence Time, ms	Percent Calcination	N_2-BET Surface Area
2-4-0383	Vicron 45-3	CH_4	-	1530	24.4	24	3.85
2-7-0383	"	CH_4	-	1530	35.5	72	7.5
5-7-0383	"	CH_4	-	1530	72.67	82	8.62
10-7-0383	"	CH_4	-	1530	63.1	52	9.62
4-8-0383	"	CH_4	-	1530	142.1	67	7.39
1-9-0383	Ash/Vicron	CH_4	-	1530	142.1	81	10.23
2-9-0383	"	CH_4	-	1530	63.1	78	9.50
3-9-0383	"	CH_4	-	1530	24.4	82	10.65
4-9-0383	Dolomite	CH_4	-	1530	24.4	93	7.65
8-9-0383	"	CH_4	-	1530	63.1	93	9.7
9-9-0383	"	CH_4	-	1530	142.1	92	12.64
4-11-0383	$Ca(OH)_2$	CH_4	-	1530	63.1	71	8.2
7-11-0383	"	CH_4	-	1530	142.1	68	7.17
6-10-0383	"	CH_4	-	1530	24.4		8.47
2-10-0383	Mich Marl	CH_4	-	1530	142.1	99	3.08
3-10-0383	"	CH_4	-	1530	63.1	97	3.07
4-10-0383	"	CH_4	-	1530	24.4	98	3.52
1-4-0383	Vicron 45-3	CH_4	-	1360	53.7	32	7.57
3-7-0383	"	CH_4	-	1360	78.8	66	10.66
4-7-0383	"	CH_4	-	1360	161.2	77	9.38
1-8-0383	"	CH_4	-	1360	142.5	32	4.67
3-8-0383	"	CH_4	-	1360	341.3	74	8.80
2-11-0383	$Ca(OH)_2$	CH_4	-	1360	53.7	60	6.50
3-11-0383	"	CH_4	-	1360	142.5	70	8.41
8-11-0383	"	CH_4	-	1360	341.3	78	8.31
1-12-0383	Vicron 45-3	CH_4	O_2	1670	133.6	91	5.63
3-12-0383	"	CH_4	O_2	1670	67.8	100	5.24
2-12-0383	"	CH_4	O_2	1670	58.8	94	5.56
4-12-0383	"	CH_4	O_2	1670	33.0	91	5.63

TABLE E-1. BET SURFACE AREA SAMPLES DATA (CONT.)

Test No.	Sorbent	Fuel	Diluent	Peak Temperature °C	Residence Time ms	Percent Calcination	N_2 BET Surface Area, m^2/g
5-12-0383	Vicron 45-3	CH_4	N_2	1640	22.6	87	6.01
2-28-0383	"	CH_4	O_2	1670	21.4	81	4.71
3-28-0383	"	CH_4	O_2	1670	31.3	78	7.53
3-29-0383	"	CH_4	O_2	1670	122.5	69	7.39
1-28-0383	"	CH_4	CO_2	1670	23.2	81	5.72
1-29-0383	"	CH_4	CO_2	1670	33.9	62	7.20
2-29-0383	"	CH_4	CO_2	1670	140.0	81	7.58
3-4-0383	"	CH_4	-	1640	22.8	33	5.06
1-7-0383	"	CH_4	-	1640	33.2	78	3.71
6-7-0383	"	CH_4	-	1640	68.1	84	7.85
9-7-0383	"	CH_4	-	1640	59.1	78	6.28
5-8-0383	"	CH_4	-	1640	133.9	81	7.17
1-24-0383	"	CH_4	-	1640	33.2	80	3.86
4-24-0383	"	CH_4	-	1640	59.1	75	9.27
5-9-0383	Dolomite	CH_4	-	1640	22.8	63	5.15
7-9-0383	"	CH_4	-	1640	59.1	95	6.13
1-11-0383	$Ca(OH)_2$	CH_4	-	1640	22.8	57	12.28
5-11-0383	"	CH_4	-	1640	59.6	80	6.55
6-11-0383	"	CH_4	-	1640	133.9	74	6.49
1-10-0383	Dolomite	CH_4	-	1640	133.9	95	8.90
4-4-0383	Vicron 45-3	CH_4	-	1830	20.2	37	4.55
5-4-0383	"	CH_4	-	1830	39.5	54	4.28
7-7-0383	"	CH_4	-	1830	60.7	76	6.08
8-7-0383	"	CH_4	-	1830	52.6	83	5.52
6-8-0383	"	CH_4	-	1830	120.2	76	5.00
2-24-0383	"	CH_4	-	1830	29.5	86	5.07
3-24-0383	"	CH_4	-	1830	52.6	88	6.89
2-22-0283	"	H_2	-	1805	10.9	48	5.35
3-23=0283	"	H_2	-	1805	68.7	45	4.26
1-21-0283	"	H_2	-	1280	26.4	10	1.80

TABLE E-1. BET SURFACE AREA SAMPLES DATA (CONT.)

Test No.	Sorbent	Fuel	Diluent	Peak Temperature °C	Residence Time, ms	Percent Calcination	N_2 BET Surface Area, m^2/g
3-22-0283	Vicron 45-3	H_2	-	1280	26.4	52	2.06
1-23-0283	"	H_2	-	1280	160.9	34	2.31
1-22-0283	"	H_2	-	1600	18.6	31	3.86
5-22-0283	"	H_2	-	1600	120.0	42	3.78
2-8-0383	Asn/Vicron	H_2	-	1600	---	0	4.61
6-9-0383	Dolomite	H_2	-	1600	---	0	0.90
9-11-0383	$Ca(OH)_2$	H_2	-	1600	---	0	12.10
5-10-0383	Mich Marl	H_2	-	1600	---	0	1.52
1-1-0483	Vicron 45-3	H_2	-	1835	>200	---	2.84
2-1-0483	"	H_2	-	1835	>200	---	1.78
3-1-0483	"	H_2	-	1585	>200	---	2.78
4-1-0483	"	H_2	-	1542	>200	---	5.38
5-1-0483	"	H_2	-	1410	>200	---	5.47
6-1-0483	"	H_2	-	1280	>200	---	6.15
13-1-0483	"	H_2	-	1685	>200	---	2.01
1-21-0383	"	CH_4	-	1680	---	6.7	4.02
2-21-0383	"	CH_4	-	1680	---	40	2.30
1-22-0333	"	CH_4	-	1360	---	35	4.23
2-22-0383	"	CH_4	-	1360	---	24	1.29
3-22-0383	---	---	-	1360	---	0	0.62
11-2-0483	Mich Marl	CH_4	-	1360	78.0	83	5.90
6-12-0483	"	CH_4	-	1360	237	87	9.63
4-12-0483	"	CH_4	-	1640	234	83	4.28
2-12-0483	"	CH_4	-	1640	---	0	2.39
2-11-0483	"	CH_4	-	1360	54	86	7.06
1-11-0483	"	CH_4	-	1630	23	94	4.76
3-12-0483	"	CH_4	-	1630	33	73	8.92
7-12-0483	"	CH_4	-	1630	96	97	3.86
5-12-0483	"	CH_4	-	1630	96	51	7.01
1-13-0483	Dolomite	CH_4	-	1360	237	90	19.48

TABLE E-1. BET SURFACE AREA SAMPLES DATA (CONT.)

Test No.	Sorbent	Fuel	Peak Temperature ^{o}C	Residence Time,ms	Percent Calcination	N_2-BET Surface Area, m^2/g
3-13-0483	Dolomite	CH_4	1360	78	93	11.07
5-13-0483	"	CH_4	Raw	---	0	1.60
4-13-0483	"	CH_4	1360	374	95	11.07
2-13-0483	"	CH_4	1360	54	59	11.31
1-8-0483	Vicron 45-3	H_2	1400	65	90	5.19
2-8-0483	"	H_2	1600	60	92	3.08
3-8-0483	"	H_2	1200	86	80	15.12
7-13-0483	$Ca(OH)_2$	CH_4	1360	374	96	7.36
9-13-0483	"	CH_4	1360	54	90	9.63
6-13-0483	"	CH_4	Raw	---	0	14.09
8-13-0483	"	CH_4	1360	78	88	11.17
2-14-0483	Kaolin	CH_4	1630	68	---	1.11
1-14-0483	"	CH_4	1360	161	---	1.24
3-14-0483	"	CH_4	Raw	---	0	9.39
4-14-0483	5K95V*	CH_4	1630	68	70	2.44
5-14-0483	"	CH_4	1360	161	30	5.38
6-14-0483	"	CH_4	Raw	---	0	1.22
3-15-0483	10K90V*	CH_4	Raw	---	0	1.54
1-15-0483	"	CH_4	1630	68	80	1.96
2-15-0483	"	CH_4	1360	161	44	5.69
9-14-0483	25K75V*	CH_4	Raw	---	0	3.72
7-14-0483	"	CH_4	1360	161	40	5.52
8-14-0483	"	CH_4	1630	68	80	1.78
1-16-0683	MW125	CH_4	1630	22	92	5.1
2-16-0683	"	CH_4	1515	24	74	7.15
1-17-0683	"	CH_4	1630	134	100.2	4.39
2-17-0683	"	CH_4	1515	142	85.2	7.48
3-17-0683	"	CH_4	1360	341	75	8.12
4-17-0683	"	CH_4	1360	142.5	69.2	9.56
5-17-0683	"	CH_4	1515	63	37	2.53

TABLE E-1. BET SURFACE AREA SAMPLES DATA (CONT.)

Test No.	Sorbent	Fuel	Peak Temperature °C	Residence Time, ms	Percent Calcination	N_2-BET Surface Area, m^2/g
1-20-0683	MW125	CH_4	1630	60	38	4.32
2-20-0683	"	CH_4	1630	68	74	4.2
3-20-0683	"	CH_4	1515	73	56	4.66
4-20-0683	"	H_2	1200	86	30	4.11
1-21-0683	"	CH_4	1360	79	58	3.96
2-21-0683	"	CH_4	1515	36	49	6.06
3-21-0683	"	CH_4	1630	33	42	4.78
4-21-0683	"	CH_4	1360	54	32	3.23
5-21-0683	"	---	Raw	---	0	0.45
6-21-0683	Bentonite	CH_4	1360	161	70	24.3
7-21-0683	"	CH_4	1630	68	76	33.65
8-21-0683	"	---	Raw	---	0	139.2
1-22-0683	25B75V	CH_4	1630	68	87	2.68
2-22-0683	"	CH_4	1360	161	44	6.46
3-22-0683	"	---	Raw	---	0	24.52
4-22-0683	10B90V	CH_4	1360	161	83	4.00
5-22-0683	"	CH_4	1630	68	---	3.3
6-22-0683	"	---	Raw	---	0	11.42
1-23-0683	5B95V	CH_4	1630	68	91	4.87
2-23-0683	"	CH_4	1360	161	85	5.11
3-23-0683	"	---	Raw	---	0	6.20
4-23-0683	CaS	CH_4	1360	161	82	4.84
1-27-0683	"	CH_4	1515	73	77	5.81
2-27-0683	"	CH_4	1630	68	67	9.42
3-27-0683	"	CH_4	1485	156	80	4.51
4-27-0683	"	---	Raw	---	0	1.09
1-28-0683	10K90V	H_2	1200	86	---	3.59
2-28-0683	Kaolin	H_2	1200	86	---	2.45
3-28-0683	25K75V	H_2	1200	86	73	2.32

TABLE E-1. BET SURFACE AREA SAMPLES DATA (CONT.)

Test No.	Sorbent	Fuel	Peak Temperature °C	Residence Time, ms	Percent Calcination	N_2-BET Surface Area, m^2/g
1-29-0683	5K95V	H_2	1200	86	77	1.96
3-29-0683	Bentonite	H_2	1200	86	89	8.92
5-29-0638	25B75V	H_2	1200	86	60	12.47
1-30-0683	10B90V	H_2	1200	86	66	5.56
2-30-0683	5B95V	H_2	1200	86	83	9.46
4-30-0683	Vicron 45-3	H_2	1200	86	81.6	5.65
6-30-0683	Al_2O_3	CH_4	1630	68	---	0.65
8-30-0683	5A195V	CH_4	1630	68	93	4.37
10-30-0683	5A195V	CH_4	1360	161	64	5.23
1-1-0783	"	H_2	1200	86	61	7.35
3-1-0783	5Na95V	H_2	1200	86	30	1.45
5-1-0783	"	CH_4	1630	68	46	3.49
7-1-0783	"	CH_4	1360	161	54	2.08
1-5-0783	5Fe95V	H_2	1200	86	70	2.17
2-5-0783	"	CH_4	1630	68	79	5.49
4-5-0783	"	CH_4	1360	161	88	2.03
6-5-0783	Vicron 45-3	---	Raw	---	0	0.64
7-5-0783	Bentonite	---	Raw	---	---	121.6
8-5-0783	Kaolin	---	Raw	---	---	7.13
9-5-0783	5B95V	---	Raw	---	---	6.08
10-5-0783	10B90V	---	Raw	---	---	10.37
11-5-0783	25B75V	---	Raw	---	---	17.9
12-5-0783	5K95V	---	Raw	---	---	0.93
13-5-0783	10K90V	---	Raw	---	---	1.40
14-5-0783	25K75V	---	Raw	---	---	2.41
15-5-0783	Al_2O_3	---	Raw	---	---	0.54
16-5-0783	5A195V	---	Raw	---	---	0.58

TABLE E-1. BET SURFACE AREA SAMPLES DATA (CONT.)

Test No.	Sorbent	Fuel	Peak Temperature ^oC	Residence Time, ms	Percent Calcination	N_2-BET Surface Area, m^2/g
18-5-0783	5Na95V	---	Raw	---	--	0.61
19-5-0783	5Fe95V	---	Raw	---	--	1.02
1-6-0783	5Si95V/140	CH_4	1360	161	31	2.10
3-6-0783	5Si95V/140	CH_4	1630	68	--	1.98
5-6-0783	5Si95V/140	H_2	1200	86	44	3.48
1-7-0783	5Si95V/240	CH_4	1200	86	--	1.77
3-7-0783	5Si95V/240	CH_4	1630	68	50	2.14
5-7-0783	5Si95V/240	CH_4	1360	161	82	2.47
1-8-0783	Si240	CH_4	1630	68	--	1.32
3-8-0783	Si140	CH_4	1630	68	--	1.04
5-8-0783	Type 4A	CH_4	1630	68	--	1.07
7-8-0783	54A95V	CH_4	1630	68	--	1.63
1-23-0783	Vicron 45-3	CH_4	1630	68	66	6.68
2-23-0783	"	H_2	1200	86	45	8.37
3-23-0783	"	CH_4	1360	161	64	6.62
4-23-0783	"	CH_4	1515	73	73	5.92
5-25-0783	5K95V	H_2	1200	86	--	3.75
1-26-0783	10K90V	H_2	1200	86	63	2.39
2-26-0783	"	CH_4	1360	161	--	2.07
1-28-0783	"	CH_4	1515	73	--	1.55
2-28-0783	"	CH_4	1630	68	--	1.51
3-28-0783	25K75V	H_2	1200	86	41	2.29
4-28-0783	25K75V	CH_4	1360	161	36	2.71
5-28-0783	"	CH_4	1515	73	52	1.78
6-28-0783	"	CH_4	1630	68	32	4.38
1-29-0783	5B95V	H_2	1200	86	--	7.73
2-29-0783	5B95V	CH_4	1515	73	--	4.74

TABLE E-1. BET SURFACE AREA SAMPLES DATA (CONT.)

Test No.	Sorbent	Fuel	Peak Temperature °C	Residence Time, ms	Percent Calcination	N_2-BET Surface Area, m^2/g
3-29-0783	10B90V	CH_4	1515	73	--	2.44
1-3-0883	"	H_2	1200	86	77	8.98
2-3-0883	25B75V	H_2	1200	86	78	9.66
3-3-0883	"	CH_4	1515	73	--	2.39
1-4-0883	Bentonite	CH_4	1515	73	--	5.48
2-4-0883	"	CH_4	1630	68	--	3.51
3-4-0883	"	CH_4	1360	161	--	2.04
4-4-0883	"	H_2	1200	86	--	4.86
5-4-0883	54A95V	H_2	1200	86	74	3.62
6-4-0883	"	CH_4	1360	161	84	3.32
1-5-0883	5Na95V	H_2	1200	86	30	7.04
2-5-0883	"	CH_4	1630	68	52	5.5
1-8-0883	5A195V	CH_4	1630	68	90	5.05
2-8-0883	"	CH_4	1360	161	82	5.81
3-8-0883	"	H_2	1200	86	79	10.11
4-8-0883	5K95V	CH_4	1360	161	78	1.94
5-8-0883	5K95V	CH_4	1515	73	76	2.68
6-8-0883	"	CH_4	1630	68	56	3.71
7-8-0883	5Fe95V	CH_4	1630	68	96	1.51
8-8-0883	"	H_2	1200	86	89	7.45
1-22-0883	5Si24095V	H_2	1200	86	62	10.50
3-22-0883	"	CH_4	1360	161	--	2.43
5-22-0883	"	CH_4	1515	73	94	2.98
7-22-0883	"	CH_4	1630	68	94	3.18
1-23-0883	5Fe95V	H_2	1200	86	87	2.47

TABLE E-1. BET SURFACE AREA SAMPLES DATA (CONT.)

Test No.	Sorbent	Fuel	Peak Temperature °C	Residence Time, ms	Percent Calcination	N_2-BET Surface Area, m^2/g
2-23-0883	5Fe95V	CH_4	1630	68	95	1.18
4-7-0983	5K95V	H_2	1200	86	78	2.64
6-7-0983	"	H_2	1200	86	63	2.90
7-7-0983	5K95MW	H_2	1200	86	74	5.17
8-7-0983	5K95MW	CH_4	1630	68	91	2.14
1-20-0983	5K95V	H_2	1200	86	51	3.16
2-20-0983	"	CH_4	1630	68	66	3.04
1-23-0983	5Si24095V	H_2	1200	86	67	6.10
3-23-0983	"	CH_4	1360	161	66	7.94
1-26-0983	"	H_2	1200	86	70	4.61
3-26-0983	"	CH_4	1630	68	67	4.57
1-27-0983	"	CH_4	1630	68	56	2.98
3-27-0983	Dolomite	H_2	1200	86	52	25.83
1-26-1083	5K95D	H_2	1100	93	62	19.56
2-26-1083	"	H_2	1200	86	31	19.51
3-26-1083	"	CH_4	1360	80	94	7.06
4-26-1083	"	CH_4	1360	161	95	5.75
5-26-1083	"	CH_4	1515	73	95	4.19
6-26-1083	"	CH_4	1630	68	97	2.53
1-28-1083	10K90Ca	H_2	1100	93	--	7.75
2-28-1083	"	H_2	1200	86	--	5.87
3-28-1083	"	CH_4	1360	80	--	3.73

TABLE E-2. VICRON 45-3/KAOLIN SEPARATE INJECTION RESULTS

Test No.	Injection Mode	Fuel	Peak Temperature °C	Residence Time, ms	Sorbent	Percent Calcination	N_2-BET Surface Area, m^2/g
1-15-0983	Parallel	H_2	1200	86	V/K	85	5.64
4-14-0983	"	H_2	1200	86	V	86	10.33
3-15-0983	"	CH_4	1630	68	V/K	95	3.18
5-14-0983	"	CH_4	1630	68	V	94	3.47
3-14-0983	Delayed	CH_4	1630	68	V/K	67	6.57
1-14-0983	"	CH_4	1630	68	V	88	7.64
1-12-0983	"	H_2	1200	86	V/K	47	7.33
5-9-0983	"	H_2	1200	86	V	79	7.51
3-9-0983	Coaxial	CH_4	1630	68	V/K	81	5.65
2-8-0983	"	CH_4	1630	68	V	81	5.64
1-9-0983	"	H_2	1200	86	V/K	79	4.51
1-8-0983	"	H_2	1200	86	V	73	7.50
1-7-1083	Delayed	H_2	1200	86	V/K		5.50
2-7-1083	Delayed (reversed)	H_2	1200	86	V/K		3.40
3-7-1083	Delayed	CH_4	1630	68	V/K		3.88
4-7-1083	Delayed (reversed)	CH_4	1630	68	V/K		4.01

Parallel - Separate Injection of Vicron 45-3 and Kaolin with parallel injection tubes.

Delayed - Coaxial Injection with Vicron 45-3 injected through the center tube downstream of the kaolin injection point.

Coaxial - Coaxial Injection with both Vicron 45-3 and kaolin injected at the same burner face.

TABLE E-3. SULFUR CAPTURE DATA (REACTIVITY PROBE)

Test No.	Sorbent	Fuel	Peak Temp, °C	Probe Residence Time, ms	Probe Temp, °C	SO_2 Concentration Percent	Utilization Percent	Calcination Percent
1-13-0783	Vicron 45-3	CH_4	1630	330	1060	5.8	5.9	58.3
1-14-0783	"	CH_4	1515	190	1060	3.5	9.4	56.6
1-18-0783	"	H_2	1200	890	1060	18.2	14.8	68.3
2-18-0783	"	H_2	1200	540	1060	11.5	17.4	72.7
3-18-0783	"	H_2	1200	790	1060	8.3	16.0	77.3
4-18-0783	"	H_2	1200	890	1060	in-filter only	2.1	48.1
1-19-0783	25K95V	H_2	1200	890	1060	18.2	5.4	19.1
2-19-0783	"	CH_4	1630	940	1060	18.2	6.2	42.1
5-23-0783	Vicron 45-3	H_2	1200	890	1060	18.2	17.2	66.3
6-23-0783	"	H_2	1200	890	1060	18.2	19.7	69.1
1-25-0783	5K95V	H_2	1200	890	1060	18.2	3.5	47.5
2-25-0783	"	H_2	1200	890	1060	18.2	2.5	18.9
3-25-0783	"	CH_4	1515	980	1060	19.5	1.2	16.9
4-25-0783	"	CH_4	1630	950	1060	19.5	1.0	68.4
2-23-0983	5Si24095V	H_2	1200	520	1060	5.6	15.3	59.0
4-23-0983	"	CH_4	1360	560	1060	6.2	9.1	71.9
2-26-0983	"	CH_4	1515	570	1060	6.0	6.5	62.4
2-27-0983	"	CH_4	1630	550	1060	6.0	5.8	73.6
4-27-0983	Dolomite	H_2	1200	520	1060	5.6	47.4	81.5
5-27-0983	"	CH_4	1360	560	1130	6.2	25.8	91.3
6-27-0983	"	CH_4	1515	570	1140	6.0	23.4	81.0
1-28-0983	"	CH_4	1630	550	1140	6.0	14.9	84.3
2-28-0983	Vicron 45-3	H_2	1200	520	1130	5.6	11.0	60.1
3-28-0983	"	CH_4	1360	560	1120	6.2	10.4	62.5
1-29-0983	"	CH_4	1515	570	1100	6.0	10.0	63.7
2-29-0983	"	CH_4	1630	550	1125	6.0	10.2	71.6
3-29-0983	Ca(OH)$_2$	H_2	1200	520	1110	5.6	22.7	97.8
4-29-0983	"	CH_4	1360	570	1110	6.2	15.9	98.4

TABLE E-3. SULFUR CAPTURE DATA (REACTIVITY PROBE) (CONTINUED)

Test No.	Sorbent	Fuel	Peak Temp, °C	Probe Residence Time, ms	Probe Temp, °C	SO_2 Concentration Percent	Utilization, Percent	Calcination, Percent
1-30-0983	$Ca(OH)_2$	CH_4	1515	570	1110	6.0	98.6	98.6
2-30-0983	$Ca(OH)_2$	CH_4	1630	550	1140	6.0	97.0	97.0
1-3-1083	5K95D	H_2	1200	520	1110	5.6	74.5	74.5
2-3-1083	5K95D	CH_4	1360	560	1110	6.2	84.4	84.4
3-3-1083	5K95D	CH_4	1515	570	1120	6.0	43.0	43.0
4-3-1083	5K95D	CH_4	1515	570	1120	6.0	80.2	80.2
1-10-1083	5K95D	CH_4	1630	550	1110	6.0	91.2	91.2
1-13-1083	10K90Ca	H_2	1200	520	1110	5.6	94.0	94.0
2-13-1083	10K90Ca	CH_4	1360	570	1120	6.2	96.9	96.9
1-14-1083	10K90Ca	CH_4	1515	570	1120	6.0	97.7	97.7
2-14-1083	10K90Ca	CH_4	1630	550	1120	6.0	96.1	96.1
3-14-1083	Vicron 45-3	H_2	1200	520	1120	5.6	62.0	62.0
1-17-1083	Vicron 45-3	H_2	1360	570	1120	5.2	80.5	80.5
2-17-1083	5K95D	H_2	1360	560	1120	5.2	88.4	88.4
3-17-1083	5K95D	H_2	1515	570	1120	6.0	87.8	87.8
4-17-1083	5K95D	H_2	1200	520	1110	5.6	99.9	99.9

TABLE E-4. IN-FLAME SULFUR CAPTURE DATA

Test No.	Sorbent	Fuel	Air, l/s	Diluent/ l/s	Stoichiometric Ratio	Peak Temp. °C	N_2-BET Surface Area, m^2/g	Utilization, Percent
1-18-0483	Vicron 45-3	CH_4/H_2S[1]	0.54	$O_2/0.24$	3.53	1300	2.0	
1-19-0483	"	"	0.54	$O_2/0.24$	3.53	1260		8.4
2-19-0483	"	"	0.60	$O_2/0.18$	2.90	1280	4.1	
3-19-0483	"	"	0.60	$O_2/0.18$	2.90	1255		8.2
1-20-0483	"	"	0.66	$O_2/0.12$	2.27	1285	3.1	
2-20-0483	"	"	0.66	$O_2/0.12$	2.27	1265		9.9
1-21-0483	"	"	0.72	$O_2/0.06$	1.65	1335	4.1	
2-21-0483	"	"	0.72	$O_2/0.06$	1.65	1325		5.8
1-22-0483	"	"	0.79	---	1.02	1405	3.1	
1-25-0483	"	"	0.79	---	1.02	1405		3.9
1-26-0473	"	"	0.72	$N_2/0.06$	0.94	1405	5.0	
2-26-0483	"	"	0.72	$N_2/0.06$	0.94	1410		2.3
3-26-0483	"	"	0.66	$N_2/0.12$	0.86	1350	6.2	
4-26-0483	"	"	0.66	$N_2/0.12$	0.86	1355		4.3
5-26-0483	"	"	0.60	$N_2/0.18$	0.78	1245	5.9	
1-28-0483	"	"	0.60	$N_2/0.18$	0.78	1235		15.1

[1] 6.15% H_2S in CH_4

APPENDIX F

Quality Control Evaluation Report

1. Experimental

A. Temperature Measurements

Temperature measurement was the primary determinant of repeatability of experimental conditions. Three temperatures were measured routinely in this program:

1) Flame gas temperature
2) Reactivity probe entrance temperature
3) Reactivity probe midpoint (furnace) temperature

In addition, particle temperatures were measured in one system by two-color pyrometry. This system and the associated uncertainties were discussed in Section 3.2.4.

B. Gas Flow Rates

All gas flow rates were measured by suitably sized rotometers which, with one exception, were all manufactured by Dwyer Instruments Inc. The exception was a Matheson Tube Cube flowmeter calibrated for low flow rates of sulfur dioxide.

In general, flowmeters were not calibrated because temperature, not stoichiometry, was the significant control variable. Calibration for H_2 and SO_2 are shown in Figures F-1 and F-2.

Flow rates were corrected for pressure and specific gravity (relative to air) using the formula

$$Q = Q^o \left[\frac{P}{101.3\text{kPa}} \times \frac{1}{\text{S.G.}} \right]^{1/2}$$

Where:

Q = true flow rate

Q^o = measured flow rate

P = outlet rotometer pressure, kPa

S.G. = gas specific gravity

Corrections for ambient temperature were not made. All of the flowmeters were factory calibrated and specified accurate to ±5 percent or better of the full scale reading. In general, conditions were repeatable within the ability to read the flowmeter. Variations in flow rate sufficient to alter the gas temperature significantly were small.

The outlet pressure of the rotometer was measured using the stagnation configuration shown in Figure F-3. This configuration ensured that pressure measurements were not affected by aerodynamic or venturi effects.

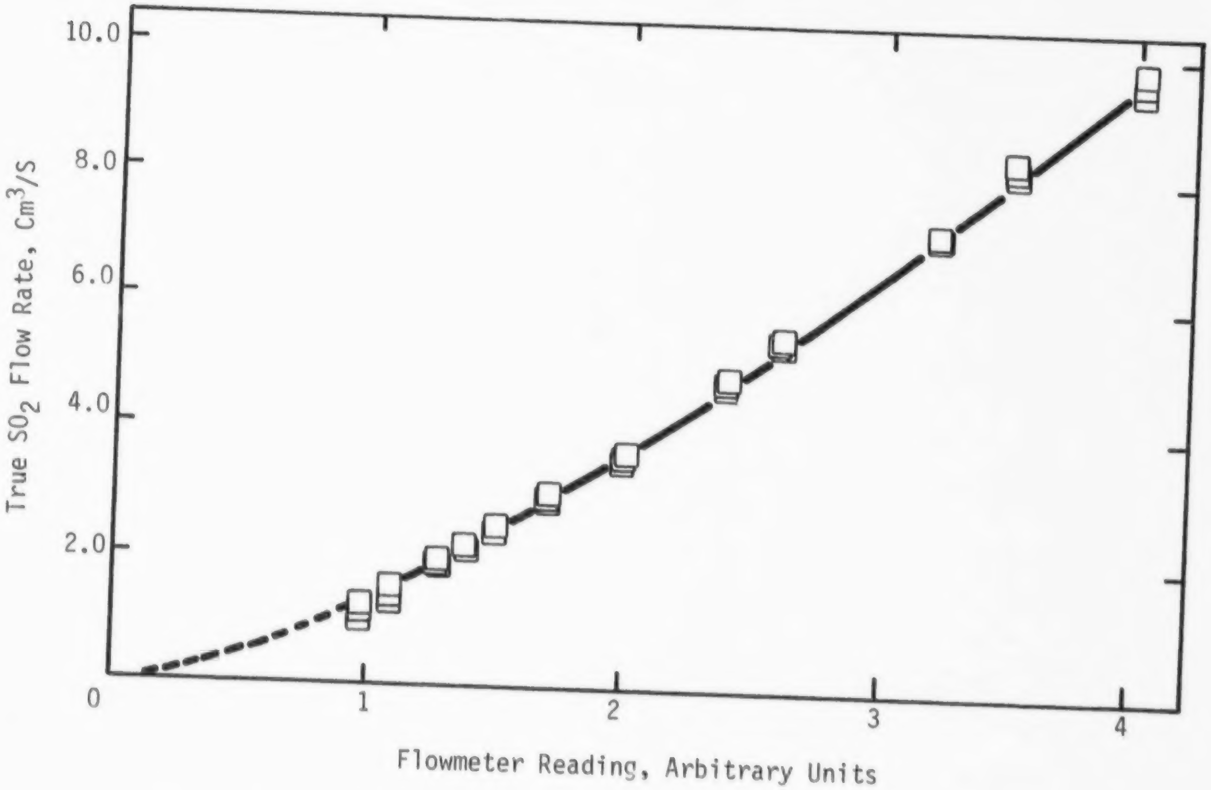

Figure F-1. Calibration of the SO_2 flowmeter at room temperature with negligible outlet pressure.

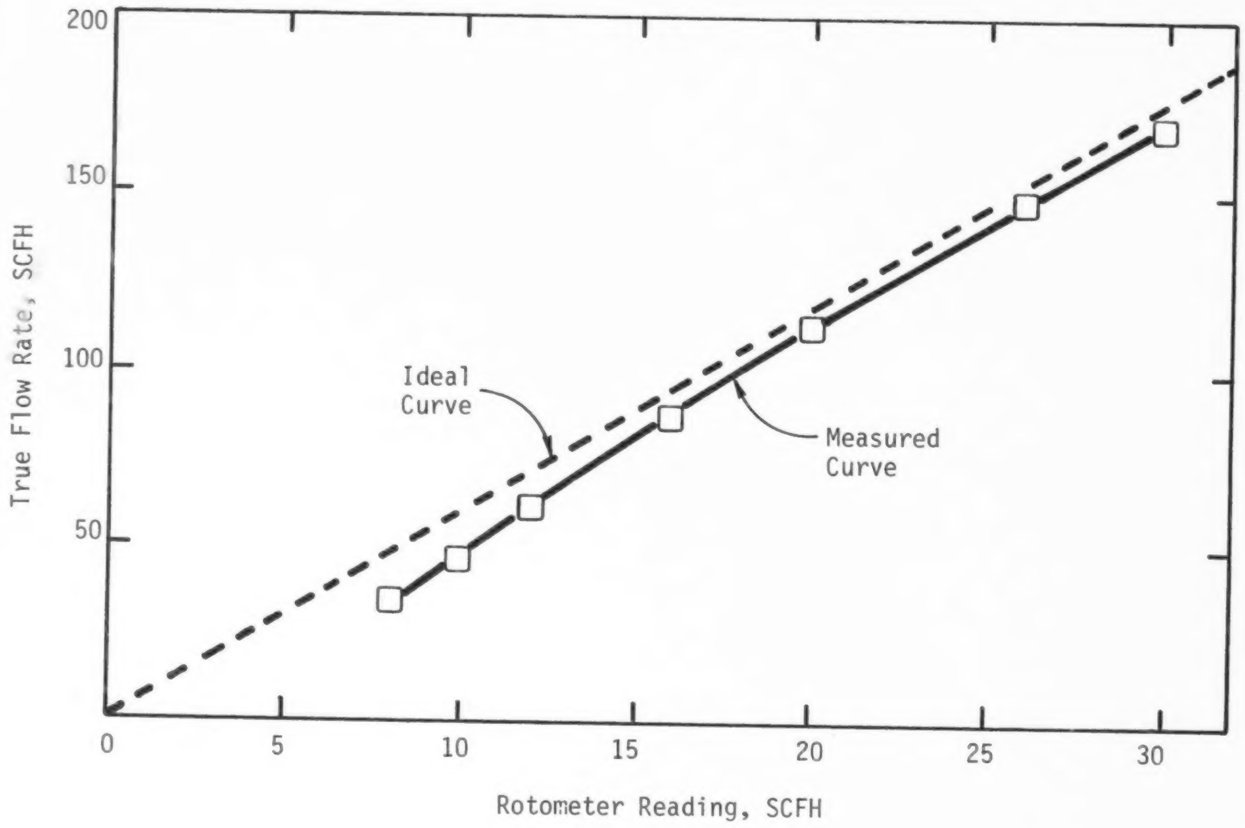

Figure F-2. H_2-rotometer calibration curve. Data were obtained using a dry-test volume displacement meter corrected for pressure and ambient temperature.

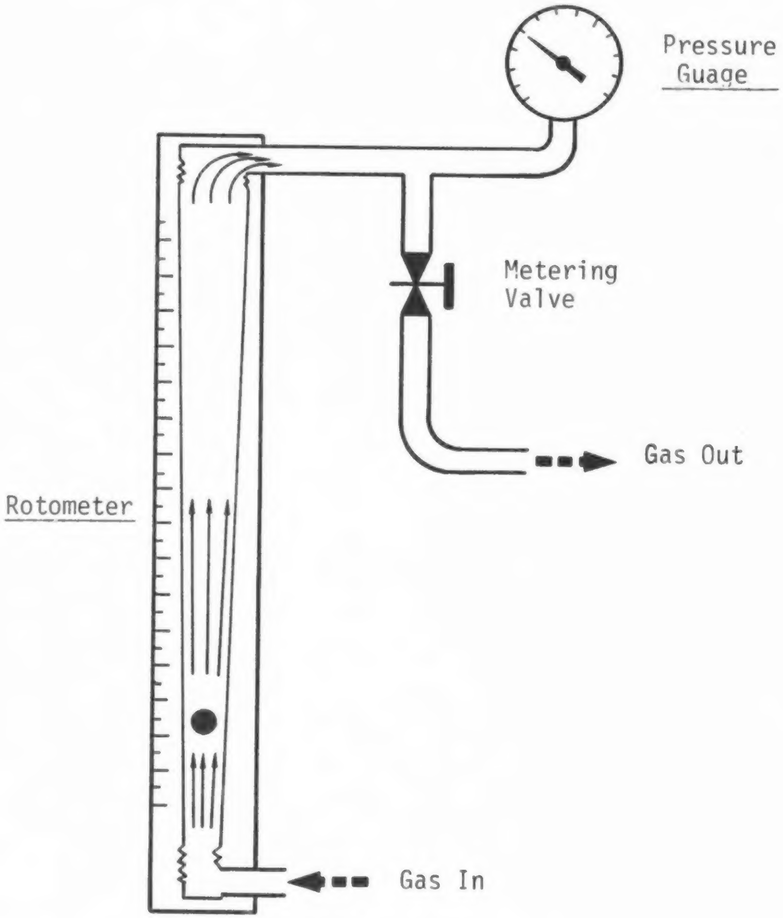

Figure F-3. Configuration for stagnation pressure measurement at rotometer outlet. Pressure measurements are used to correct measured gas flow rates.

C. Measurement of Sorbent Flow Rates

Sorbent flow rates were regulated and monitored for two reasons which could impact the repeatability of the experiments. 1. to avoid thermally overloading the reactor volume occupied by the sorbent stream, and, 2. to maintain a favorably low calcium-to-sulfur ratio in the reactivity probe. Sorbent feed rates were not infinitely adjustable and were dependent on the operating conditions of the fluidized bed as well as those of the offtake tube assembly. However, suitable flow rates could be attained and were generally reproducible even if the sorbent flow was halted for a few minutes and then restarted.

The objective of monitoring the sorbent feed rates was to ensure that no change in feed rate had occurred which might impact the validity or representativeness of a sample. Feed rates were measured immediately before and after each sample was collected and the results recorded.

Procedure

After the desired fluidized bed operating conditions were set and a visibly steady sorbent flow rate was obtained, the sorbent feed tube was placed into a tared 50 ml Erlenmeyer flask. The sorbent was ejected into the flask for either 30 or 60 seconds depending on the flow rate. The flask was then reweighed. An electronic balance with automatic tare and zero was used so that the sorbent mass was obtained directly. This procedure was performed immediately before and immediately following flame injection and sampling.

During the filling of the flask, fine material was carried out of the flask by the transport gas. Several means were used to trap the fine material. These included:

- Filling the flask with shredded paper to provide a high surface area and tortuosity to trap the fines.

- Placing water in the flask to act as a dust trap.

- Fitting paper and glass fiber filters to the mouth of the flask.

- Plugging the mouth and neck of the flask with a fiber such as glass wool.

The latter technique was the most effective at reducing the visible efflux of fines from the flask. However, it was found that the fines constituted a negligible fraction (could not be measured) of the total mass of material collected so this precaution was generally disregarded.

Typical data to demonstrate the reproduceability of sorbent feed rates are shown in Table F-1.

TABLE F-1. REPRODUCIBILITY OF SORBENT FLOW RATES BEFORE AND AFTER SAMPLE COLLECTION

	Flow Rate, g/min		
Sorbent	Before Sampling	After Sampling	Change
25K75V	0.60	0.58	-0.02 g/min
5B95V	0.80	0.80	0
10B90V	0.85	0.88	0.03
Bentonite	0.40	0.34	-0.06
Kaolin	0.30	0.25	-0.05
Kaolin	0.43	0.22	-0.21
Vicron 45-3	0.51	0.42	-0.09
Vicron 45-3	0.48	0.63	+0.15
Vicron 45-3	0.64	0.70	+0.06

E. Peak Centerline (Axial) Gas Temperatures

As discussed in Section A. the peak centerline temperatures served as the main check on reproduceability of conditions in the thermal decomposition reactor tests. Using a 0.2mm (.008") diameter butt-welded type S (Pt/Pt-10%Rh) thermocouple inserted 6.5-7.0 cm from the burner surface the axial temperature was matched to that of the main flame. The procedure was as follows.

1. The main burner flame temperature was set at the desired level by adjusting the fuel flow rate.
2. Sorbent flow conditions were established.
3. Sorbent flow was stopped.
4. The centerline of the reactor was located by the "thermal well" produced by the transport gas.
5. Methane was introduced to the transport gas at the burner until the desired temperature was reached.
6. The main flame temperature was rechecked, usually this was then too high and had to be reset.
7. The centerline temperature was rechecked, it generally was too low.
8. Steps 6. and 7. were repeated until the radial profile near the center of the reactor was flat at 6.5-7.0 cm.

Following this procedure carefully each time an experiment was performed ensured continuity of experimental conditions against potential variations in measured gas flow rates or sorbent injection conditions.

2. Analytical

A. BET Analysis

Specific surface area measurements constituted the primary diagnostics employed in this study. Measurements were carried out at 77K using N_2 adsorption isotherm analysis by the Brunauer-Emmett-Teller (BET) technique on an instrument manufactured by Quantachrome. This method provides a representative measure of specific surface area for a given material. The repeatability of the measurements was checked by multiple analyses of randomly chosen samples throughout the period of the program. Results of the repeatability tests are listed in Table F-2.

In addition, two standards, supplied by Quantachrome Inc., were analyzed to determine the overall accuracy of both the instrument and operation. These standards were No. 8008, SiO_2, 5.15 m^2/g and No. 7008, Al_2O_3, 1.97 m^2/g. Analyses are given in Table F-3.

TABLE F-2. REPRODUCIBILITY OF BET SPECIFIC SURFACE AREA MEASUREMENTS

Sample Description	Surface Area m^2/g	Standard Deviation
Vicron 45-3, partly calcined	5.06 4.79	3.9%
Bentonite	137.25 141.06	1.9%
Al_2O_3	0.58 0.54	5.1%

TABLE F-3. BET SPECIFIC SURFACE AREA STANDARDS TESTING

BET Standard	Actual Surface Area m^2/g	Measured Surface Area, m^2/g	Difference m^2/g
No. 8008 SiO_2	5.15	4.25	-0.90
No. 7008 Al_2O_3	1.97	1.40	-0.57
		mean difference	-0.74 m^2/g
		standard deviation	0.23 m^2/g

B. Perkin-Elmer 240B Elemental Analyzer

The Perkin-Elmer 240B elemental analyzer was used to determine the CO_2 and H_2O content of solid samples. For unsulfated samples this information was used to directly determine the extent to which the sample was calcined (mol-% basis). Recalibration of the instrument was carried out each time a series of samples was analyzed. In addition, both accuracy and precision studies were performed. Standards for the accuracy study were benzethonium chloride monohydrate, 2,5-bis-(4-biphenylyl) oxazole and acetanilide. The precision study utilized the five replicate samples of benzethonium chloride monohydrate. Results of these test are shown in Table F-4. Accuracy was +1.0 ± 2.5 percent for carbon and -0.6 ± 3.0 percent for hydrogen. The relative precision was ±0.2 percent for carbon and ±1.4 percent for hydrogen.

TABLE F-4. ACCURACY AND PRECISION TESTS FOR THE PERKIN-ELMER 240B ELEMENTAL ANALYZER

Accuracy Tests

Standard	Actual Composition -Percent-		Measured Difference -Percent-	
	Carbon	Hydrogen	Carbon	Hydrogen
Benzethonium chloride monohydrate	69.58	9.51	+3.4	-2.5
			3.4	1.3
			2.8	4.8
			3.3	3.6
			3.3	2.5
2.5-bis(4-biphenylyl) oxazole	86.84	5.13	0.1	+0.4
			0.1	2.3
			-3.2	3.7
			3.0	4.3
Acetanilide	71.09	6.71	+0.3	-2.2
			0.4	0.6
	$\bar{x}$		+1.0	-0.6
	s		2.5	3.0

Precision Tests

Standard		Measured Composition -Percent-	
		Carbon	Hydrogen
Benzethonium chloride monohydrate		71.92	9.29
		71.95	9.39
		71.53	9.05
		71.88	9.17
		71.88	9.27
	$\bar{x}$	71.83	9.23
	s	0.17	0.13

C. Leco SC-32 Sulfur Analyzer

The Leco SC-32 sulfur analyzer was used to determine the sulfur content of sulfated and sulfidated sorbents as well as possible trace levels of sulfur in the sorbents and mineral additives. The sulfur contents were then used, along with the 240B data, to determine directly the extent of calcination of sulfated sorbents as well as the calcium utilization efficiency. The SC-32 sulfur analyzer was calibrated prior to running each sample. In addition, a series of tests was run to determine the accuracy and relative standard deviation of the instrument. The standard materials were four coals (0.96 percent S, 2.05 percent S, 1.68 percent S, and 3.02 percent S) provided by Leco as calibration standards. Results of these tests are shown in Table F-5.

The Leco instrument measures sulfur content by igniting the sample in an oxygen-rich atmosphere at high temperature. The resultant volume of SO_2 is measured and the percent-by-weight of sulfur is calculated internally by the instrument. Test involving inorganic sulfur as sulfate showed poor recovery and reproduceability. To solve this problem several combustion accelerators were tested. Vanadium pentoxide was found to work satisfactorily with sulfated limestones. The V_2O_5 is ground to a powder and added to the sample after taring and weighing.

TABLE F-5. ACCURACY AND RELATIVE STANDARD DEVIATION DETERMINATIONS FOR THE LECO SC-32 SULFUR ANALYZER

	Measured Percent Sulfur			
Coal Sulfur Content	0.96%S	2.05%S	1.68%S	3.02%S
	0.93	2.10	1.73	3.02
	0.93	2.05	1.68	2.98
	0.96	2.13	1.65	3.13
	0.96	2.07	1.62	
	0.92	1.98	1.67	
	0.94	2.03	1.72	
	0.94	2.08	1.63	
	0.95	2.05	1.64	
	0.99	2.03	1.65	
	0.93	2.05	1.63	
	0.94	2.00	1.66	
	0.94	2.04	1.68	
	1.00	2.12	1.69	
	0.97	2.08	1.64	
		2.02	1.75	
		2.07	1.74	
		2.09	1.68	
		2.00		
		2.06		
$\bar{x}$	0.95	2.06	1.67	3.04
RSD	2.5%	2.0%	2.4%	2.6%
$\frac{\bar{x}-x}{x}$x100%	-1.04%	+0.49%	-0.60%	0.66%

D. Overall Check of Chemical Analyses by Mass Balance

In order to provide an overall check on the accuracy of the chemical analyses, a mass balance was performed for each sample. The data returned from the 240B instrument were %C, %H and % ash. The ash value was obtained from the net weight of the sample after ignition in the instrument.

For unsulfated limestones (e.g. Vicron 45-3) the sample was assumed to contain CaO, $CaCO_3$ and $Ca(OH)_2$ only. Trace impurities and Mg compounds were ignored. The carbon content was then stoichiometrically equivalent to $CaCO_3$ with a factor of 8.33; hydrogen, inturn, equivalent to $Ca(OH)_2$ with a factor of 37. Calcium oxide, the remaining compound, was determined by difference. The mass balance involved simply calculating the total calcium in the sample from the CaO, $CaCO_3$ and $Ca(OH)_2$ measurements. The percent calcium was then compared with the percent calcium in the ash, which was assumed to be all CaO.

With unsulfated dolomite samples, the same procedure was employed, except that the separately determined Mg/Ca ratio was used to correct the percent Ca (from H and C measurements) to percent CaO plus MgO. The total CaO plus MgO was then compared with the percent ash, which was assumed to be MgO plus CaO.

With sulfated samples the Leco SC32 sulfur analyzer results also were employed. The sulfur was assumed to be $CaSO_4$ with a stoichiometric factor of 4.25. During the 240B analysis the $CaSO_4$ was retained in the ash. The CaO was determined as $100-(CaSO_4 + CaCO_3 + Ca(OH)_2)$ and the ash value was compared with

$$CaSO_4 + CaO + \frac{56}{100} CaCO_3 + \frac{56}{74} Ca(OH)_2$$

Example calculations are shown below.

Unsulfated Vicron 45-3 Sample 1-23-0683

% C = 1.42 = 11.83% $CaCO_3$ = 4.73% Ca

% H = 0.29 = 10.73% $Ca(OH)_2$ = 5.80% Ca

% CaO = 100-11.83-10.73 = 77.44% = 55.31% Ca

% Ash = 92.60 = 66.14% Ca

4.73 + 5.80 + 55.31 = 65.84% Ca

$$\text{mass balance} = \frac{65.84}{66.14} \times 100\% = 99.55\%$$

Unsulfated Dolomite Sample 3-27-0983

% C = 4.32 = 36.0% $CaCO_3$ = 20.16% CaO

% H = 0.25 = 9.25% $Ca(OH)_2$ = 7.00% CaO

100-(36.0 + 9.25) = 54.75% CaO + MgO

% Ash = 81.27

total CaO + MgO = 20.16 + 7.0 + 54.75 = 81.91

$$\text{mass balance} = \frac{81.91}{81.27} \times 100\% = 100.79\%$$

Sulfated Vicron 45-3 Sample 3-32-0383

% C = 2.30 = 19.17% $CaCO_3$ = 7.67% Ca

% H = 0.10 = 3.7% $Ca(OH)_2$ = 2.0% Ca

% S = 3.64 = 15.47% $CaSO_4$ $CaSO_4$ = 4.55% Ca

% CaO = 100-(19.17 + 3.7 + 15.47) = 61.66 = 44.04% Ca

% Ash = 91.65 = CaO + $CaSO_4$

91.65-15.47 = 76.18% CaO = 54.41% Ca

7.67 + 2.0 + 44.04 = 53.71% Ca

$$\text{mass balance} = \frac{53.71}{54.41} \times 100\% = 98.71\%$$

3. Samples Quality Assurance

A. Calcination Check for Sample Quality and Comparability

In order to ensure comparability of data collected at a fixed experimental condition, the extent of calcination was measured for each sample. At short residence times and/or low temperatures calcination was generally incomplete as a result of the experimental conditions. At longer times, however, low extents of calcination indicated a spurious pulse, or slugging, in the sorbent feed system. The results of slugging in the feed system were associated with surface areas either higher or lower than the norm.

At peak temperatures of 1360°C and higher, samples collected at distances greater than 10 cm were generally rejected if extents of calcination were lower than 80 percent. At 1200°C, lower extents of calcination were observed overall and so samples were retained with extents of calcination of 50 percent or greater.

B. Additional Criteria for Acceptance/Rejection

In addition to the baseline levels of calcination, comparability with other data was also used as a criterion for acceptance. Samples which were clearly out of line with those collected at both shorter and larger residence times were rejected. Also rejected were samples collected at long residence times which showed a substantial decrease in the level of calcination from the samples collected at shorter times.

Repeats of some samples were collected in order to determine both repeatability of conditions and the effects of possible unknown systematic variables. Sample repeats are apparent in the main test of this report, primarily with Vicron 45-3, for calcination, surface area and sulfur capture tests.